Spatial analysis of the O-, H- and Sr- isotope composition of Cape Town groundwater

Rosy Finlayson (FNLCLA002)

Supervisor: Prof. Chris Harris

Co-supervisor: Prof. Judith Sealy

UNIVERSITY OF CAPE TOWN

IYUNIVESITHI YASEKAPA • UNIVERSITEIT VAN KAAPSTAD

Abstract

Hydrogen, oxygen and strontium isotope data, as well as electrical conductivity (EC) and pH, are presented for 256 water samples, collected over the years of 2017, 2020 and 2021 from predominantly the eastern slopes of the Cape Peninsula mountain range, Cape Town. The aim is to characterise aquifers and to improve the understanding of Cape Town groundwater. The range in the δD and $\delta^{18}O$ values of the water was -19.9‰ – 13.7‰ and -4.37‰ – 2.35‰, respectively. The EC range was 0.11 mS/cm – 58.7 mS/cm and the pH range was 4.00 – 7.93 ($\bar{x}$ = 6.44). The relatively good quality of the groundwater EC (median= 0.72 mS/cm), as well as the stable isotope composition, is consistent with a lack of seawater infiltration into the groundwater. Whereas a single aquifer can contain water with varying composition (e.g. the EC of Pinelands' water) the data are consistent with either multiple localised aquifers or compartments within the regional Cape Flats Aquifer (CFA) and scree aquifer on the eastern slopes of the mountains. The increase in the δD and $\delta^{18}O$ values of the eastern slopes' groundwater with depth indicates that the aquifer is stratified. The overall variation in the stable isotope composition indicated that the aquifers were primarily recharged by local, present-day rainfall. The increase of the δD and $\delta^{18}O$ values of the groundwater towards lower altitudes was attributed to 1) an inherited signature from the rainfall, caused by altitude and amount effects, and/or 2) evaporative enrichment of the return flow of abstracted groundwater. The recharge rates of the groundwater are thought to be slower than for the springs (which are recharged by approximately 50% within 3 years) because the recharge area and volume of water contained in the scree aprons from which the springs are derived is smaller than the groundwater. EC as high as 58.7 mS/cm is attributed to dissolution of salt from the substrate. The range $^{87}Sr/^{86}Sr$ ratios for the subset of the 10 samples was 0.70935 – 0.73023 ($\bar{x}$ = 0.71417). Variability in the $^{87}Sr/^{86}Sr$ ratios was attributed to varying amounts of interaction of the water with the local geology and sediments.

Acknowledgements

Firstly, I would like to thank my supervisor, Prof. Chris Harris, and my co-supervisor, Prof. Judith Sealy, for the advice, guidance, help in the field, draft edits and support throughout this year. Secondly, thank you to Dr. Alastair Sloan for the assistance with creating an isoscape. Thank you to my parents, Nicholas Soutar and my peers for their encouragement. The financial assistance of BIOGRIP towards this research is hereby acknowledged. Funding for the analytical work was provided by a CIMERA grant. Stable isotope analyses were done by Warrick Joe in 2017 and 2020, and Joshua Mirkin in 2021 in Adam West's lab in the Department of Biological Sciences, and strontium isotope analyses were done by Petrus le Roux, Fayrooza Rawoot and Kerryn Gray in the Department of Geological Sciences. Finally, thank you to Dianne Steele for your time and great help with my references.

Contents

List of Figures

List of Tables

Chapter 1: Introduction

Between 2015 and 2017, the Western Cape experienced its worst drought on record in over 100 years, culminating in a threat to cut off municipal water supply to over 4 million people, a scenario termed "Day-Zero". As a result, the City of Cape Town (CoCT) implemented extreme water restrictions, which exacerbated the unequal access to water in the region – a basic human right. Water shortages are predicted to become increasingly common in Cape Town due to climate change and the rising demand for water from a growing population (Midgley et al., 2005). The Western Cape water system is primarily reliant on surface reservoirs and hence rainfall, making the CoCT highly vulnerable to climate perturbations (Midgley et al., 2005). In addition, the scarcity of water is further exacerbated by leaking water mains. In 2009, water losses (including leakages, burst pipes, administrative errors, meter inaccuracies and meter tampering) by the CoCT were estimated at 25%, and in 2018 it was reported that water losses were estimated at 16% (City of Cape Town, 2018a). Groundwater has therefore been suggested as an alternative water source to alleviate the water stress experienced by the region. It is more resilient to the effects of climate breakdown because it is impacted less directly and more slowly by changing conditions. During droughts, it experiences lower rates of evaporation than surface water bodies because it is stored underground in larger volumes. Furthermore, it is less susceptible to contamination by pollution than surface water sources (Department of Water Affairs [DWA], 2010). Groundwater abstraction is also significantly cheaper than seawater desalination. As a result, groundwater is considered key to Cape Town's strategy of adaptation to climate breakdown (DWA, 2010). This study determines the isotope composition of groundwater across Cape Town as well as other physiochemical characteristics such as electrical conductivity (EC) and pH, to gain an understanding of Cape Town's groundwater.

1.1 Study site

The study site is situated along a narrow strip that stretches from Table Mountain, rising 1086 m above sea-level in the north, to Cape Point, covering an area of ~330 km^2 (only urban area included; Figure 1.1). It extends from the suburb of Bakoven, on the western slopes of Table Mountain around the coast to Mouille Point, and down to Simon's Town on the eastern slopes of Swartkop (Figure 1.2). The topography of the study area is steep along the elevated sandstone cliffs of the Cape Peninsula mountains, and relatively flat and low-lying in the Cape Flats District.

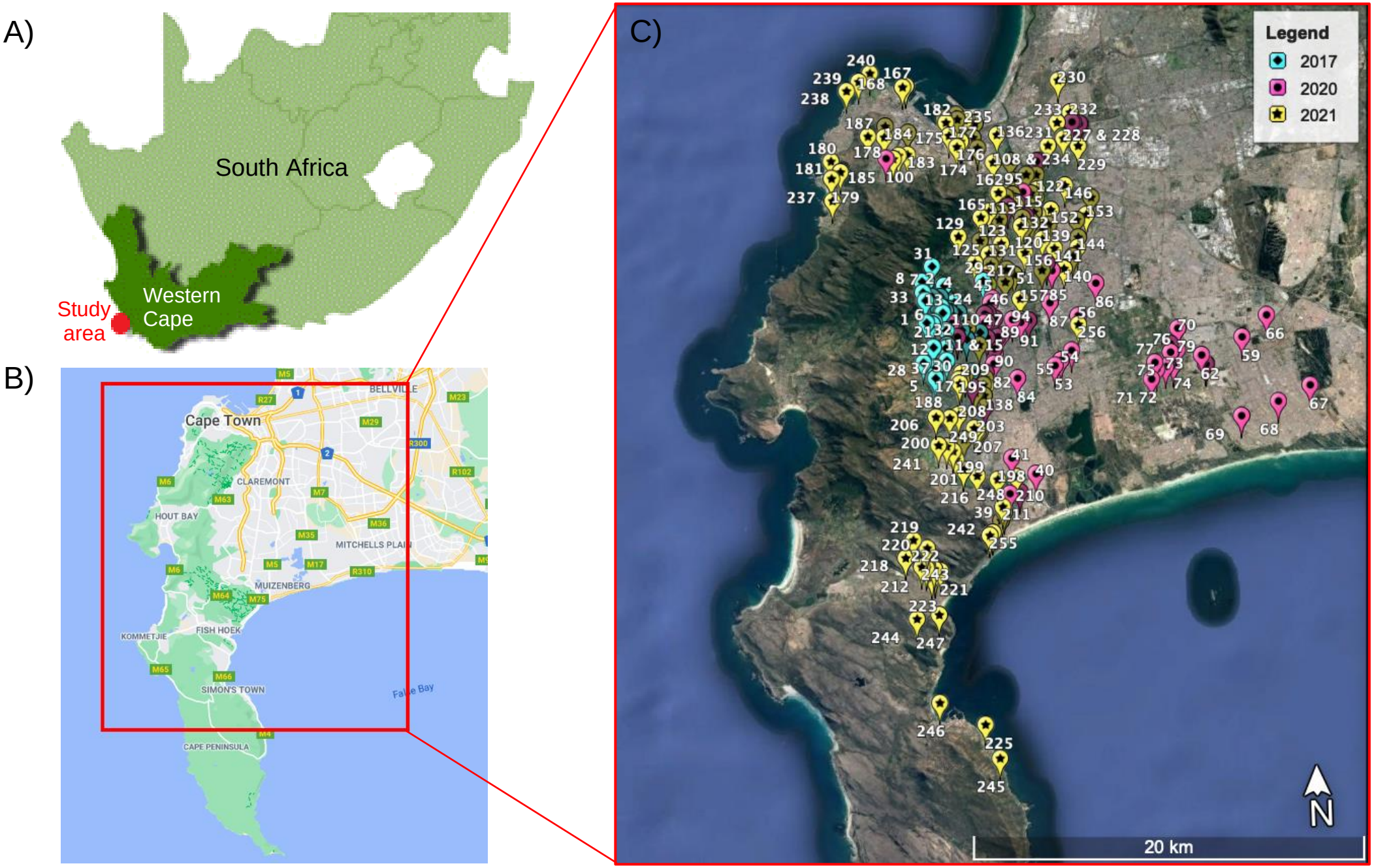

Figure 1.1: The location of the study area in the context of A) South Africa and the Western Cape province, B) greater Cape Town (Google Maps, 2021) and C) the Cape Peninsula (Google Earth Pro, 2019a), showing the collection points of the water samples (where the number refers to the sample number and the colour refers to the year of sample collection).

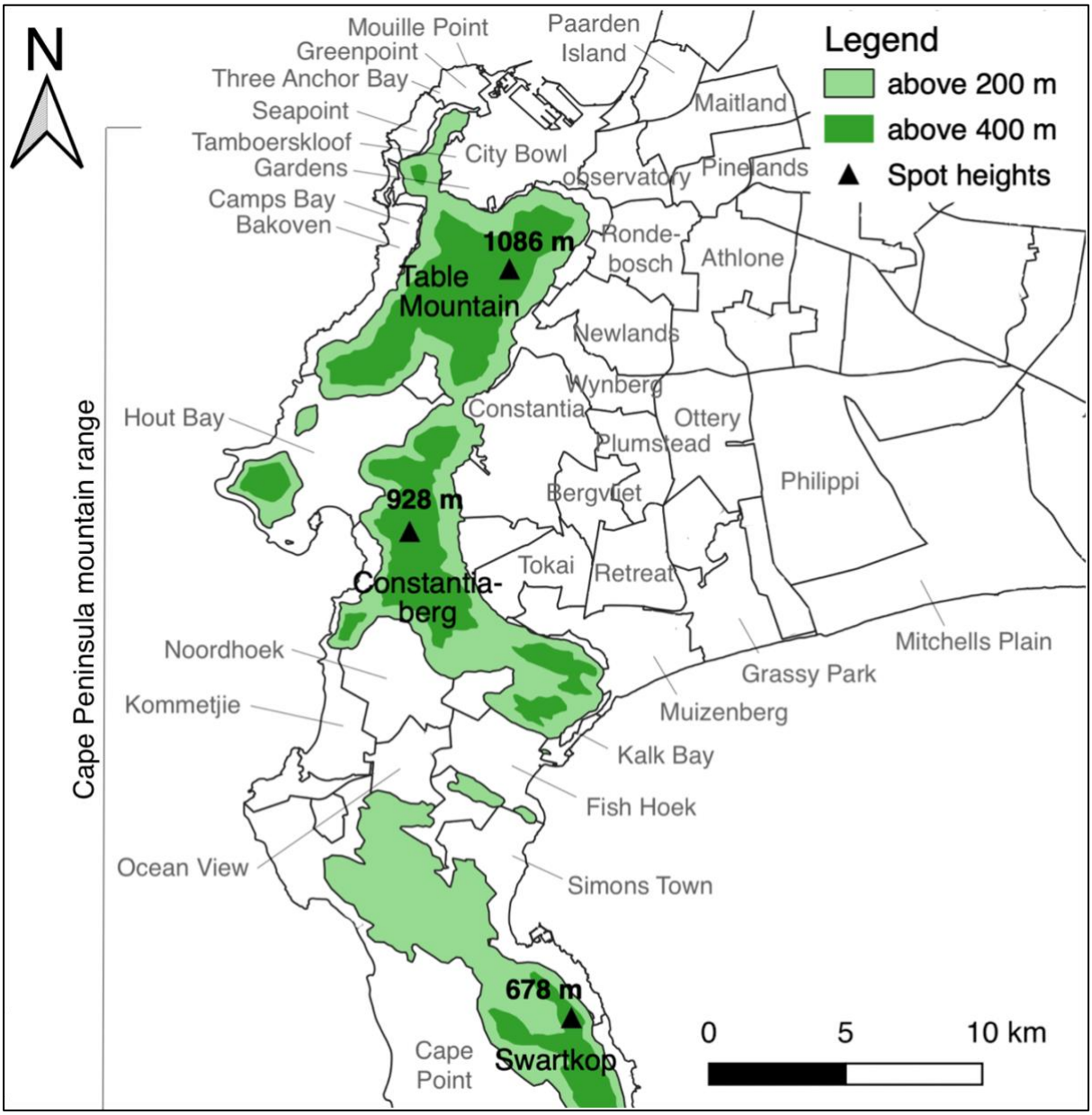

Figure 1.2: The suburbs and the Cape Peninsula mountain range of the study area.

1.2 Historical background

Cape Town has a long history related to the accessibility of freshwater. In pre-colonial times, the Khoisan, whose ancestors inhabited Cape Town hundreds of thousands of years ago nicknamed the area as "the place of sweet-waters" (Deacon and Deacon, 1999; Dippenaar, 2016), and in 1647, it was the availability of freshwater which made the Cape an attractive location for the refreshment outpost for the Dutch to supply ships that travelled the spice route for trade purposes ("Cape Province", 2013). Under Dutch colonial rule, water was primarily supplied from waterways originating from the lower slopes of Table Mountain until water

shortages associated with a growing population and dry summer conditions drove the development of a system of reservoirs and canals. The canals were eventually decommissioned between 1827 and 1850 and closed in 1901 due to waste pollution deteriorating the water quality (Dippenaar, 2016). Up until 1891, Cape Town was mainly supplied with water from the springs located at the foot of Table Mountain, and up until 1921, the city was supplied with water almost exclusively from the Woodhead Dam on top of Table Mountain (CoCT, 2018b). Thereafter, the Steenbras Scheme was set up to augment the supply of water to the CoCT (CoCT, 2018b). Today, water is supplied via the Western Cape Water Supply System from several rivers, reservoirs and dams located in different catchment areas which are connected by extensive pipelines (CoCT, 2018b). There are 5 reservoirs on Table Mountain, which were constructed to store and supply water related to orographic rainfall events ("Cape Province", 2020) and 6 main dams, including the upper and lower Steenbras Dams, the Berg River, Voelvlei, Wemmershoek and the Theewaterskloof Dam, which are located outside of Cape Town. Many of the springs from the lower slopes of Table Mountain are also still in use. For example, the Oranjezicht springs, including the Main spring, located on the northern slopes of Table Mountain, is used to irrigate the Greenpoint Urban Park (Western Cape Government, 2011a). The Newlands and Albion springs, located on the eastern slopes of Table Mountain, are also still utilized today. The Newlands spring continues to supply freshwater to the Newlands commercial Brewery and the Albion spring contributes to the city's bulk water supply (Newlands Brewery, n.d.; CoCT, 2018b). Springs related to the Newlands spring system also supply schools within the vicinity.

1.3 The hydrological cycle

The water cycle details how water is continuously circulated and distributed throughout the hydrosphere. There is a fixed amount of water in continuous flux. Water occurs in the atmosphere in vapour form, condensing to clouds which produce precipitation. As a result, water is introduced to the land and ocean surfaces. On the land surface, water can a) infiltrate into the subsurface, or b) continue to flow on the land surface in the form of run-off. In scenario b) the water will eventually form rivers, which transport water to the ocean. Some water returns to the atmosphere through evaporation. Water that has infiltrated the subsurface is used by plants, which release the water back into the atmosphere through transpiration. The remaining infiltrated water moves as interflow into rivers, springs, and wetlands, or it progresses deeper into the ground, eventually recharging aquifers. Groundwater can also flow and discharge into

rivers. Rivers progress towards the ocean, carrying erosion debris and dissolved salts in the process. Once the rivers reach the ocean, evaporation of seawater results in the production of freshwater rainfall because salts have a low solubility in water vapour.

The depiction of this system is simplistic. Little attention is provided to the changing nature of groundwater storage and movement; the incorporation of the water in rocks, magmas, and rock-forming minerals; as well as the interchange of water between the physical environment and living organisms. Even in this simplistic form, the sensitivity of the water cycle to interference is evident. The acceleration of climate change over the last century has resulted in higher temperatures and altered precipitation patterns globally, and it is expected to continue to increasingly affect the balance and distribution of water (Intergovernmental Panel on Climate Change, 2021). Moreover, development and construction interfere with natural water drainage channels and infiltration. Humans have effectively become part of the water cycle, and it must be analysed as such. For example, the Kingdom of Saudi Arabia is increasingly dependent on groundwater due to the low rates of rainfall (<50 – 100 mm mean annual rainfall) and the lack of surface water sources, as well as the growing demand by the agricultural sector, fuelled by the promotion of investment in farming by the government of the Kingdom of Saudi Arabia over the last 3 decades (Youssef et al., 2020). This growing demand has resulted in the over-exploitation of groundwater sources, which have been classified as non-renewable (rate of abstraction > rate of recharge). Over-exploitation of the groundwater sources has led to the formation of sinkholes in extensive cropland areas with karst bedrock such as the Al Jouf area (Youssef et al., 2020). As the groundwater level decreases, the roof of the underlying cavity loses buoyancy, resulting in subsidence (Youssef et al., 2020). The formation of sinkholes can have major consequences including the destruction of infrastructure and loss of life. Therefore, it is important to understand anthropogenic effects on the water cycle in order to manage groundwater resources effectively to ensure sustainable use.

1.3.1 Surface water bodies

Over 98% of the water used by the CoCT is supplied from surface water bodies (CoCT, 2018b). Surface water is derived from precipitation. It includes rivers, lakes, wetlands, reservoirs etc. There are 4 major drainage basins of the CoCT: the Peninsula, the Eastern Pluton, the Cape Flats, and the Diep River Basins. The rivers in the Peninsula region have

formed steeply incised valleys into the Table Mountain Group (TMG) towards the south, and the Cape Granite Suite and Malmesbury Group towards the north (Dippenaar, 2016). The Eastern Pluton forms a radial drainage pattern, and the Diep River Basin directs the surface water southwards towards the Milnerton Lagoon (Dippenaar, 2016). The Cape Flats drainage occurs over flat sandy deposits. It is mainly controlled by the Diep River and Kuils River paleo-channels (Dippenaar, 2016). There are also numerous wetlands present in the area due to sediment build-up reducing flow rates (Dippenaar, 2016). Wetlands are important ecological features because they prevent floods, they act as filters which improve water quality, and they provide habitats for plants and animals. Vleis are an example of a marsh or floodplain wetland. They are low-lying areas that collect water during the rainy season (Merriam-Webster, n.d.). As previously mentioned, there are several dams and reservoirs that have been constructed on Table Mountain to supply fresh water to the CoCT.

1.3.2 Springs

Springs are an interface between surface and groundwater (e.g., Dippenaar, 2016). They form where the surface topography and the water table intersect e.g., many of the springs on Table Mountain occur where the water table intersects a rock with low permeability (such as shale or mudstone layers) or at geological contacts (e.g., between the TMG sandstone, and the Malmesbury Group or Cape Granite Suite) at the land surface (Dippenaar, 2016). Generally, contact springs produce relatively high yields because they emanate from aquifers that have relatively large storage capacities due to fractures and faults creating a larger volume of space for groundwater (Wu, 2008). There are also other types of springs such as depression springs, springs associated with faults and perched springs. Depression springs occur as a result of weathering and erosion exposing the aquifer to the Earth's surface, whereas springs associated with faults occur when water moves in fractured zones (often from great depths). Perched springs are also present on Table Mountain. They form as a result of interflow i.e., they are not associated with the main water table (Dippenaar, 2016). They generally have fast flow rates and emanate from perched water tables with limited storage capacities in comparison to aquifers that supply contact springs (Wu, 2008). Abstraction of groundwater does not affect perched springs because they are not connected to the regional groundwater flow system (Kotze, 2002). The springs on Table Mountain therefore occur over a range of altitudes and appear to emanate from multiple aquifers rather than from a single aquifer.

1.3.3 Groundwater

Groundwater is water that occurs below the surface of the Earth in the saturated zone (e.g. American Water Works Association, 2014). Potential useable water is stored in aquifers. An aquifer is a body of permeable and porous, or fractured rock, that holds groundwater. Low permeability rocks and sediments are referred to as aquitards, and impermeable rocks and sediments are referred to as aquicludes (e.g. American Water Works Association, 2014). The porosity of the aquifer determines the amount of water that is stored within an aquifer. Primary (intergranular) aquifers refer to aquifers that form at the same time as the geological formation. For example, the intergranular porosity of sand creates an aquifer which forms at the same time as the alluvial material is deposited. Secondary (fractured) aquifers are formed after the formation of the geological unit i.e. the water moves through spaces that are created post-deposition. This type of aquifer occurs in hard rocks that become fractured through deformation. Water mainly flows along the fractures and minor amounts of water is stored in a porous matrix, which is less permeable than the fractures (e.g., American Water Works Association, 2014). Fractured aquifers are generally heterogenous and can vary relatively drastically (up to several orders of magnitude) in permeability, hydraulic conductivity and storativity over short distances (Brown et al., 2003). This is due to anisotropic flow that occurs as a result of preferential flow along fractured zones. The denser and more interconnected the fracture network, the larger the storage capacity of the aquifer. Groundwater flow in secondary aquifers in the South African context is predominantly a function of vertical and sub-vertical fractures related to faults, fault zones and dykes, and horizontal bedding plane fractures associated with the release of tensional forces, zones of weathering or tectonic uplift (Brown et al., 2003).

Aquifers can be further characterised as confined, unconfined, or semi-confined. A confined aquifer is sealed by an overlying, low permeability geological layer known as an aquitard or aquiclude (e.g. American Water Works Association, 2014). The water within the confined aquifer is usually confined at a higher pressure than atmospheric pressure, and has restricted interaction with the surface environment (e.g. American Water Works Association, 2014). In comparison, unconfined aquifers are at atmospheric pressure i.e. they are affected directly by atmospheric processes. The water table is the ‘top’ of the aquifer, where the aquifer is saturated (e.g. American Water Works Association, 2014). Semi-confined aquifers are an

intermediate between confined and unconfined aquifers. They are partially covered by low permeability rock and have slower recharge rates than unconfined aquifers.

Aquifers are recharged by rainfall, run-off or surface water that infiltrates and percolates into the unsaturated zone of the ground until it reaches the saturated zone. Recharge rate refers to the percentage of rainfall that infiltrates into an aquifer. The rate of recharge is dependent on the interaction of a number of factors including the climate, geology, topography, soil, and vegetation cover. For example, high intensity rainfall events recharge aquifers more rapidly than low intensity rainfall events. However, rain splash during very heavy down pours can reduce the infiltration due to a sealing effect (Wu, 2005). The geological structure also plays an important role in aquifer recharge. Faults in competent rocks can provide conduits for fluids to flow along. In addition, the dip of strata can influence the rate of recharge of an aquifer. Escarpment that dips away from the source of recharge at a steeper angle than the slope angle, recharges an aquifer more effectively than escarpment that dips at a shallower angle than the slope angle or escarpment that dips in the other direction (figure 1.3; Wu, 2005). Furthermore, flatter areas allow for greater volumes of recharge than areas with steep slopes because water flows rapidly down slopes i.e. there is less time for percolation and infiltration to occur on a steeper slope (Sophocleous and Buchanan, 2003). The nature of the soil also determines recharge rates (Wu, 2005). Sandy soils are more porous and permeable than clay soils and therefore have higher rates of recharge. Aquifers in sparsely or non-vegetated areas are recharged more rapidly than vegetated areas due to evapotranspiration (Gee and Hillel, 1998). However, in steeply sloped areas, vegetation cover can promote groundwater infiltration by slowing down the movement of the water and allowing it time to seep into the ground (Dippenaar, 2016). The types of vegetation also influence the rates of recharge. Alien vegetation generally requires more water than indigenous plants, which reduces the amount of the water that can infiltrate deep into the ground to recharge an aquifer (Fourie et al., 2002; Department of Water Affairs, 1986, cited in Wu, 2005). Therefore, favourable recharge conditions are created when heavy rainfall is received by non-vegetated, porous sandy soil or permeable bedrock that is fractured and occurs near the surface of the Earth in flat or gently sloping areas (De Vries and Simmers, 2002).

Boreholes and wellpoints are constructed to extract groundwater to provide a continuous supply of water for business or domestic purposes. Wellpoints generally tap into shallow primary aquifers and reach a maximum depth of ~15 m, while boreholes are typically

drilled to depths of >20 m. A wellpoint usually requires a surface-mounted centrifugal pump, whereas a borehole usually requires a submersible pump to draw groundwater to the surface.

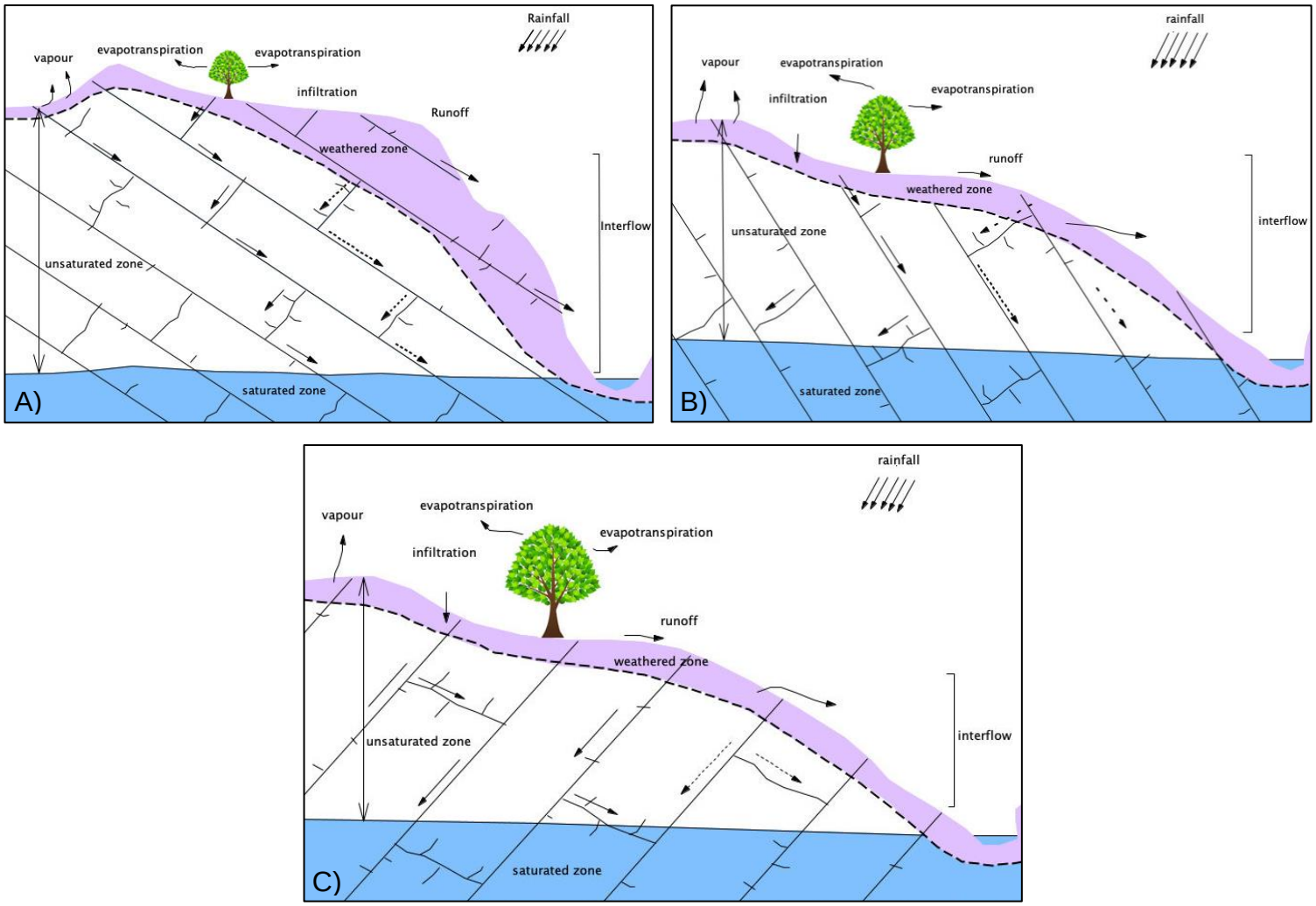

Figure 1.3: The relationship between the recharge rate of an aquifer and inclined escarpment when A) the dip angle is less than the slope angle, B) the dip angle is steeper than the slope angle and C) the dip angle is in the opposite direction to the source of recharge (adapted from Wu, 2005).

1.3.4. Seawater

Seawater intrusion into aquifers has been identified as a concern in coastal regions due to overextraction of groundwater. Saline water exists below the ocean like freshwater exists below the land surface. Saltwater has a marginally higher density than freshwater. Therefore, extensive pumping of groundwater can result in saline groundwater moving upwards (and laterally) and infiltrating into freshwater aquifer systems. This can cause permanent damage

because it is difficult for freshwater to replace the saline water again (Alfarrah and Walraevens, 2018).

1.3.5. Cape Town water quality

Water quality refers to the suitability of the water for a particular use in terms of its biological, chemical, and physical attributes (Western Cape Government [WCG], 2011b). It is measured by multiple parameters including EC and pH. EC is an easy method for measuring the salt content of water in the field (Anderson and Cummings, 1999). Water with an EC of >2.5 mS/cm is not recommended for human consumption and the pH of drinking water typically ranges between 6.5 and 8.5 (Anderson and Cummings, 1999; World Health Organization, 2007). Water quality fluctuates in time and space, and therefore it requires continuous monitoring in order to facilitate effective management (WCG, 2011b). It can be affected by natural influences including the geological and meteorological characteristics of the drainage basin, and human intervention such as the construction of dams and pollution (WCG, 2011b). For example, the natural causes of EC include the dissolution of minerals in soils, rocks, and decomposing plant material (Department of Water and Forestry, 1996), whereas anthropogenic causes include the accumulation of chemicals from fertilizers and pollution due to poor sanitation and waste disposal, the increase in salinity of return flow of extracted groundwater for irrigation due to evaporation, and the ingress of seawater into the aquifer due to over-abstraction (Aza-Gnandji et al., 2013). The accumulation of dissolved particles such as salts can impair the water quality and result in it becoming unusable (United States Geological Survey [USGS], n.d.). Similarly, pH can be affected by several factors such as the geochemistry of the rocks and soils in the catchment area, photosynthesizing plants and respiring organisms (Wu, 2008), and contamination caused by anthropogenic activities associated with industries, agriculture, mining, and urbanization (Ramjukadh et al., 2018).

There are various sources of contamination to the Cape Town water system. This makes it difficult to pinpoint the major sources. Contributors to water pollution include sewage effluent, illegal discharges associated with commercial and industrial activities into stormwater bodies (such as detergents from car washes) and run-off from residential gardens and farms (Day et al., 2020). Poor water quality poses a risk to human health and the integrity of ecosystems. In addition, the cost of managing symptomatic and reactive issues is much greater than preventing it (Day et al., 2020).

1.3.6. The effects of anthropogenic climate change on water quality

Climatic variation results in localised changes in the hydrological cycle. Numerous climate models predict that the Western Cape will experience warmer and more variable precipitation in the future as a result of anthropogenic induced climate change (Midgley et al., 2005). In addition, an increased frequency of extreme weather events such as storms, fires, floods, and droughts are expected for the Western Cape due to climate breakdown (Western Cape Government, 2018). Recently, Cape Town experienced one of its worst droughts on record (Otto et al., 2018). This is expected to be an increasing phenomenon in the future (Otto et al., 2018). The interval between drought periods is decreasing and as a result the likelihood of the occurrence of a prolonged drought has doubled (Otto et al., 2018). Periods of drought have been linked to a reduction in water quality because there is less rainfall available to dilute contaminants (Day et al., 2020). In areas where there is poor service provision, such as informal settlements, high-volumes of rainfall do not dilute pollutants, instead, storms and flooding events mobilise waste that has built up in the streets and drainage channels, and transport it into the water system (Day et al., 2020).

1.4 Isotopes

Isotopes are defined as variations of an element that differ in mass number (e.g. Sharp, 2017). They occupy the same position on the periodic table, but have differing numbers of neutrons (e.g. Sharp, 2017). Due to these differing numbers of neutrons, isotopes of a particular element have slightly different physical properties from one another, resulting in the potential for fractionation (e.g. Sharp, 2017). Fractionation is the process of partitioning isotopes based on relative mass difference (e.g. Sharp, 2017). Molecules made up of light isotopes form weaker intermolecular bonds than molecules made up of heavier isotopes (e.g. Hoefs, 2009). Weaker bonds are easier to break, therefore lighter isotopes generally move through a reaction faster resulting in a shift of the ratio of the heavier isotopes to the lighter isotopes (e.g. Hoefs, 2009). Factors such as temperature and pressure control the degree of fractionation (e.g. Hoefs, 2009). At lower temperatures, greater amounts of fractionation occur. Equilibrium fractionation and kinetic effects are the two predominant mechanisms of fractionation (e.g. Hoefs, 2009). During equilibrium fractionation, isotopes are exchanged (e.g. Hoefs, 2009). For example, under high temperatures, mineral recrystallisation and crystal growth processes frequently approach thermodynamic equilibrium (Sharp, 2017). In contrast, kinetic effects are

one-way effects in which reactions are irreversible (e.g. Sharp, 2019). Evaporation in an open system is an example of a kinetic effect (e.g. Sharp, 2019). Isotopes are classified as either stable or radioactive (e.g. Hoefs, 2009). Stable isotopes do not decay, whereas radioactive isotopes decay and radiogenic isotopes are the product of decay (e.g. Hoefs, 2009).

1.4.1 Stable isotope variation in precipitation

Hydrogen and oxygen isotopes are conservative tracers that provide a means for tracking hydrological processes because they fractionate in predictable ways in the water cycle (e.g. Craig, 1961). The isotopic composition of the ocean is relatively uniform across the globe because it is such a large, well-mixed reservoir (e.g. Craig, 1964). In contrast, the isotopic composition of precipitation is variable (Craig, 1961; Dansgaard, 1964). There are 5 major factors that affect the isotopic composition of precipitation: 1) temperature, 2) altitude, 3) continentality 4) latitude, and 5) amount (Dansgaard, 1964). A colder air mass contains less moisture than a warmer air mass, therefore the isotopic values of precipitation produced from a colder air mass is lower than a warmer air mass due to the loss of heavier isotopes to liquid (e.g. Sharp, 2017). Seasonal effects are linked to temperature - during cooler months, precipitation has lower isotopic values than in warmer months (e.g. Sharp, 2017). Precipitation received at higher altitudes produces lower isotopic values than at lower altitudes because as an air mass rises, it condenses, which results in a preferential rainout of heavier isotopes (e.g. Sharp, 2017). Continentality effects result in precipitation becoming isotopically lighter further from the source due to the air mass experiencing rainout as it progressively moves further away (e.g. Sharp, 2017). Similarly, latitudinal effects result in the isotopic values of rainfall decreasing as the latitude increases as a result of increased rainout as well as decreased temperatures (e.g. Sharp, 2017). An amount effect results in lower isotopic values during periods of heavy precipitation and higher isotopic values during periods of less precipitation because during heavy rainfall events the proportion of lighter isotopes precipitating is higher than during milder conditions (e.g. Sharp, 2017). In addition, during heavier rainfall events, less evaporative enrichment of the raindrops occur as they fall to the ground than during milder conditions (Dansgaard, 1964). The isotopic values of precipitation are also dependent on the reservoir from which the water vapour is evaporated i.e. isotopic values of precipitation differ for different oceanic sources (e.g. Harris et al., 1999).

The positive, linear and interdependent relationship between oxygen and hydrogen isotopes in rain waters around the world is called the global meteoric water line (GMWL) (figure 1.4 of Craig, 1964). Although oxygen and hydrogen behave similarly, hydrogen fractionates to a greater extent than oxygen because the relative mass difference between the hydrogen isotopes is greater than the relative mass difference between the oxygen isotopes (Sharp, 2017). The GMWL therefore has a relatively steep slope with a gradient of 8 and a y-intercept of 10 (figure 1.4 of Craig, 1961). Samples that plot on the GMWL with low delta values are predominantly collected from high latitude, high altitude and inland regions, whereas the samples that plot on the GMWL with high delta values are predominantly collected from areas with tropical climatic conditions (figure 1.4; Sharp, 2017). Samples that do not plot on the GMWL have been influenced by other isotopic processes such as exchange with minerals in rocks, and evaporation. The GMWL ultimately represents the weighted local meteoric water lines (LMWLs) from regions around the globe (Sharp, 2017). A LMWL is derived from precipitation that falls within a local area. They generally have shallower gradients than the GMWL (Gat, 1996). The LMWL of Cape Town has been determined by Harris et al. (2010) as $\delta D = 5.55*\delta^{18}O + 6.11$ using the least squares method (LSM) and $\delta D = 6.41*\delta^{18}O + 8.66$ using the reduced major axis (RMA) method, based on rainfall data collected at UCT from 1996 – 2008. The LSM is a statistical approach commonly used to determine the line of best fit. It is calculated by minimizing the sum of the residuals i.e., the vertical distances between the actual values and the predicted values (Harper, 2014). This method of regression analysis is used to determine the relationship between an independent and dependent variable (Harper, 2014). It assumes that the independent variable has no errors (Harper, 2014). By contrast, the RMA method is used to determine the line of best fit for dependent x and y variables (Harper, 2014). It assumes that there are errors in both variables (Harper, 2014). It is determined by minimizing the sum of both the horizontal and vertical distances (Harper, 2014). It is the preferred method for calculating the LMWL. Deuterium excess (d-excess) is a parameter that is used to measure the vertical displacement from the GMWL due to changes in relative humidity. It is calculated using the equation: d-excess= $\delta D - 8*\delta^{18}O$. It is mainly influenced by kinetic effects related to evaporation (Sharp, 2017). Typical d-excess values range from 0 to +25 (Gat and Carmi, 1970; International Atomic Energy Agency, 1992).

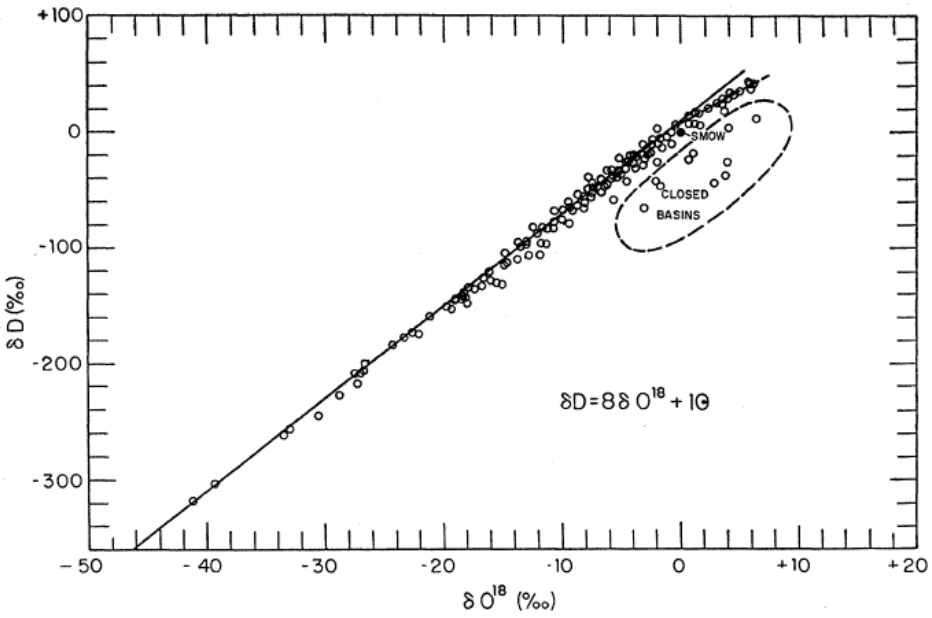

Figure 1.4: Plot of δD vs. δ^{18}O values for the meteoric water world-wide. The GMWL (Craig, 1961) is the line of best fit through the data.

1.4.2 Stable isotope variation in surface water bodies

The oxygen and hydrogen isotope values of surface water bodies should reflect the isotopic composition of run-off and therefore precipitation. Where the isotopic composition of surface water bodies differs substantially from the isotopic composition of the local rainfall, it indicates mixing with other sources of water and/or the influence of transportation processes. Mixing occurs when water with various origins combine together. For example, surface water received in different catchment areas may have distinct oxygen and hydrogen isotope signatures. The isotopic composition of the mixture of the waters should therefore reflect the amount of water contributed by the different sources. Evaporation is an example of a transportation process. During evaporation, the heavier isotopes remain in the residual liquid and the lighter isotopes are removed in the water vapour (Dansgaard, 1964). The higher rate of diffusion for hydrogen in comparison to oxygen results in differing amounts of enrichment in the δD and δ^{18}O values of the residual liquid. This effect results in a local evaporation line (LEL) with a gradient less steep than the LMWL, of between 4 and 7, depending on the temperature and relative humidity (figure 1.5; Bowen et al., 2018). The d-excess value of the residual liquid becomes more negative, while the d-excess value of the vapour becomes more positive. The evaporated signal is reduced by the addition of precipitation. Therefore, areas that experience seasonal rainfall with periods of extended dry conditions with minimal recharge of

surface water bodies, may show evidence of seasonal variation in the isotopic composition of the surface water.

1.4.3 Stable isotope variation in groundwater

Gat and Tzur (1967) report that the stable isotope values of groundwater are usually affected by <1% by surface processes i.e. the stable isotope composition of groundwater is relatively unaffected by seasonality and other short-term fluctuations in climatic conditions (figure 1.5). Studying the stable isotope composition of groundwater is therefore very useful for tracing and quantifying the contribution of different water masses with distinct origins and identifying the encroachment of extraneous water sources such as seawater. The isotopic composition of groundwater can be compared to the local rainfall, surface water bodies, surface run-off, spring water and other sources to determine its source(s) of recharge. For example, groundwater, recharged by precipitation infiltrating directly into the aquifer through sand, produces a different isotopic signature to groundwater recharged by surface run-off infiltrating into crystalline or limestone aquifer pockets (Gat, 1996). The difference in the isotopic signatures of these groundwaters occurs because they are recharged by different sources of water and they are not influenced by atmospheric processes (such as evaporation) to the same extent i.e., groundwater in the crystalline or limestone confined aquifer is less affected by the atmosphere than groundwater in the unconfined sandy aquifer.

Other information such as the rate of recharge and the altitude of recharge of an aquifer can also be determined by analysing the stable isotope composition of groundwater. Recharge rates can be estimated by comparing the groundwater to the local precipitation. Unconfined aquifers with rapid recharge rates have isotopic values that are very similar to the local precipitation i.e. they plot on the GMWL (figure 1.5). If they have very different isotopic values to the recent precipitation this could indicate that the aquifer is confined and contains ancient waters (figure 1.5). The isotopic composition of the ancient waters may indicate paleo-climatic conditions (Gat, 1996). The springs at the foot of Table Mountain are thought to be recharged by ~50% in <3 years. This is based on the findings of Harris et al. (2010) who determined the d-excess value was significantly lower (~6) for the years of 2005 and 2006 in comparison to the rest of the rainfall dataset from 1996 – 2008 which typically had annual d-excess values of ~16. This difference in isotopic composition of the rainfall is reflected by the springs and was used to determine the approximate recharge rate. Isotopic data can also track the mean altitude

of recharge, since recharge at higher altitudes results in more negative isotopic values and recharge at lower altitudes results in less negative isotopic values. For instance, the Main spring has lower δD and δ^{18}O values and is situated at a higher average altitude of recharge than the Albion spring, which has higher δD and δ^{18}O values and is located at a lower altitude of recharge, at the foot of Table Mountain on the eastern slopes (Harris, 2017).

Stable isotopes can also be used to investigate anthropogenic influences on the groundwater system. For example, February et al. (2004) hypothesizes that over-abstraction of groundwater from the TMG Aquifer poses a major threat to certain endemic species of fynbos vegetation in the Western Cape. This is a cause for concern because many boreholes have been drilled in recent years in response to the 2015 - 2017 drought. Stable isotopes can also be helpful for identifying water losses from leaking water mains. Surface water bodies have a distinct isotopic signature to groundwater. Groundwater generally has an isotopic composition that represents the long-term average of the weighted mean precipitation (West et al., 2014). In comparison, surface water usually has a composition that is similar to the local precipitation but often is enriched due to the effects of evaporation (West et al., 2014). Analysis of the stable isotope composition of groundwater by Harvey and Silbray (2001) revealed that leaking canals constructed for irrigation purposes in the cropland of Nebraska recharged a shallow alluvial aquifer and a deeper underlying aquifer in the area. They stated that sealing of the canals would have a large impact on a nearby wetland that relies on this water source in the summer months (Harvey and Silbray, 2001). Similarly to this study, leaking water mains can be identified through the analysis of the stable isotopes.

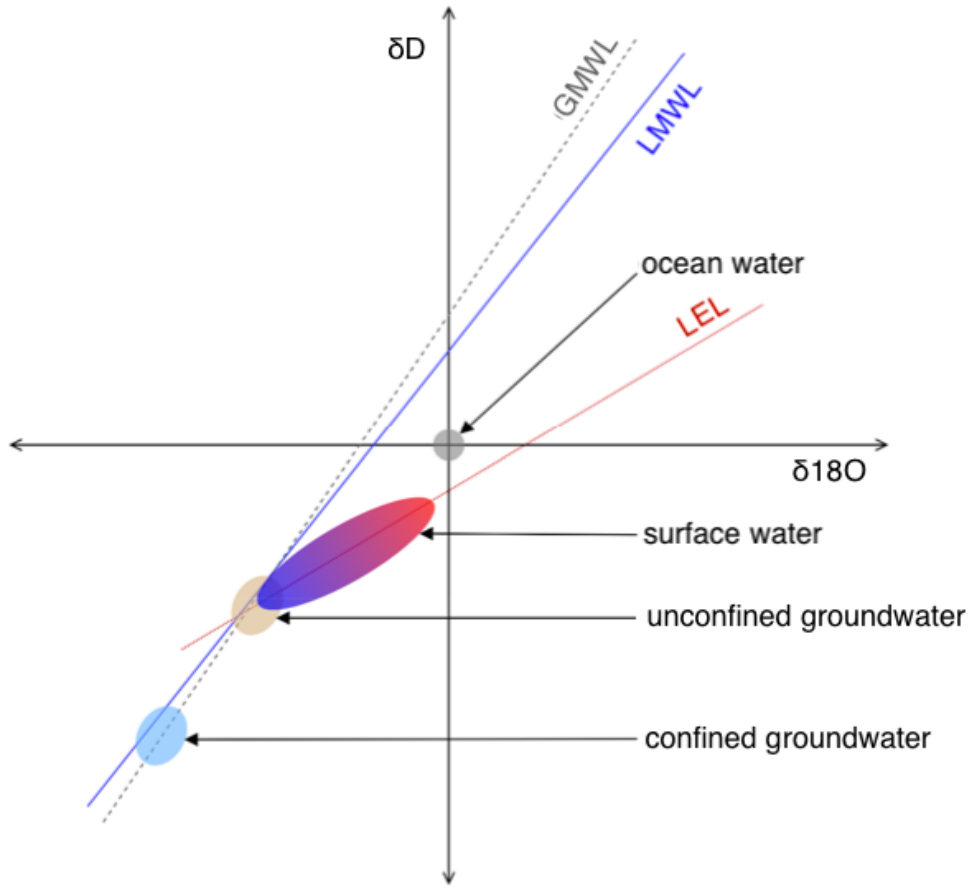

Figure 1.5: δD vs. δ^{18}O values of hypothetical surface water, confined and unconfined groundwater bodies in comparison to the GMWL, LMWL and the local evaporation line (LEL) (de Wet et al., 2020).

1.4.4 Radiogenic isotopes in the hydrological cycle

On Earth, there are two sources of strontium: 1) primordial strontium formed from nucleosynthesis during Earth's formation, and 2) the daughter product formed from the decay of rubidium (^{87}Rb). Radiogenic strontium (^{87}Sr) is the daughter product that forms from the decay of ^{87}Rb, whereas ^{86}Sr is non-radiogenic. The half-life of the decay of ^{87}Rb to ^{87}Sr is 47.2 x 10^9 years (McMullen et al., 1966). Water inherits the ^{87}Sr/^{86}Sr ratio of the rock with which it interacts through chemical reactions such as mineral dissolution and ion exchange. The strontium concentration and isotope ratio can be different for different rocks types (Sharp, 2017). Therefore, mixing of water bodies that have interacted with different rock types can greatly affect the isotope ratio of the water (Sharp, 2017). Rocks containing calcium (Ca^{2+}) are likely to have higher concentrations of strontium because Ca^{2+} in minerals such as plagioclase feldspar, gypsum, dolomite, and calcite is often substituted for by Sr^{2+}. Radiogenic strontium (^{87}Sr) in nature is gradually increasing as a function of the decay of ^{87}Rb. Therefore, older rocks with high Rb concentrations have higher ^{87}Sr/^{86}Sr than younger rocks with low Rb

concentrations. This results in the $^{87}Sr/^{86}Sr$ ratio of water varying as a function of age and concentration of Rb in the source rock with which it interacts (e.g. Weaver at al. 1999).

The $^{87}Sr/^{86}Sr$ ratio is used to investigate groundwater because it is a good tracer for the source rocks of the chemical constituents in water for a number of reasons: it is soluble in water, it occurs in a wide variety of rocks and it varies considerably in minerals (McNutt, 2000). The $^{87}Sr/^{86}Sr$ can be used to identify the movement of water in the groundwater system and allow us to determine if there is connectivity between aquifers. The $^{87}Sr/^{86}Sr$ can also be used in addition to EC to determine if there is interaction of groundwater with seawater or anthropogenic inputs (e.g. Jørgensen et al. 2008). Strontium isotopes are therefore used in conjunction to stable isotopes in this study to characterise the types of water in the aquifers across Cape Town.

The modern ocean has a relatively constant strontium isotope ratio of 0.7092 because it a well-mixed reservoir. The strontium isotope ratio of the modern ocean is derived from a combination of a component with high $^{87}Sr/^{86}Sr$, sourced from continental weathering with a strontium isotope ratio of ~0.7120, and a component with low $^{87}Sr/^{86}Sr$, sourced from hydrothermal alteration of the oceanic crustal material with a strontium isotope ratio of 0.7035 (Halverson et al., 2007). The seawater strontium isotope ratio has varied slightly in the past, between a value of ~0.7070 and 0.7092, since the Precambrian due to varying amounts of ^{87}Sr-enriched continental and ^{87}Sr-depleted mantle inputs (figure 1.6; Halverson et al., 2007; Kharaka and Hanor, 2014).

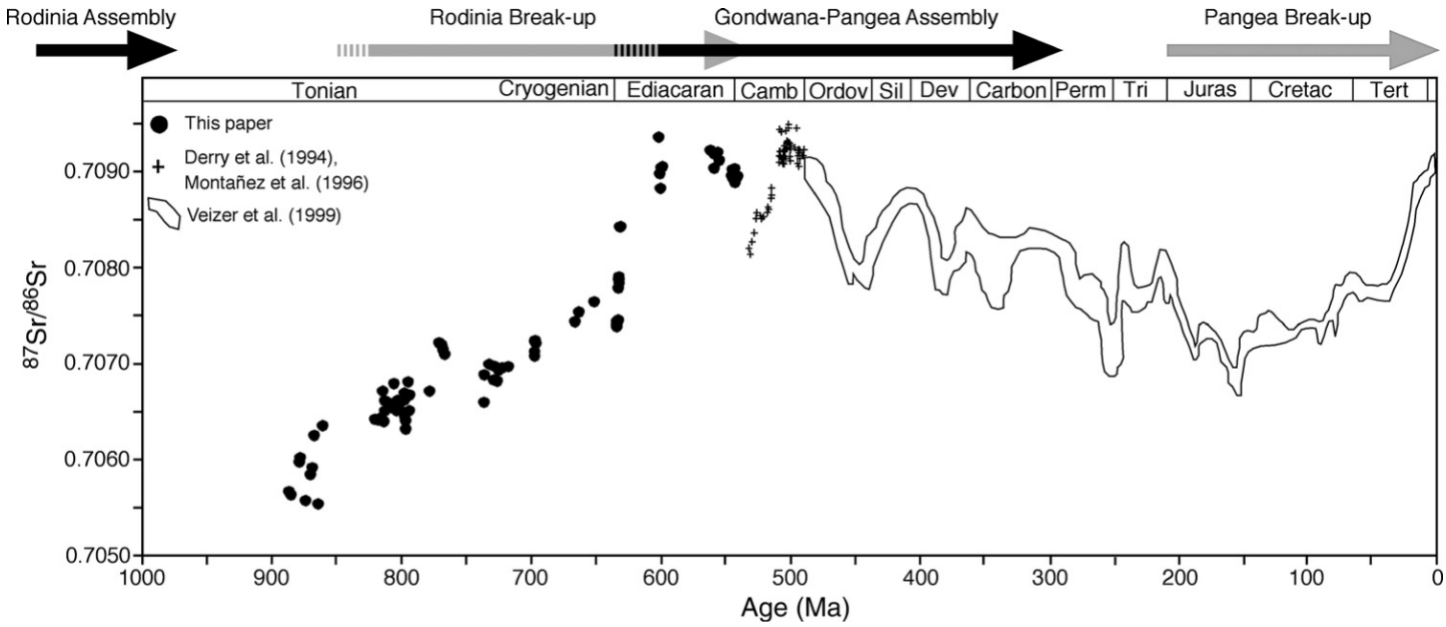

Figure 1.6: Variation of $^{87}Sr/^{86}Sr$ in seawater over the last 1000 Ma (Halverson et al., 2007).

The cause of the high salinity of groundwater from Struisbaai, located approximately 200 km southeast of Cape Town in the Overberg District of the Western Cape, has been investigated by Weaver et al. (1999) using strontium isotopes. The low strontium isotope ratio ($\bar{x}$ $^{86}Sr/^{87}Sr$= 0.7092) of the groundwater suggests that strontium is not sourced from the TMG quartzites or the Bokkeveld Shales (that have relatively high strontium ratios of 0.713 and 0.718, respectively) which are present in the area (Weaver et al., 1999). However, it is important to note that Weaver et al. (1999) states that the very low concentration of strontium in the TMG quartzites of <0.05 indicates that the strontium isotope ratio in the TMG quartzites may not be representative. Weaver et al. (1999), therefore, attributed the high salinity of the Struisbaai Aquifer to either: 1) seawater ingress, 2) sea spray, or 3) interaction with the underlying marine sediments. Weaver et al. (1999) states that the Struisbaai Aquifer is most likely recharged by rainfall which interacts with and dissolves material from the Bredasdorp Formation, which contains Neogene and Quaternary marine sediments such as dunes and beach deposits with large proportions of calcarenites, shells and aeolianites. These marine-derived sediments of the Bredasdorp Formation have an identical $^{87}Sr/^{86}Sr$ ratio to seawater because they have inherited their $^{87}Sr/^{86}Sr$ ratio from the shell deposits within the formation. Shells have the same strontium isotope composition as the ocean during the time of their formation. Another study, performed by van Gend et al. (2020), used $^{87}Sr/^{86}Sr$ data in addition to δD, $\delta^{18}O$ and hydrochemistry data to determine the source of salinity of groundwater from the Buffels River catchment in the

semi-arid to arid region of Namaqualand, South Africa. The δD and $\delta^{18}O$ of the groundwater revealed that its salinity was not caused by evaporation. Instead, the $^{87}Sr/^{86}Sr$ ratios along with major geochemistry of the groundwater, revealed that the salinization of the aquifer is related to the deposition of marine aerosols on vegetation and soils during evaporation, which is dissolved by rainfall that recharges the aquifer, as well as ion-exchange reactions that occur in the soil along the flow path of the rainfall infiltrating into the ground. Rainfall can also transport marine aerosols more directly to the aquifer by flushing it out of the atmosphere (van Gend et al., 2020).

1.4.5 Isoscapes

An isoscape is defined as a geographical map of predicted isotopic compositions across a landscape based on the interpolation of data or the development of process-level models that use isotope fractionation to understand and visualise isotope value predictions across space (West et al., 2008; Bowen, 2010). Isoscapes have broad applications in numerous fields including hydrology, geology, ecology, anthropology, forensics etc.

West et al. (2014) produced the first groundwater and tap water isoscape for South Africa. Tap water from extensive regions across the study area was found to have similar δD and $\delta^{18}O$ values to groundwater. This indicated that the tap water was either sourced from groundwater or that both groundwater and tap water had isotopic compositions that reflected the weighted mean annual δD and $\delta^{18}O$ values of the precipitation (West et al., 2014). In other regions the tap water and groundwater isotopic compositions differed. This was attributed to 1) the influence of evapoconcentration on tap water that is transported or stored at the Earth's surface or 2) tap water reflecting the isotopic composition of recent rainfall while the groundwater reflects the long-term weighted mean annual isotopic signature i.e. the groundwater is not as directly affected by recent precipitation events as tap water in some areas (West et al., 2014).

Additionally, an isoscape of bio-available $^{87}Sr/^{86}Sr$ has been produced by Copeland et al. (2016) for the Greater Cape Floristic Region (GCFR) which is located along the southern coast of South Africa. Bio-available strontium refers to strontium that is absorbed by plants which is in turn inherited by animals who consume the plants. Bio-available strontium can differ from the average $^{87}Sr/^{86}Sr$ ratios of bedrocks due to chemical weathering releasing

strontium at different rates from minerals which have different $^{87}Sr/^{86}Sr$ ratios. The construction of the isoscape was done by determining the bio-available $^{87}Sr/^{86}Sr$ ratios of plants (including shrubs, grasses, forbs etc.) from 171 localities within the GCFR (Copeland et al. 2016). Through the development of a robust isoscape, the pattern of fossil ungulate movements during the Middle and Late Pleistocene could be determined (Copeland et al. 2016).

1.5 Project aims

The aims of this project are, therefore, to:

(i) Collect new data and compile with existing water data from across Cape Town

(ii) Measure the EC and pH of each of the new water samples

(iii) Measure the O- and H- isotope composition of the new water samples

(iv) Measure the Sr- isotope composition of a subset of the new water samples for exploratory purposes in order to investigate if Sr isotopes are likely to be useful in this context for gaining additional information on the flow path of the groundwater

(v) Construct a map of the distribution and isotopic composition of the new and existing water samples

(vi) Construct similar maps for EC and pH

(vii) Explain any variations in EC, pH, δD, $\delta^{18}O$ and $^{86}Sr/^{87}Sr$

(viii) Construct an isoscape of the new and existing data

(ix) Explain any patterns in the isoscape

Chapter 2: Site description

2.1 Climate

The study area experiences a Mediterranean-type climate with cool, wet winters and warm, dry summers. Cape Town's temperature ranges from an average of 13℃ in winter to an average of 21℃ in summer (International Atomic Energy Agency and World Meteorological Organization, 2006). The variation in temperature across the study area is minor as a result of the moderating effect of the ocean surrounding the narrow landmass of the Cape Peninsula (Cowling et al., 1995). The area is influenced by both the cold Benguela current on the west coast and the warm Agulhas current on the east coast. In winter, north-westerly winds dominate, whereas in summer, southerly and south-easterly winds, commonly known as the "Cape Doctor", prevail (South African National Parks, 2021). Wind speeds often exceed gale force (Cowling et al., 1995). Cape Town rainfall varies by location. The mean precipitation received annually is ~600 mm/yr (Harris et al., 1999). Localised microclimates are created by topographical and geographical features. The Cape Town International Airport, situated in the Cape Flats, receives an average of as low as 500 mm/yr of rainfall (figure 2.1; Cowling et al., 1995). In comparison, the University of Cape Town, situated on the slopes of Table Mountain, receives up to 2000 mm/yr of rainfall on average due to the influence of orographic rainfall (figure 2.1; Harris et al., 1999). Fog also provides a significant amount of moisture to the CoCT throughout the year, with the highest frequency of fog events occurring in winter (van Schalkwyk and Dyson, 2013). Advection fog is common and is related to the cold Benguela current on the west coast (van Schalkwyk and Dyson, 2013). It is often blown inland from a north-westly direction (van Schalkwyk and Dyson, 2013). Annual evaporation rates exceed the rates of precipitation by almost twice the amount (Department of Water Affairs and Forestry [DWAF], 2008). The Western Cape is therefore classified as a water stressed region (City of Cape Town [CoCT], 2018b).

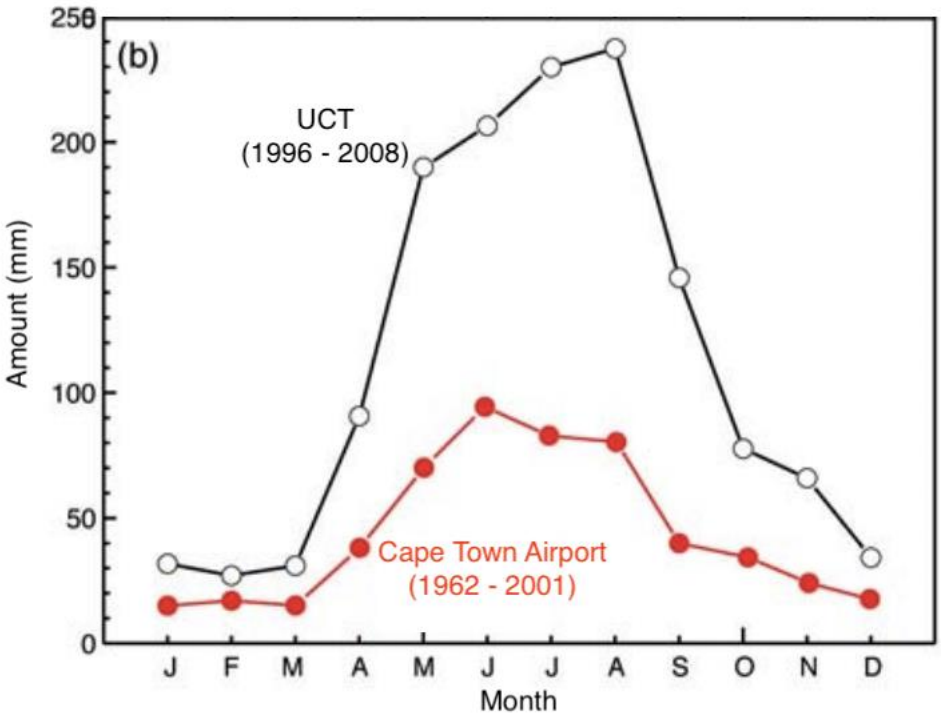

Figure 2.1: The mean monthly amount of rainfall received by UCT (1996 – 2008) and the Cape Town International Airport (1962 – 2001) (Harris et al., 1999).

2.2 Vegetation

The study area is located in the southern extent of the Cape Floristic Region biodiversity hotspot, which is dominated by fynbos species that typically grow in nutrient-poor soils on calcareous and leached quartzite rocks (Cowling et al., 1995). Renosterveld, which predominantly consists of shrubs and grasses, is found on fertile soils derived from shales in relatively low-lying areas, and has largely been replaced by agricultural crops or housing (figure 2.2; Cowling et al., 1995).

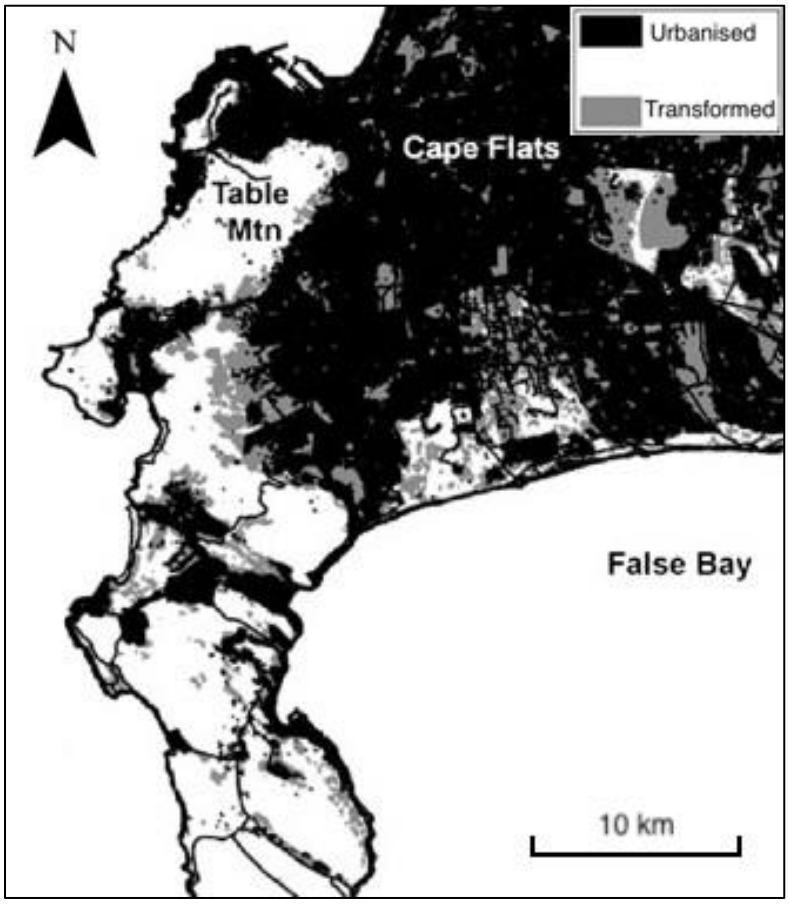

Figure 2.2: The extent of urbanization and transformation of the study area by afforestation, alien invasion and agriculture (adapted from Rebelo et al., 2011).

2.3 Geology and sediment deposits

The major rock types of the greater Cape Town area are the Malmesbury Group, intruded by the Peninsula Granite, both of which are unconformably overlain by the TMG, and covered in places by Quaternary deposits (Tankard and Rogers, 1978). Several Cretaceous normal faults and dolerite dykes also cut across the study area orientated in a predominantly NW-SE direction (figure 2.3; Council of Geoscience [CGS], 1990). On the slopes of the Cape Peninsula mountain range the Malmesbury Group, Cape Granite Suite, TMG and mountain scree deposits are present. In the Cape Flats, the TMG is absent and the Quaternary deposits unconformably overlie the Malmesbury Group and the Cape Granite (figure 2.3; CGS, 1990).

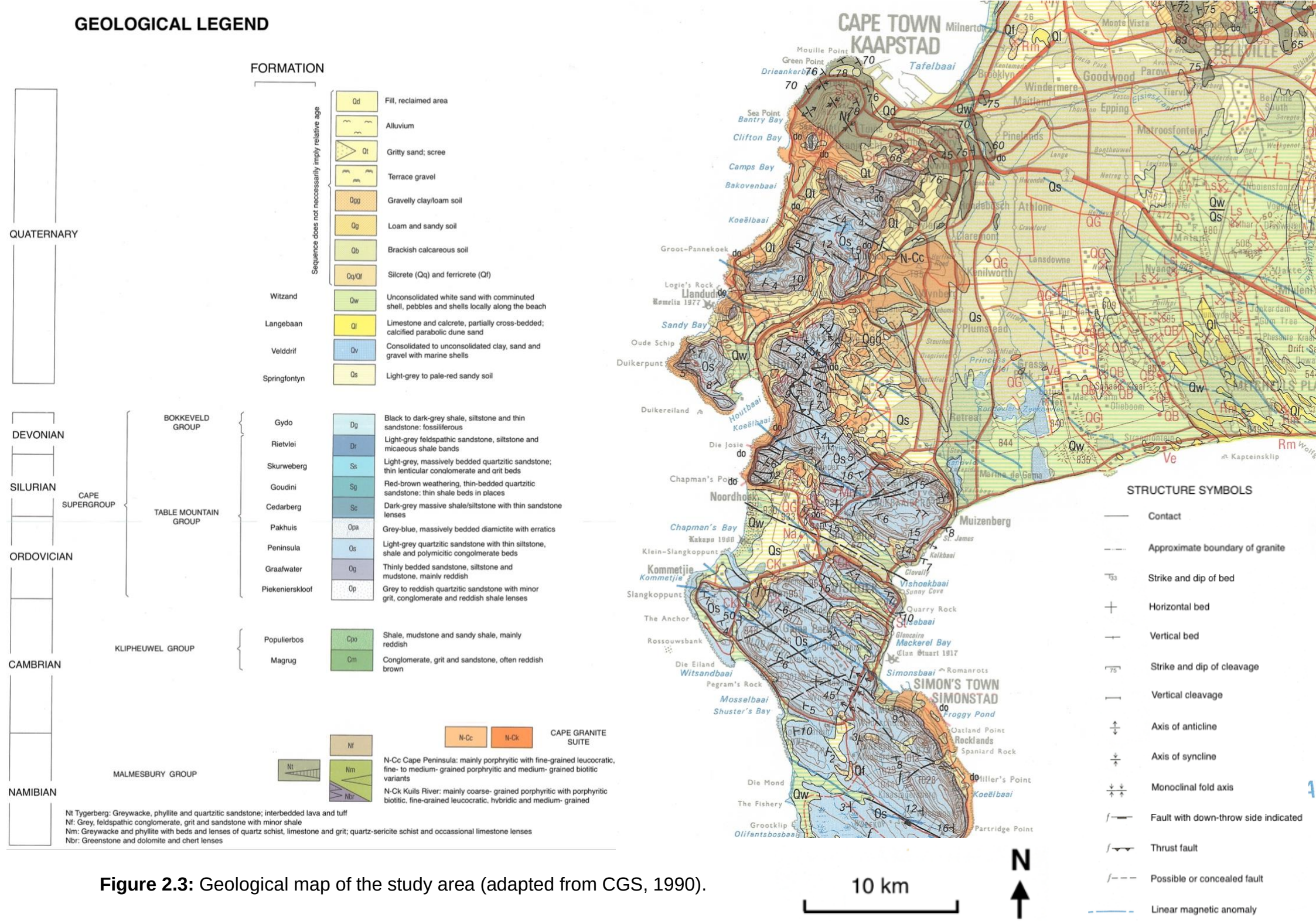

Figure 2.3: Geological map of the study area (adapted from CGS, 1990).

2.3.1 Malmesbury Group

The Malmesbury Group was deposited in the Neoproterozoic. It is separated into three techno-stratigraphic terranes by NW trending faults: 1) the southwestern Tygerberg, 2) the central Swartland and the 3) northeastern Boland terranes by Hartnady et al. (1974, cited in Rozendaal et al., 1999). The Tygerberg and Swartland terranes are divided by the Colenso fault, and the Swartland and Boland terranes are divided by the Piketberg-Wellington fault system (Rozendaal et al., 1999). The Tygerberg terrane is present within the study area. It is a thick turbidite succession that formed on a continental margin in the early Adamaster Ocean in response to the break-up of Rodinia ~780-750 Ma (Rozendaal et al., 1999). The metasedimentary sequence is composed of rhythmic alterations of immature quartzite, phyllitic shales, siltstone, and fine-grained greywacke with some sporadic, thin beds of conglomerate and impure limestone (Rozendaal et al., 1999; Dippenaar, 2016). The sequence has been metamorphosed to low-grade greenschist facies conditions and folded tightly in the NW direction by multiple deformation events, resulting in the strike of the beds being orientated at ~90° (Rozendaal et al., 1999). The thickness of the Tygerberg Formation is poorly constrained, however it is expected to be on the order of 10s of km in thickness. It is exposed in the north and northeast of the study area for ~3 km along the coastline between the City Bowl and Seapoint and along the lower slopes of Table Mountain, due to erosion of the overlying TMG (Gresse et al., 2006). Cross-bedding, ripple cross-lamination, ripple marks, graded bedding and slumping sedimentary structures are displayed within this exposure (Von Veh, 1982).

2.3.2 Cape Peninsula batholith

The Cape Granite Suite intruded into the Malmesbury Group ~555 – 515 Ma as a result of the Saldanian Orogeny during the assembly of Gondwana (Scheepers and Schoch, 2006). There are 3 groups of plutons of the Cape Granite Suite in the Cape: the northern group, the eastern group and the southwestern group (Scheepers and Schoch, 2006). The Peninsula Granite is 1 of 6 major batholiths that form part of the southwestern group (Scheepers and Schoch, 2006). It is located furthest southwest and it lies beneath the Cape Peninsula mountains (Theron, 1984). The Cape Peninsula granitoids of the Tygerberg terrane formed syn- and post-tectonic activity and have S-type chemical compositions (Harris and Vogeli, 2010). S-type granites are generally metaluminous to slightly peraluminous in composition and they often contain sedimentary enclaves (Scheepers, 1995). The Cape Peninsula Granite is a coarse-grained, porphyritic rock that is made up of quartz, feldspar, and biotite. It is exposed as

rounded boulders through uplift and erosion. The Seapoint migmatite zone is a famous exposure of the contact between the Peninsula granite and the hornfels of the Malmesbury Group (Scheepers and Schoch, 2006).

2.3.3 Table Mountain Group (TMG)

The TMG is the lowermost group of the Cape Supergroup. It is a vast deposit that extends across the Western Cape and into the Northern Cape and Eastern Cape provinces. It was deposited approximately 500 – 440 Ma ago in a passive margin basin (Thamm and Johnson, 2006). In the study area the Graafwater Formation forms the base of the TMG. It consists of stacked cycles of interlayered mudstones, maroon siltstones, and sandstones (de Beer, 2002). The fine-grained mudstone increases in proportion upwards towards the top of each cyclical unit (Compton, 2004). It is approximately 70 m thick (Compton, 2004). It is overlain by the Peninsula Formation, which is made up of well-sorted, thickly bedded quartzitic sandstone and thin beds of pebbly sandstone (de Beer, 2002). It is approximately 550 m thick on Table Mountain and it occurs up to a thickness of 1800 m elsewhere in the Cape Fold Belt (Compton, 2004). The sharp depositional contact between the Graafwater Formation and the Peninsula Formation signifies a change in the depositional environment (de Beer, 2002). There are two interpretations to explain this shift in the depositional environment: 1) the formations are coastal deposits that have experienced transgression or 2) the formations are river deposits that have experienced regression (Compton, 2004). In the first interpretation, the Graafwater Formation is thought to be deposited on a tidal mud flat or in a quiet estuary, and the Peninsula Formation is thought to be a beach deposit (Compton, 2004). The challenging interpretation suggests that the Graafwater Formation was deposited in a floodplain setting with meandering rivers, and the Peninsula Formation was deposited in a braided river system (Compton, 2004). The Pakhuis Formation occurs above the Peninsula Formation on the highest points of Table Mountain, for example at Maclears Beacon (Compton, 2004). It contains lithified clusters of angular pebbles and boulders formed due to glacial outwash when South Africa was situated close to the South Pole ~440 - 420 Ma ago (Compton, 2004). The Cedarberg Formation and the Nardouw Subgroup are absent in the study area because they have been eroded away (figure 2.4). The TMG forms an angular unconformity with the underlying Malmesbury Group and a nonconformity with the Cape Granite Suite (figure 2.5). It has experienced two major events of deformation: 1) the Cape Orogeny (~250 Ma) and 2) the break-up of Gondwana (Brown et al., 2003). Burial of the TMG during the Cape Orogeny metamorphosed the TMG to lower greenschist facies conditions (Frimmel et al., 2001).

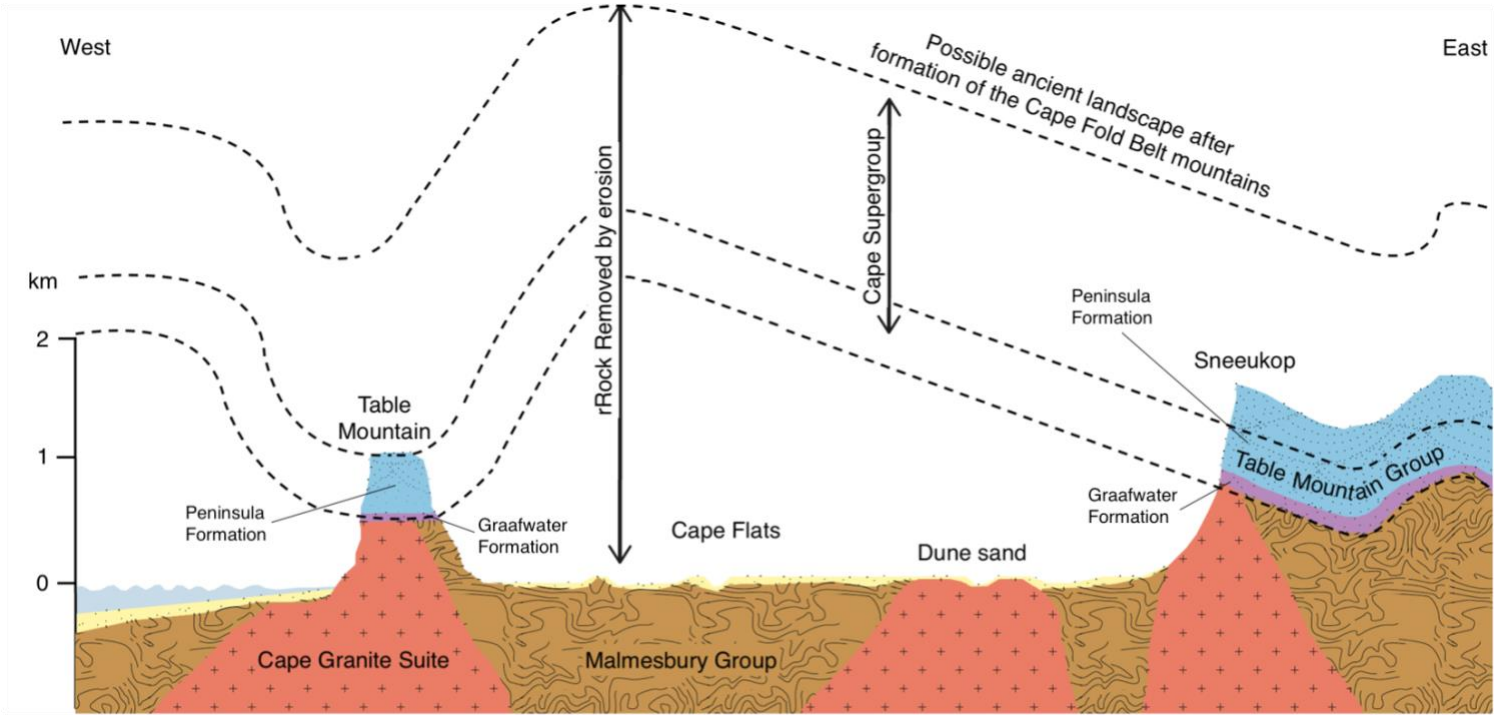

Figure 2.4: E-W geological cross-section through the Cape Peninsula, Cape Flats, and Hottentots-Holland Mountains (adapted from Compton, 2004). Vertical exaggeration= 30. Scree deposits are omitted for clarity.

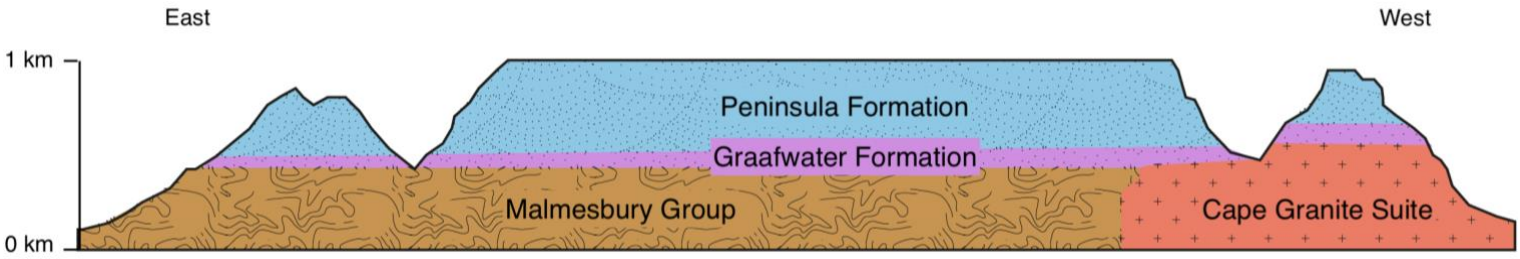

Figure 2.5: The geological formations of Table Mountain, Devil's Peak and Lion's Head (adapted from University of Cape Town. Geological Department, 2021).

2.3.4 Dolerite dykes

The dolerite dykes intrude the basements rocks and TMG in the study area. Their emplacement is related to the fragmentation of Gondwana and the opening of the South Atlantic Ocean which occurred ~132 Ma (Reid et al., 1991).

2.3.5 Quaternary deposits

The Quaternary deposits in the study area consist of the mountain scree and the Sandveld Group. The mountain scree is comprised of soil and weathered material derived from the Malmesbury Group, Cape Granite Suite and Graafwater Formation as well as boulders from the Peninsula Formation (Diamond and Harris, 2019). It covers the lower slopes of the Cape Peninsula mountains (Diamond and Harris, 2019). The scree is thought to have formed under cooler and wetter conditions of the Pleistocene Epoch based on a study conducted on the scree slopes of the Hex River Mountains, which form part of the Cape Fold Belt (Boelhouwers, 1993). It is relatively inactive and stable today due to the growth of vegetation (Diamond and Harris, 2019).

The Sandveld Group consists of marine, fluvial and aeolian sands derived from beaches, and the erosion of the Malmesbury Group and the TMG (Botha, 2006). They form a thin, lens-shaped deposit that lies parallel to the continental margin. It is up to 50 m thick over the Cape Flats (Wigley, 2004). The Sandveld Group was deposited on a passive continental margin that formed in response to the split of South America and Africa, during the breakup of Gondwana, in the Early Cretaceous (Wigley, 2004). It is present from False Bay to Elands Bay (GCS, 1990). During the Pliocene and Pleistocene, sea-levels fluctuated from 25 m above, and 120 m below, modern-day mean sea level due to glacial-interglacial cycles (Compton, 2004). Sand and shell deposits accumulated during periods of transgression associated with warmer temperatures and sea-level rise, and calcrete-cemented sands were deposited during periods of regression associated with cooler temperatures and a drop in sea level (Compton, 2004).

The formations within the Sandveld Group that occur in the study area include the Elandsfontyn, Varswater, Langebaan, Velddrif, Springfontyn and Witzand Formations. The Elandsfontyn Formation is the basal formation of the Sandveld Group. It contains several upward-fining sequences of angular, finely to coarsely grained sands, gravel, and peat clays (Roberts et al., 2008). It was likely deposited in a coastal plain depositional environment with a meandering river system under subtropical palaeo-climatic conditions (Roberts et al., 2008). The Varswater Formation is a marine deposit that consists of phosphoritised clayey sands, fine to medium grained sands and gravel (Roberts et al., 2008). Lenticular lignite bodies also occur intermittently, which suggests a lagoon and coastal plain depositional environment (Roberts et al., 2008). The overlying Langebaan Formation is made up of very fine to medium-grained, well-sorted aeolian sand (Wigley, 2004). It contains numerous fossils including the

Trigonephrus globulus dune species as well as other terrestrial snails, and several vertebrates (mainly mammals) such as antelope and rodents (Wigley, 2004). The Velddrif Formation is a littoral limestone deposit (Wigley, 2004). The Diepriver member contains fluvial gravel, littoral sand, and marine clay (Wigley, 2004). These characteristics suggest that it was deposited in an estuarine/lagoon depositional environment (Roberts et al., 2008). The Springfontyn Formation is an aeolian deposit that is characterized by fine to medium grained, well-sorted quartzose with sporadic peat layers (Wigley, 2004). The Witzand Formation was deposited in the Holocene. It is the youngest subdivision of the Sandveld (Browning and Roberts, 2015) and it consists of unconsolidated to semi-consolidated calcareous aeolian bioclastic-siliciclastic sands which are fine to coarsely grained and moderately to well sorted (Browning and Roberts, 2015). The deposit is whiteish to slightly reddish. Low angle laminations and northward, steeply dipping cross beds are present (Browning and Roberts, 2015). The snail, *Trigonephrus globulus,* is abundant, and rhizoids and insect burrows occur within semi-consolidated sands (Browning and Roberts, 2015).

2.3.6 Ferricrete

"Koffieklip" is a hard near-surface ferricrete layer that forms due to reduced groundwater, rich in dissolved iron, interacting with oxygenated surface waters or the atmosphere (Cole, 2011). In the study area, the iron is sourced from the Malmesbury Group and precipitates as iron oxide minerals that are cemented together (Cole, 2011). These layers have not been dated but they are presumed to represent the palaeo- water table.

2.4 Hydrogeology

There are two main aquifer systems that have been identified as sources of drinking water by the CoCT: the TMG Aquifer which has recently been tapped into, and the Cape Flats Aquifer (CFA) which has the potential to supply ~30% of Cape Town's current potable water demands (City of Cape Town [CoCT], 2019).

2.4.1 Malmesbury Group

The Malmesbury Group forms a secondary aquifer in Cape Town. It is separated from the CFA system by an aquiclude, which formed in response to wave erosion of the upper levels of the basement rock during cycles of marine transgression and regression during the Quaternary period (DWAF, 2008). It is a confined to semi-confined aquifer which results in it

being less vulnerable to contamination by pollution (Colvin and Saayman, 2007). It produces a relatively low yield (~0.1 – 0.5 L/s) of relatively poor-quality water with EC values that range between 1 – 10 mS/cm (Table 2.1; Colvin and Saayman, 2007; Conrad et al., 2019). Groundwater flow is concentrated along faults, fractures, bedding planes and foliation planes and is hindered by the abundance of mica and clay minerals (Colvin and Saayman, 2007; Münch and Conrad, 2007). Conrad et al. (2019) presents hydraulic conductivity data of 0.001 – 0.86 m/d for the Malmesbury Group beneath the CFA.

2.4.2 The Cape Peninsula batholith

Granitic rocks are typically aquicludes and do not store or transmit water. However, the Cape Granite Suite has experienced fracturing and weathering which has resulted in it forming a secondary aquifer with a low hydraulic conductivity of ~0.06 m/d (Table 2.1; Conrad et al., 2019). Agyare-Dwomoh (2020) reports that its EC varies between 0.04 mS/cm – 1.10 mS/cm (Table 2.1). Recharge from the overlying TMG from cross-cutting structures may transmit higher quality water to the Cape Granite aquifer (Rosewarne, 2002). Very little research has been conducted on the Cape Granite aquifer.

2.4.3 The Table Mountain Group (TMG)

The TMG Aquifer has been recognized as one of the largest aquifer systems in South Africa due to its substantial aquifer rock volume of >100 000 km^3 (Brown et al., 2003). It is made up of two main aquifer units: the Peninsula Aquifer and the Skurweberg Aquifer. The Peninsula Formation, arguably, has the greatest potential for large-scale water abstraction because it is a thick deposit which is present across the entirety of the extensive TMG outcrop.

The TMG Aquifer is a secondary aquifer that exploits the highly fractured nature of the Peninsula Formation. Prior to brittle deformation, the TMG lacked primary porosity due to the precipitation of quartz cement and the partial recrystallisation of quartz grains during metamorphism (de Beer, 2002). However, the formation of faults and joints resulted in the generation of secondary porosity within the highly competent, resistant sandstone quartzites of the TMG. Dense fracture zones within the TMG have generated highly permeable fluid pathways. The anisotropic nature of the fracture network within the TMG Aquifer results in it being heterogenous in terms of its hydrogeological characteristics i.e. the storage, transmissivity and infiltration vary across the TMG deposits. In a study conducted on a

borehole at Rietfontein Farm, located ~ 10 km from the town of Graafwater in the northwest of the Western Cape, it was found that groundwater flow of the TMG Aquifer is controlled by shallowly-dipping bedding planes and steep fractures in the zone near the surface (<150 m deep), and primarily by steep fractures in the deeper zone (>150 m) (Figure 2.6; Lin et al., 2007). It was also discovered that groundwater predominantly flows above a depth of 400 m, and progressively reduces with increasing depth to a depth of 570 m (Lin et al., 2007). Below 570 m, Lin et al. (2007) found that there was no groundwater flow. In comparison, hot springs in a number of localities in the Western Cape have been associated with geothermal heating of rainwater that has percolated deep into the crust. For example, Diamond and Harris (2000) found that a hot spring emanated from a depth of 1760 m, along horizontal bedding planes and vertical joints orientated NW-SE, NE-SW and E-W, from a borehole located ~50 km from Rietfontein spring, north of the Cape Fold Belt (Figure 2.6). In addition, studies of the hydraulic conductivity of the TMG indicate that it ranges by location with values of 1.99 – 1.99 x 10^{-3} m/d (Table 2.1; Rosewarne, 2002).

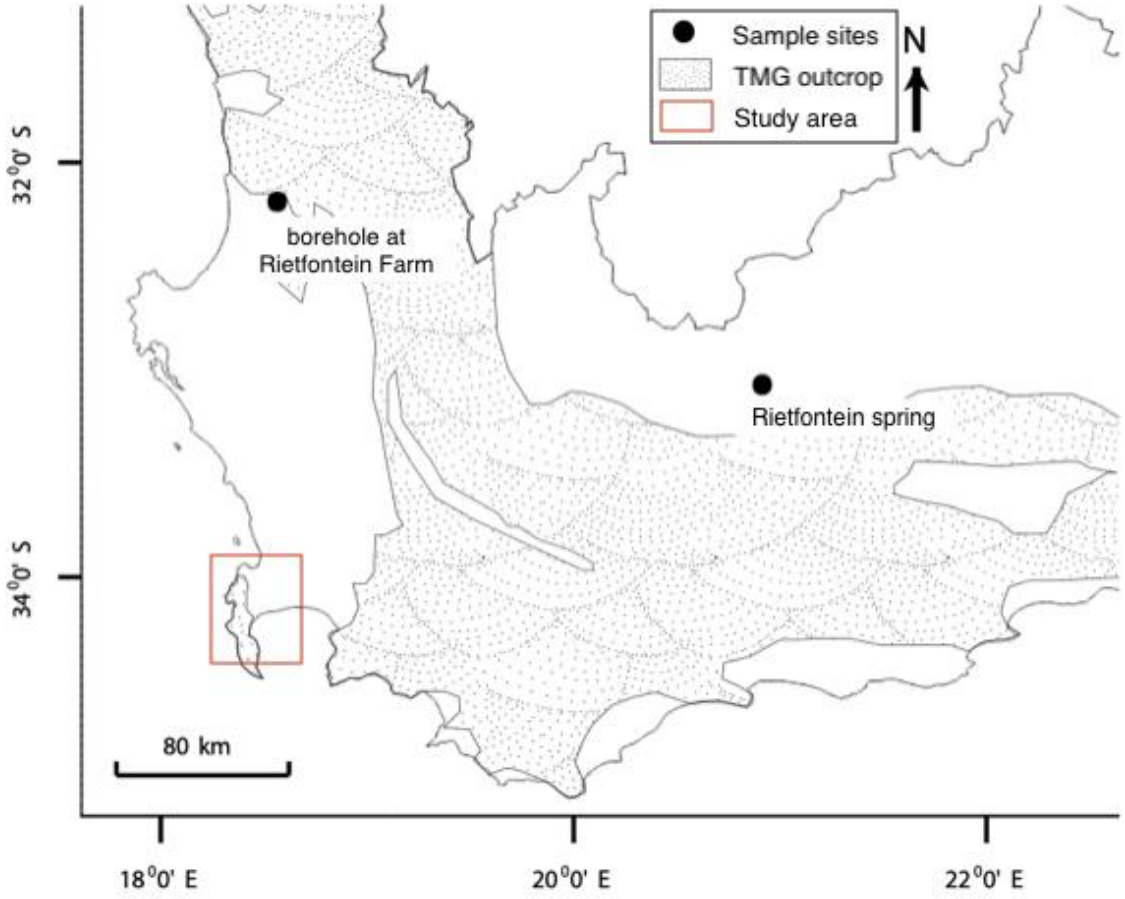

Figure 2.6: Location of the Rietfontein Farm borehole sample and the Rietfontein spring sample in relation to one another and the study area in the Western Cape province.

The Peninsula Formation on Table Mountain is an example of a horizontal terrain aquifer (Wu, 2005). It is recharged by rainfall received at high altitudes in areas that have rugged outcrops and coarse sandy soils that are derived from the weathering of sandstone (Wu, 2005; Weaver at al., 1999). The rainfall infiltrates vertically along joints in the Peninsula Formation of Table Mountain and discharges into the ocean via faults, seepage zones, and springs (Wu, 2005).

Groundwater from the TMG Aquifer has been characterised as high quality due to its low EC values of ~0.1 – 0.3 mS/cm (Table 2.1; Wu, 2005). The predominantly unconfined nature of the aquifer, in coastal regions, has resulted in it being susceptible to contamination by pollution (Rosewarne, 2002). However, the majority of its recharge area is outside of urban areas because it is usually located at high altitudes (Rosewarne, 2002). The ^{14}C-derived residence time has been calculated by Kotze et al. (2000) as 1500 years, based on a study conducted on the Kamanssie mountains, located ~550 km east of Cape Town, and 2000 years, based on a study conducted by Hartnady and Jones (2007), on the hot springs in Citrusdal, located ~180 km north of Cape Town. In comparison, Miller et al. (2017) states that the groundwater has a relatively short turnover time (indicated by its short residence time of approximately 10 - 40 years determined through the analysis of noble gas concentrations, radioactive elements, and tritium), which suggests that the TMG Aquifer may be susceptible to climate change. It has a relatively large estimated storage volume on the order of 10^{11} to 10^{12} m^3 according to Brace (1984) and 10^{10} m^3 (with 1.5 x 10^9 m^3 stored in dams) according to Rosewarne (2002) (Table 2.1). The borehole yields are typically >5 L/s (Table 2.1; Xu et al., 2009; Netili, 2007; Hartnady and Hay, 2000). However, lowering of water levels in areas where abstraction of ~5% of the potential yield is taking place may suggest that the potential yield of the TMG Aquifer has been overestimated (Jolly and Kotze, 2002). This could have major consequences which could eventually lead to groundwater depletion if groundwater abstraction is not monitored to ensure sustainable use.

2.4.4 Dolerite dykes

Typically, dolerite dykes are semi-permeable to impermeable (van Wyk and Witthueser, 2011). However, thermal fracturing of the surrounding host rocks can result in the formation of fluid pathways (van Wyk and Witthueser, 2011). A study conducted on the Hansrivier Dyke located in Beaufort West which is ~450 km northwest of Cape Town, identified the primary conduit for groundwater drainage in the area as pervasive jointing of the

host rock associated with the dyke (van Wyk and Witthueser, 2011). In addition, in this study it was found that more boreholes were drilled in areas that were in close proximity to contact zones between the dykes and the host rocks than elsewhere (van Wyk and Witthueser, 2011).

2.4.5 Table Mountain Group (TMG) scree

Diamond (2014) proposes that the Peninsula and scree aquifers are recharged by the same rainfall, and that over time, water from the high-lying Peninsula Aquifer slowly flows downslope to recharge the aquifers that occur on the lower slopes of Table Mountain. Diamond (2014) has identified that the springs at the foot of Table Mountain are sourced from scree aprons that surround the mountain based on an isotopic study. Similarly, Harris (2017) suggests that groundwater from Constantia is derived from a scree aquifer system on the eastern slopes of the Cape Peninsula mountain range.

The highest yielding springs at the foot of Table Mountain have been estimated to have yields of >16.50 L/s by Harris et al. (1999), and in 2008, the Main, Newlands and Albion spring flow rates were calculated to be ~25.47 L/s, ~17.93 L/s and ~34.72 L/s, respectively, by Wu (2008). In addition, Halenyane (2017) measured the mean EC of the Albion, Newlands, Main and De Waal springs as 0.17 mS/cm.

2.4.6 The Sandveld Group

The Sandveld Group forms a primary aquifer, known as the CFA. The Springfontyn Formation of the Sandveld Group has been identified as the main unit that forms the aquifer (Harris et al., 1999). Bedrock palaeo-channels infilled with gravels (Elandsfontyn Formation) have also been identified as having a high potential for groundwater yield (Hay et al., 2015). The aquifer sediments are generally rounded and well-sorted to support relatively high hydraulic conductivities of ~15 – 50 m/d (Table 2.1; Gerber, 1981). It has a relatively large estimated storage volume of 1.5 x 10^9 m^3 and borehole yields typically range between 0.5 L/s and 2 L/s (Table 2.1; Meyer, 2001). Groundwater of the CFA generally has a semi-radial flow with water moving from the relatively high-lying suburb of Durbanville, which is located northeast of the study area, to False Bay coastline in the south and Table Bay in the northwest (Hay et al., 2015). The CFA is mainly unconfined; however, it is semi-confined on a local to regional scale due to the presence of discrete clay, peat, and calcareous lenses (DWAF, 2008). The model of recharge of the CFA, created by DWAF (2008), indicates that it has a direct relationship with rainfall received in the area (figure 2.7). Aza-Gnandji found that the EC of

samples collected from the CFA ranged between 0.85 mS/cm and 2.84 mS/cm. The relatively fresh water from the CFA is currently used to irrigate gardens and sports fields in the Cape Flats and it has the potential to supply water for large-scale commercial use (Diamond and Harris, 2000). The unconfined nature as well as the shallow water table (0 m to 40 m below the surface) has resulted in the CFA being highly susceptible to contamination due to industrial activities, agricultural processes, and urban development (figure 2.8; Diamond and Harris, 2000; Adelana and Xu, 2006). The most vulnerable region of the CFA has recently experienced rapid urbanization in the form of both formal and informal housing (Colvin and Saayman, 2007). Run-off from informal settlements has been identified as a major non-point source of contamination to the CFA in a report by the City of Cape Town Catchment, Stormwater and River Management (Adelana and Xu, 2006).

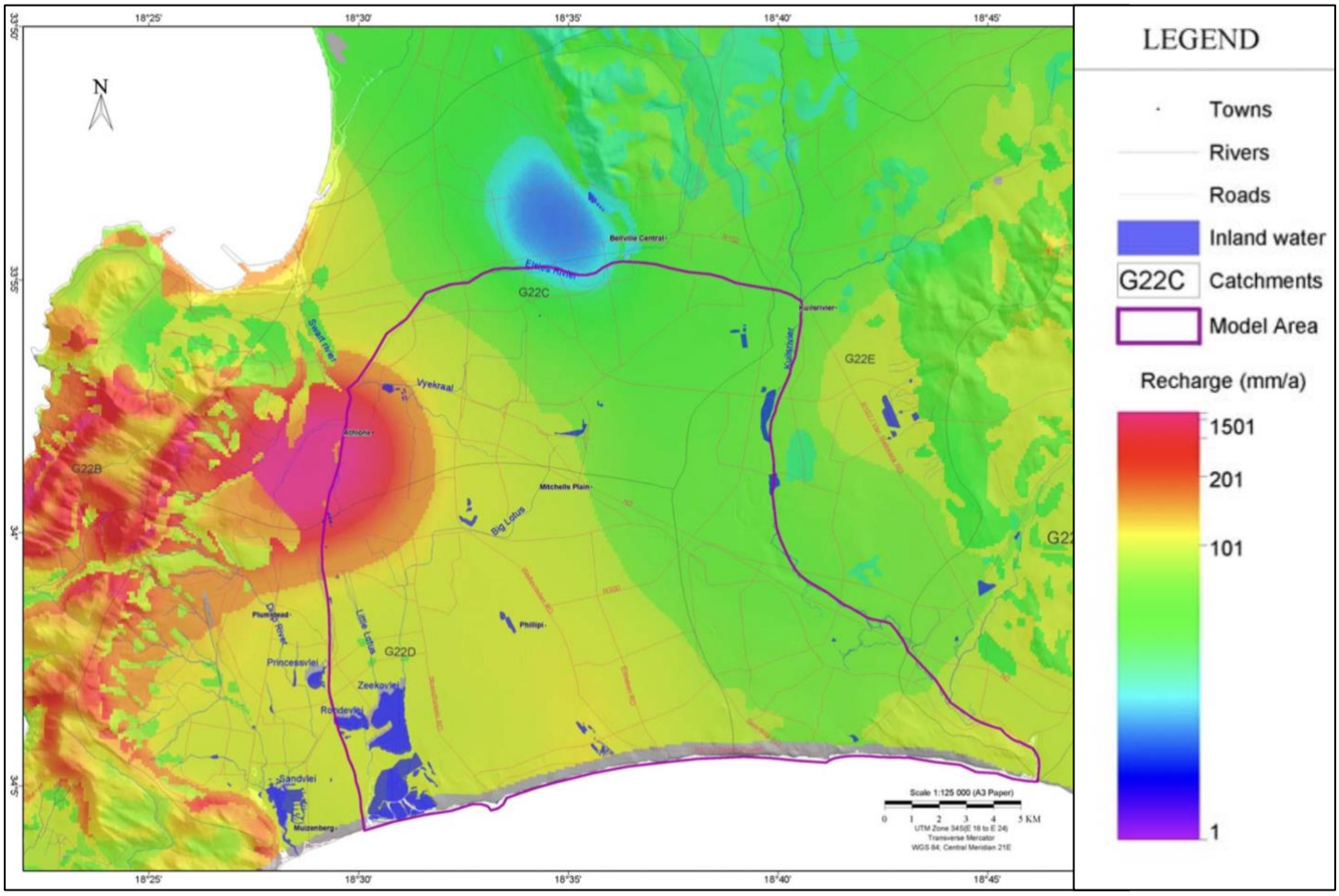

Figure 2.7: Model of the recharge rate of the CFA produced by DWAF (2008) based on the Breede River Basin study method outlined in Department of Water Affairs and Forestry [DWAF] (2007). The recharge rate is calculated as a percentage of the rainfall. The effect of the geology is considered in the model. Where the model area is outlined in purple.

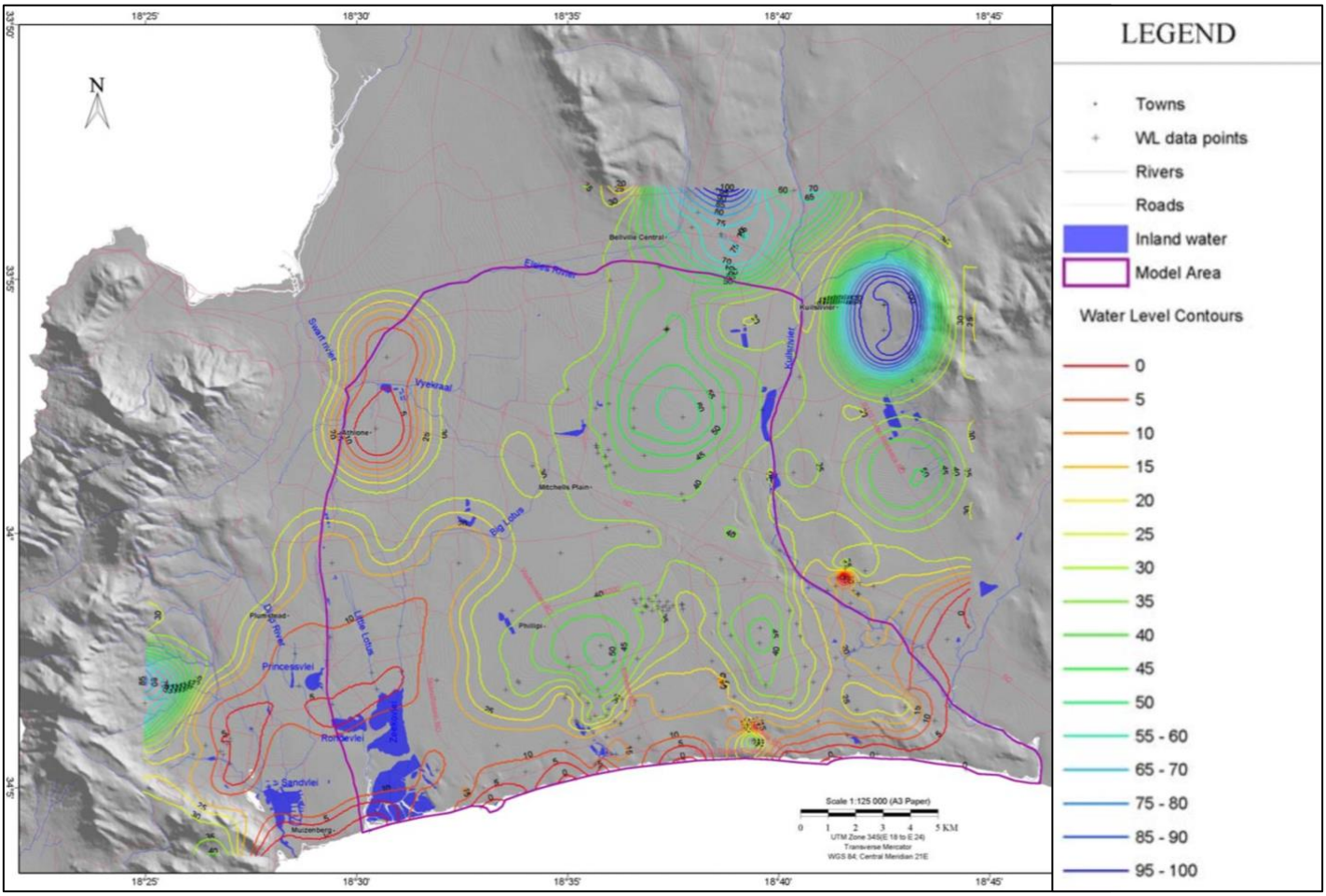

Figure 2.8: CFA groundwater level model produced by DWAF (2008) based on data, measured in mamsl, from the National Groundwater Database (data from 175 boreholes), Wessels and Greeff (1980) (47 data points) and specified points along the coastline. Where the model area is outlined in purple.

Table 2.1: Summary of the hydrological characteristics of the local geology.

oldest ⟶ youngest

	Malmesbury Group	**Cape Granite Suite**	**TMG**	**Dolerite dykes**	**TMG scree** (based on spring studies)	**Sandveld Group**
Hydraulic conductivity (m/d)	0.001 – 0.86	~0.06	1.99 – 1.99 m^{-3}	NA	NA	~15 – 50
Storage volume (m^3)	No information available (NA)	NA	10^{10} – 10^{12}	NA	NA	1.5 x 10^9
Yield (L/s)	~0.1 – 0.5	NA	>5	NA	>16.5	0.5 – 2
EC (mS/cm)	1 – 10	0.04 – 1.10	~0.1 – 0.3	NA	0.17	0.85 – 2.84

NB: These are general values, and they vary considerably due to folding, fracture density etc.

Chapter 3: Methods

3.1 Sample collection and field measurements

Two-hundred and fifty-six water samples from boreholes, wellpoints, springs, rivers and stagnant surface water bodies were collected in 4 rounds of sampling. In the 1st round of sampling, 37 groundwater samples were collected by Harris (2017) from Constantia homeowners around 11 October 2017 (Table 3.1). In 2020, 57 water samples (3 surface water samples and 54 groundwater samples) were collected from the Southern Suburbs and Cape Flats between 21 January and 29 February, and in the 3rd round of sample collection, 16 water samples (1 river and 15 groundwater samples) were collected by Harris (2020) from Oranjezicht, Mowbray, Pinelands, Rondebosch, Bergvliet, and Constantia over the same time period as the 2nd round of sample collection (Table 3.1). In the 4th round of sample collection, 146 water samples (5 spring water, 4 river and 137 groundwater samples) were collected from Bakoven along the coast to Greenpoint, the City Bowl, Southern Suburbs and the Cape Peninsula between 18 January and 17 February 2021 (Table 3.1). All 4 batches of the samples were collected in summer to avoid the short-term influence of heavy winter rainfall events on the oxygen and hydrogen isotope results, and the distribution of the data points was dependent on where boreholes have been drilled i.e., there is no data for areas where no one resides such as the very steep upper slopes of Table Mountain etc. (Figure 1.1).

Table 3.1: Summary of the 4 rounds of sampling.

Round #	Data collector	# samples	Date	Year	Area
1	Chris Harris	37 groundwater	11 Oct	2017	Constantia
2	Clare Finlayson	57 (3 surface and 54 groundwater)	21 Jan – 29 Feb	2020	Southern Suburbs and Cape Flats
3	Chris Harris	16 (1 river and 15 groundwater)	21 Jan – 29 Feb	2020	Oranjezicht, Mowbray, Pinelands, Rondebosch, Bergvliet, and Constantia
4	Clare Finlayson	146 (5 spring, 4 river and 137 groundwater)	18 Jan - 17 Feb	2021	Bakoven along the coast to Greenpoint, the City Bowl, Southern Suburbs and the Cape Peninsula

Two strategies of sample collection were adopted: 1) a field campaign and 2) crowd-sourcing. The field campaign involved collection of samples from institutions that could be accessed by the public such as schools, hospitals, businesses etc. Some samples were also collected from private residences. Samples were collected in ~150 millilitre laboratory bottles. A combination of glass and plastic bottles were used. The laboratory bottles were rinsed with the sample water before being filled to prevent contamination. The bottles were then filled to the brim and sealed to prevent evaporation of the sample. Where it was not possible to pump the water to the surface, a teflon baler was used to manually extract water from the water table (~1-5 m deep) in the wellpoint. EC and water temperature were measured on-site. This was done using a WTW-conductivity multimeter in the first 3 rounds of sampling by placing a TeltraCon350i probe into a bucket filled with the sample water. The bucket was rinsed prior to the EC and water temperature measurement to prevent contamination. The EC readings measured by the WTW-conductivity multimeter were not calibrated in the field. Standard solutions, containing KCl with EC measurements of 1.41 mS/cm and 0.76 mS/cm, that were prepared in the UCT laboratory according to the protocol outlined by the Environmental Change Network technical note 3, indicate that minimal corrections were required (Adamson, 2006). In the 4th round of sampling, samples 183 – 233 and 250 – 252 were measured using the WTW-conductivity multimeter and samples 110 – 182, 234 – 249 and 253 – 256 were measured using a Hannah instruments HI-199300 waterproof pH meter depending on the availability of equipment. Calibration of the Hannah instruments HI-199300 was done every morning before sample collection using a standard solution prepared in the UCT laboratory with an EC of 12.88 mS/cm. EC is a proxy for the total dissolved salts, and water temperature gives an indication of the depth that water is from (in mid-summer, colder water is generally from a deeper level (>5 m).

In the crowd-sourcing method, members of the public collected their own samples in 0.5 - 1.5 litre plastic bottles following a similar method to the field campaign strategy i.e. the bottles were rinsed with the sample water prior to collection and then filled to the brim to seal the sample. The samples were brought to Alphen Hall in Constantia in the 1st round of sampling or UCT to measure the EC, and the oxygen and hydrogen isotope ratios. The temperature of these samples (samples 1 - 37, 89 - 94, 192 and 251 - 256) was not recorded because temperature measurements require in-situ measurements and equipment which were not available to the public.

The pH of the water samples was only measured for the water samples collected in the 4th round of sampling, using the Hannah instruments HI-199300 waterproof pH meter on the 15th of March 2021 at UCT.

3.2 Laboratory sample analysis

The samples were stored at room temperature for approximately 1-3 weeks prior to the analysis of the oxygen and hydrogen isotope ratios, and ~3 months prior to the analysis of the strontium isotope ratios.

The oxygen and hydrogen isotope values of the water were measured, simultaneously, using a L2120-i Picarro-wavelength-scanned cavity ring-down (WS CRD) spectrometer in the Department of Biological Sciences laboratory at UCT. This process involved the following steps: 1) injection of a millilitre of the sample into a vaporisation chamber which was then transferred to the infrared absorbance cavity and 2) calculation of the stable isotope values using the ringdown time at particular wavelengths (West et al., 2010). Samples containing contaminants, such as oil, were filtered by injecting the sample through a micropore filter (Diamond, 2014). Six injections per a sample were made and memory effects were removed by discarding the first three injections. The samples were then screened by Chemcorrect version 1.0.0 post-analysis to detect if there were any problematic samples following the method used by West et al. (2014). Where issues were detected, that measurement was discarded.

The oxygen and hydrogen isotope values are reported in δ notation:

$$\delta‰ = 1000.[(R_{sample}/R_{standard}) - 1]$$

where R= D/H or $^{18}O/^{16}O$

The δD and δ^{18}O values are reported relative to Standard Mean Ocean Water (SMOW). The following internal standards were analysed: 1) Adam's Cape Town Millipore Water 3 (ACTMP3) and 2) Rocky Mountain Water (RMW), which were used to recalculate the raw data to the SMOW scale. Evian water was analysed as an unknown and gave δD and δ^{18}O values of -71.9‰ (1 σ=0.52, n = 8) and -10.24‰ (1 σ=0.14, n = 8) in 2017, -71.73‰ (1 σ=0.15, n = 8) and -10.26‰ (1σ=0.13, n = 8) in 2020, and -71.29‰ (1 σ=0.26, n = 20) and -10.19‰ (1 σ= 0.08, n = 20) in 2021, respectively (Table 3.2). The accepted hydrogen isotope

value is -73.1‰ and the accepted oxygen isotope value is -10.2‰ for Evian water (Spangenberg and Vennemann, 2008).

The standard deviation of the δD and δ^{18}O values of the Evian data for 2017 – 2020 ranges from 0.15 - 0.52 and 0.08 – 0.14, respectively (Table 3.2). It is important to note that Evian water is almost pure water, whereas the water samples collected in this study may contain organic matter and have relatively high salinities. Therefore, the error for the water samples is expected to be larger than for Evian water.

Table 3.2: Evian data for the 2017, 2020 and 2021 WS CRD spectrometer runs.

2017		
Run	δD	δ^{18}O
PIC-17-042	-72.9	-10.45
PIC-17-042	-71.6	-10.37
PIC-17-042	-71.8	-10.33
PIC-17-042	-71.3	-10.05
PIC-17-042	-71.5	-10.25
PIC-17-043	-72.1	-10.07
PIC-17-043	-71.8	-10.25
PIC-17-043	-72.4	-10.17
Ave.	-71.9	-10.24
SD	0.52	0.14

2020		
Run	δD	δ^{18}O
PIC20-003	-71.8	-10.19
PIC20-003	-71.7	-10.40
PIC20-003	-71.7	-10.49
PIC20-003	-71.5	-10.24
PIC20-004	-72.0	-10.05
PIC20-004	-71.7	-10.21
PIC20-004	-71.9	-10.27
PIC20-004	-71.6	-10.20
Ave.	-71.7	-10.26
SD	0.15	0.13

2021		
Run	δD	δ^{18}O
PIC1	-71.4	-10.33
PIC1	-71.7	-10.15
PIC1	-71.4	-10.22
PIC1	-71.3	-10.05
PIC2	-71.5	-10.06
PIC2	-71.0	-10.30
PIC2	-71.6	-10.20
PIC2	-71.6	-10.18
PIC3	-71.3	-10.16
PIC3	-71.2	-10.01
PIC3	-71.4	-10.21
PIC3	-71.1	-10.23
PIC4	-71.2	-10.19
PIC4	-71.4	-10.16
PIC4	-71.2	-10.28
PIC4	-70.7	-10.13
PIC5	-71.4	-10.19
PIC5	-71.6	-10.25
PIC5	-71.1	-10.29
PIC5	-70.7	-10.23
Ave.	-71.3	-10.19
SD	0.26	0.08

Strontium isotope ratios were only measured in 10 of the water samples and were chosen based on their range in oxygen and hydrogen isotope values, EC, depth, and their relatively wide spatial distribution within the study area. No special bottling procedure was

followed - precipitation of strontium onto the inside of the container was not considered a problem because it is a ratio that is being measured. These samples were prepared for analysis and measured following the method outlined by van Gend (2020). Approximately 2 - 10 millilitres of the groundwater samples were dried. Thereafter, the precipitate from each aliquot underwent a second drying cycle after a few drops of concentrated nitric acid was added. A volume of 1.5 millilitres of 2 moles of nitric was then added to each of the Teflon vials before loading them onto the Sr.Spec columns for standard Sr elemental separation chemistry. Finally, the collected strontium fractions were dried, dissolved into 0.2% nitric acid and diluted to a concentration of ~200 ppb. The strontium isotope ratios were measured by a NuPlasma HR mass spectrometer with a DSN-100 desolvating nebuliser, in the Geological Science laboratory at UCT. The ratios measured were compared to the standard, NIST987 which has a value of 0.710255 that was determined through bracketing analyses. The measured strontium isotope ratios were compared to natural $^{85}Rb/^{87}Rb$ and a measured ^{85}Sr signal to address Rb interference, and instrumental mass fractionation was corrected for by comparing $^{87}Sr/^{86}Sr$ measured to a known $^{86}Sr/^{88}Sr$ ratio of 0.1194 and using the exponential law.

3.3 Depth, altitude and distance data

The depth of the borehole or wellpoint was given by the owner; it refers to how deep the borehole or wellpoint has been drilled into the ground. Altitude was determined on Google Earth Pro; it indicates the height of the top of the borehole relative to the mean sea-level. It is accurate to the nearest 4 m. A rough estimate of the minimum possible horizontal distance between the water sample, and the TMG and Malmesbury Group unconformity was measured using the ruler function on Google Earth Pro (Figure 3.1).

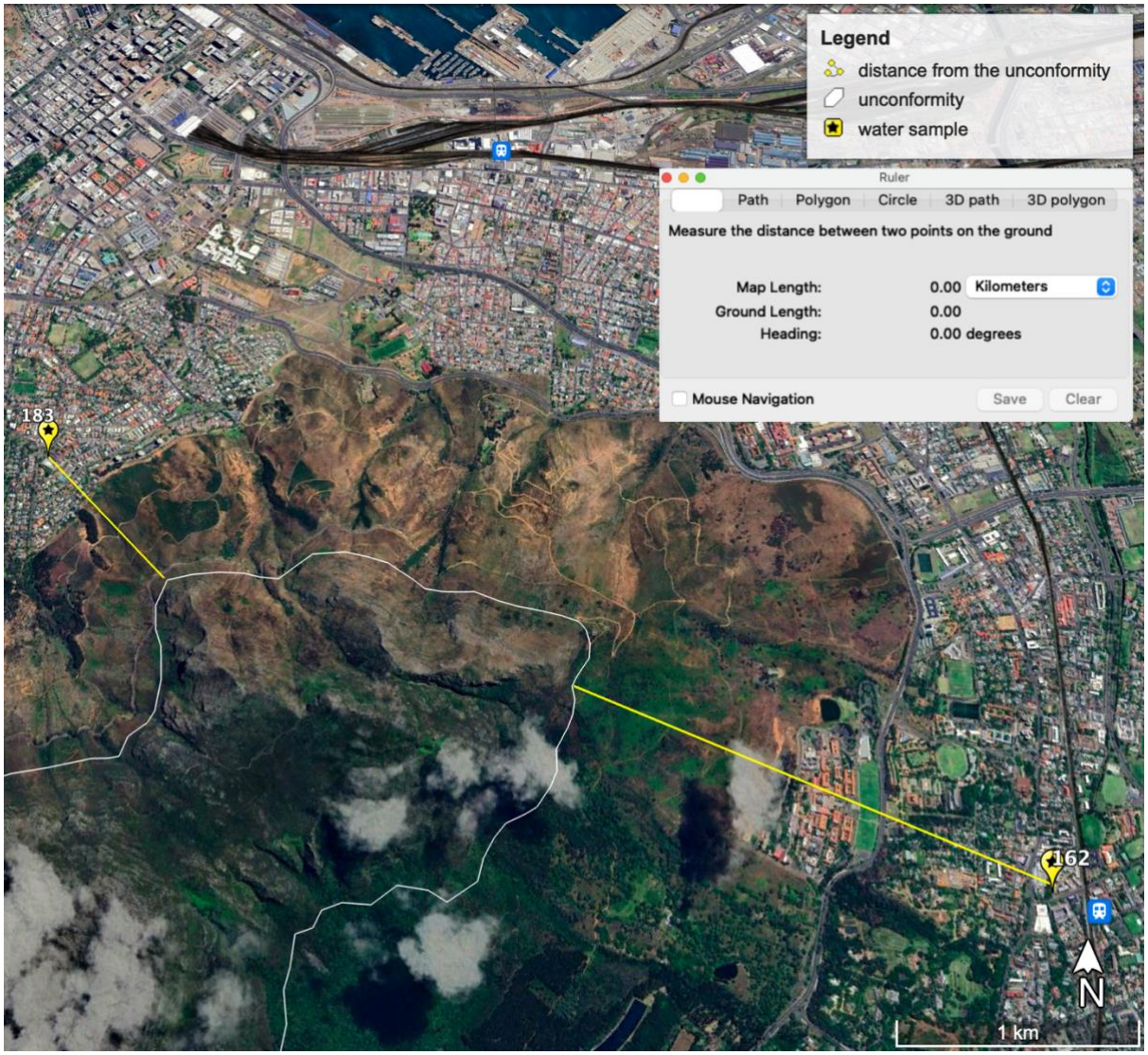

Figure 3.1: Method used to measure the approximate minimum horizontal distance between the water samples, and the TMG and Malmesbury Group unconformity (Google Earth Pro, 2019b).

3.4 Meteorological, spring and groundwater data

Monthly precipitation δD and δ^{18}O values for samples collected at UCT from the rooftop of the Geology building between late 1996 – early 2021 (Table 7.1), and the average monthly δD and δ^{18}O values of samples collected from Albion spring, Main spring and Newlands spring in September 2019, October 2019 and November 2019 were taken from the unpublished database of Harris through personal communication. The average δD and δ^{18}O values of Main spring for January 2020 are also included. In addition, the δD and δ^{18}O values of groundwater data collected by Daws (2021), in preparation for a MSc dissertation, was acquired for comparison purposes. This dataset consists of 125 groundwater samples that were

collected in spring 2020 and resampled in autumn 2021 from the western slopes of the Table Mountain and Constantiaberg massifs. The $^{87}Sr/^{86}Sr$ ratios were also acquired for 9 of the groundwater samples collected by Daws (2021). The errors for these water samples are expected to be similar to the errors of the water samples presented in this study.

3.5 Spatial modelling

In order to better visually illustrate the spatial trends within existing and new groundwater $\delta^{18}O$ measurements, isoscapes were produced in Generic Mapping Tools (GMT) v. 6.0.0.

Chapter 4: Results

All the data, except for the strontium isotope data, are included in Table 4.1. There are 4 water samples that have positive δD and $\delta^{18}O$ values. Three of these samples are stagnant surface water samples that were collected from Sandvlei (sample 39 and 41) and a lake from the Capricorn Conservation Area (sample 40) in 2020. There are also several spring and river samples included in the dataset. The spring samples include samples collected from Westerford High School in Rondebosch (sample 113), False Bay College in Muizenberg (sample 215), Greenpoint Urban Park (240), St. James (sample 242) and Boyes Drive (sample 248). The river samples include a sample collected from Elsieskraalrivier in Pinelands (sample 101), Rhodes High School in Mowbray, which was derived from the Black River (sample 130), a sample collected from the Clovelly Country Club, which was derived from the Silwermynrivier (sample 219), and a sample collected from a stream in Glencairn Heights (sample 247). The rest of the dataset consists of groundwater samples. There are some missing depth data because many institutions and homeowners do not know how deep their borehole or wellpoint is and, as previously mentioned, the samples without temperature recordings were collected via the crowd-sourcing method i.e., the members of the public did not have access to the equipment required to take in-situ temperature measurements. In addition, the temperature of samples 110 - 122 was not included due to technical issues with the equipment. The EC of sample 106 was not also recorded. The pH of only the water samples collected in 2021 were recorded due to the availability of a new instrument with enhanced capabilities.

Table 4.1: Raw dataset including the location, GPS coordinates, altitude, depth, the distance from the unconformity between the TMG and the Malmesbury Group, and the compositional data of the groundwater, spring, river, and stagnant surface water samples.

Sample #	Location	Sample type	Latitude S	Longitude E	Altitude (mamsl)	Depth (m)	Distance from unconformity (km)	Temp (℃)	pH	EC (mS/cm)	$\delta^{18}O$ (‰)	δD (‰)	d-excess (‰)
1	Constantia	groundwater	34.019503	18.428850	78		2.34			0.51	-2.69	-12.1	9.49
2	Constantia	groundwater	34.000839	18.429481	118		1.28			0.28	-3.13	-12.5	12.51
3	Constantia	groundwater	34.007692	18.432294	75		1.82			0.26	-2.85	-11.4	11.42
4	Constantia	groundwater	34.002831	18.439211	75		2.15			0.34	-2.84	-10.8	11.93
5	Constantia	groundwater	34.044964	18.432881	32		3.46			0.52	-2.70	-12.1	9.52
6	Constantia	groundwater	34.012492	18.437203	60		2.95			0.35	-2.84	-11.7	11.01
7	Constantia	groundwater	34.005619	18.427353	113		1.65			0.34	-2.98	-11.8	12.06
8	Constantia	groundwater	34.000639	18.427025	145		1.42			0.22	-3.24	-12.6	13.27
9	Constantia	groundwater	34.019478	18.443256	55		3.82			0.52	-2.55	-10.5	9.89
10	Constantia	groundwater	34.023375	18.448075	55		4.39			0.34	-3.39	-15.7	11.42
11	Constantia	groundwater	34.031408	18.438856	41		3.33			0.49	-2.79	-11.5	10.85
12	Constantia	groundwater	34.023325	18.439494	54		3.28			0.65	-2.68	-10.6	10.87
13	Constantia	groundwater	34.015222	18.437953	65		3.17			0.39	-2.70	-10.8	10.83
14	Constantia	groundwater	34.042436	18.452892	27		4.96			0.51	-2.79	-11.1	11.21
15	Constantia	groundwater	34.031408	18.438856			3.33			0.49	-2.68	-11.4	10.06
16	Constantia	groundwater	34.013525	18.441353	56		3.29			0.38	-2.85	-13.2	9.67
17	Constantia	groundwater	34.040139	18.432939	36		3.21			0.58	-2.45	-9.9	9.67
18	Constantia	groundwater	34.009144	18.434397	67		2.41			0.34	-1.66	-6.8	6.53
19	Constantia	groundwater	34.015319	18.442161	59		3.43			0.60	-2.75	-12.4	9.59
20	Constantia	groundwater	34.014881	18.441356	60		3.30			0.41	-2.46	-9.8	9.88
21	Constantia	groundwater	34.020286	18.431986	82		2.59			0.86	-2.75	-11.3	10.70
22	Constantia	groundwater	34.027567	18.450742	53		4.34			0.98	-2.51	-10.6	9.49
23	Constantia	groundwater	34.014361	18.439544	61		3.20			0.42	-3.09	-13.1	11.64
24	Constantia	groundwater	34.010628	18.444519	40		3.35			0.69	-2.32	-9.1	9.47
25	Constantia	groundwater	34.010922	18.435797	72		2.70			0.24	-2.99	-12.6	11.31
26	Constantia	groundwater	34.024692	18.458106	33		5.00			1.21	-2.76	-10.6	11.48
27	Constantia	groundwater	34.027139	18.450483	54		4.30			0.63	-2.52	-11.2	8.94
28	Constantia	groundwater	34.037653	18.426419	47		2.56			0.55	-2.89	-12.2	10.90
29	Wynberg	groundwater	34.001142	18.460700	59		3.97			0.31	-2.89	-12.2	10.94
30	Constantia	groundwater	34.030825	18.432189	65		2.71			0.55	-3.01	-13.6	10.47
31	Bishopscourt	groundwater	33.993872	18.432872	185		1.36			0.39	-2.87	-11.9	11.14
32	Constantia	groundwater	34.019256	18.433006	86		2.70			0.43	-2.76	-12.3	9.77
33	Constantia	groundwater	34.009336	18.428681	105		2.08			0.23	-2.89	-11.3	11.82
34	Constantia	groundwater	34.029811	18.439819	38		3.38			0.53	-2.85	-11.8	10.96
35	Constantia	groundwater	34.007906	18.436892	51		2.65			0.38	-2.74	-11.2	10.69
36	Constantia	groundwater	34.015247	18.446772	43		3.83			1.00	-2.39	-9.7	9.46

Sample #	Location	Sample type	Latitude S	Longitude E	Altitude (mamsl)	Depth (m)	Distance from unconformity (km)	Temp (℃)	pH	EC (mS/cm)	$\delta^{18}O$ (‰)	δD (‰)	d-excess (‰)
37	Constantia	groundwater	34.037057	18.439550			3.55			0.51	-2.61	-11.4	9.53
38	Muizenberg	groundwater	34.098097	18.477392	5	7	1.27	20.5		1.41	-2.52	-9.9	10.24
39	Muizenberg	Stagnant surface water	34.098761	18.471744	2	0	0.74	23.5		35.70	2.13	12.5	-4.57
40	Capricorn	Stagnant surface water	34.089992	18.486531	3	0	2.54	23.8		1.74	1.38	6.5	-4.54
41	Marina Da Gama	Stagnant surface water	34.082472	18.473447	2	0	1.87	24.0		35.20	2.35	13.7	-5.10
42	Plumstead	groundwater	34.019436	18.480608	20	11	6.46	22.8		1.33	-1.97	-8.1	7.69
43	Plumstead	groundwater	34.019886	18.485197	18		6.86	21.7		1.41	-1.87	-6.6	8.37
44	Plumstead	groundwater	34.027292	18.461986	26	35	5.35	25.4		0.93	-2.95	-13.0	10.59
45	Wynberg	groundwater	34.009344	18.465519	47	15	4.61	22.5		0.38	-2.88	-13.2	9.86
46	Wynberg	groundwater	34.011250	18.464522	48		4.66	23.3		0.58	-2.55	-9.9	10.53
47	Plumstead	groundwater	34.020478	18.460739	24	9	5.24	20.1		0.40	-2.68	-10.7	10.71
48	Plumstead	groundwater	34.019908	18.462167	31		4.90	19.7		0.34	-2.84	-12.5	10.27
49	Wynberg	groundwater	34.002614	18.464958	57	40	4.25	23.6		0.15	-1.68	-4.3	9.17
50	Kenwyn	groundwater	33.993936	18.496303	21	3	6.45	21.1		0.26	-2.30	-7.0	11.38
51	Kenwyn	groundwater	33.997494	18.498986	22	9	6.86	23.0		0.23	-2.39	-7.5	11.62
52	Kenwyn	groundwater	33.997194	18.493528	23		6.37	25.5		0.52	-2.67	-11.3	10.05
53	Grassy Park	groundwater	34.040903	18.498936	12		9.63	24.0		5.53	-2.39	-9.3	9.81
54	Grassy Park	groundwater	34.038506	18.502358	12		9.21	25.4		0.72	-2.32	-8.6	9.96
55	Grassy Park	groundwater	34.034236	18.508392	11		9.35	26.6		1.92	-2.75	-11.6	10.37
56	Ottery	groundwater	34.018528	18.512525	17	13	8.94	20.8		0.52	-2.67	-8.5	12.86
57	Ottery	groundwater	34.018611	18.512747	17	13	9.07	21.8		0.75	-2.67	-9.1	12.23
58	Plumstead	groundwater	34.016303	18.461428	36	6	4.80	21.1		0.62	-2.29	-7.5	10.78
59	Mitchells Plain	groundwater	34.030508	18.602722	35	40	16.66	22.6		2.08	-3.19	-13.1	12.40
60	Philippi	groundwater	34.042264	18.582575	30	34	15.84	19.3		2.15	-2.28	-7.9	10.31
61	Philippi	groundwater	34.042411	18.582261	30	34	15.86	18.9		2.35	-2.33	-8.3	10.32
62	Philippi	groundwater	34.038233	18.580042	30		15.36	19.1		1.62	-2.76	-9.9	12.14
63	Plumstead	groundwater	34.018467	18.466539	32	12	5.17	20.8		0.56	-2.69	-10.8	10.67
64	Plumstead	groundwater	34.016392	18.461064	35	25	4.59	20.9		0.49	-2.66	-9.8	11.52
65	Plumstead	groundwater	34.016128	18.462850	36	6	4.85	21.2		0.28	-1.92	-6.6	8.79
66	Mitchells Plain	groundwater	34.020844	18.616617	35	24	16.62	20.6		2.07	-3.21	-13.2	12.53
67	Mitchells Plain	groundwater	34.053456	18.606219	32	~18	17.03	20.4		0.67	-2.64	-10.6	10.53
68	Mitchells Plain	groundwater	34.060392	18.621711	25	16	15.23	22.1		0.76	-2.84	-12.1	10.60
69	Mitchells Plain	groundwater	34.066522	18.601106	17		13.22	21.9		0.71	-2.50	-10.3	9.70
70	Philippi	groundwater	34.025639	18.567361	29	9	12.64	20.5		1.80	-2.42	-8.8	10.52
71	Philippi	groundwater	34.048528	18.552028	26	42	9.94	19.4		1.05	-2.47	-8.7	11.06
72	Philippi	groundwater	34.044139	18.555111	27	47	10.57	18.9		1.74	-2.00	-6.6	9.35
73	Philippi	groundwater	34.043000	18.560083	26	40	10.99	18.6		1.26	-2.37	-8.2	10.74
74	Philippi	groundwater	34.042306	18.564417	27	45	11.30	18.9		3.38	-1.98	-5.9	9.93
75	Philippi	groundwater	34.040944	18.554139	28	70	10.63	20.0		1.91	-2.76	-10.3	11.80
76	Philippi	groundwater	34.036472	18.562944	28	45	11.52	19.2		4.82	-1.05	-1.7	6.67

Sample #	Location	Sample type	Latitude S	Longitude E	Altitude (mamsl)	Depth (m)	Distance from unconformity (km)	Temp (℃)	pH	EC (mS/cm)	$\delta^{18}O$ (‰)	δD (‰)	d-excess (‰)
77	Philippi	groundwater	34.036597	18.563308	28	45	11.53	19.0		3.62	-1.58	-4.0	8.62
78	Philippi	groundwater	34.032639	18.562917	27	45	11.80	19.5		2.74	-2.09	-5.5	11.24
79	Philippi	groundwater	34.035436	18.566781	28	45	11.91	19.1		2.61	-1.77	-6.4	7.78
80	Dreyersdal	groundwater	34.058619	18.459717	9		3.59	28.3		0.20	-1.90	-4.9	10.25
81	Diep River	groundwater	34.032306	18.465850	21		5.77	21.9		0.65	-2.45	-9.4	10.16
82	Diep River	groundwater	34.039211	18.465192	4		5.82	20.2		0.87	-2.72	-10.4	11.35
83	Bergvliet	groundwater	34.043244	18.460819	18		5.28	21.3		0.60	-3.14	-13.9	11.19
84	Elfindale	groundwater	34.046125	18.478078	14		5.41	20.4		0.64	-1.75	-7.0	6.97
85	Ottery	groundwater	34.010117	18.497147	20		7.35	23.8		0.85	-2.59	-10.7	9.97
86	Philippi	groundwater	34.003864	18.522917	19		8.89	24.2		0.35	-1.95	-6.5	9.09
87	Ottery	groundwater	34.012150	18.497233	19	10	7.54	22.4		0.93	-2.87	-11.8	11.13
88	Plumstead	groundwater	34.015733	18.462572	36	10	4.74	20.8		0.22	-1.73	-5.2	8.68
89**	Plumstead	groundwater	34.026	18.469	23		5.96			0.58	-2.73	-11.8	10.04
90**	Diep River	groundwater	34.034	18.466	22		5.85			1.23	-2.60	-10.2	10.56
91**	Plumstead	groundwater	34.020	18.480	19		6.43			0.95	-2.32	-8.8	9.80
92**	Plumst	groundwater	34.026	18.467	22		5.84			0.72	-2.37	-9.0	9.97
93**	Wynberg	groundwater	34.000	18.462	64		3.99			0.41	-2.46	-9.2	10.53
94*	Plumstead	groundwater	34.019253	18.476300	17		6.09			1.08	-2.48	-10.1	9.76
95	Rondebosch	groundwater	33.961156	18.484303	19	56	3.39	24		0.78	-3.18	-12.7	12.79
96	Rondebosch	groundwater	33.972294	18.485547	26	56	4.02	29		0.56	-2.92	-10.7	12.68
97	Pinelands	groundwater	33.930847	18.516839	12		6.63			17.39	-3.07	-13.2	11.36
98	Pinelands	groundwater	33.966017	18.480950	12	4	3.32			1.47	-2.46	-6.8	12.90
99	Pinelands	groundwater	33.929886	18.513600	10		6.39			1.68	-2.98	-11.1	12.77
100*	Oranjezicht	groundwater	33.943869	18.409567	185		1.10			1.00	-3.27	-12.6	13.52
101	Pinelands	river	33.931108	18.517464	7		6.67			0.77	-1.05	-3.4	4.94
102	Pinelands	groundwater	33.929897	18.512661	10		6.34			3.76	-3.16	-13.6	11.71
103	Mowbray	groundwater	33.947375	18.492411	11		4.00			1.32	-3.28	-13.9	12.37
104	Pinelands	groundwater	33.930997	18.516689	11	5	6.61			1.07	-2.83	-13.1	9.53
105	Pinelands	groundwater	33.930997	18.516689	11	6	6.61			0.94	-3.00	-11.7	12.26
106	Constantia	groundwater	34.026425	18.445667	59	45	3.93				-3.33	-15.7	10.92
107	Rondebosch	groundwater	33.967569	18.475872	21		2.98			0.75	-2.30	-7.4	10.94
108	Rondebosch	groundwater	33.947256	18.468517	29	100	1.77			1.10	-3.43	-11.7	15.73
109	Bergvliet	groundwater	34.049553	18.453056	22	32	5.25			0.93	-2.65	-10.1	11.12
110	Constantia	groundwater	34.019972	18.442819	56		3.56			0.32	-3.55	-15.1	13.35
111	Rondebosch	groundwater	33.967856	18.488092	21		4.04		6.36	0.62	-2.70	-10.7	10.87
112	Rosebank	groundwater	33.955956	18.479206	19		2.64		6.69	1.67	-2.66	-9.9	11.34
113	Rondebosch	spring	33.969581	18.465294	23		2.23		7.18	0.42	-2.47	-8.3	11.51
114	Newlands	groundwater	33.970575	18.468167	20	36	2.52		7.31	0.24	-2.06	-7.3	9.19
115	Rondebosch	groundwater	33.966919	18.479878	14	5	3.28		7.01	1.21	-1.94	-5.3	10.18
116	Rondebosch	groundwater	33.970564	19.216501	19		4.4		7.91	1.00	-1.93	-3.6	11.89

Sample #	Location	Sample type	Latitude S	Longitude E	Altitude (mamsl)	Depth (m)	Distance from unconformity (km)	Temp (℃)	pH	EC (mS/cm)	$\delta^{18}O$ (‰)	δD (‰)	d-excess (‰)
117	Rondebosch	groundwater	33.963219	18.474814	21	30	2.52		7.59	0.90	-2.72	-10.0	11.73
118	Rondebosch	groundwater	33.967153	18.475533	21	6	2.89		7.90	0.29	-2.33	-6.9	11.71
119	Rondebosch	groundwater	33.970314	18.490233	18		4.25		7.22	0.98	-1.59	-4.2	8.48
120	Rondebosch	groundwater	33.972203	18.491967	16		4.38		7.30	0.32	-2.02	-6.4	9.73
121	Rondebosch	groundwater	33.972994	18.483603	26		3.81		7.15	1.03	-2.24	-9.5	8.46
122	Rondebosch	groundwater	33.960306	18.492108	9	75	4.04		6.93	1.16	-2.85	-13.1	9.73
123	Claremont	groundwater	33.984469	18.472061	29		3.90	24.2	6.80	0.32	-2.19	-5.7	11.78
124	Claremont	groundwater	33.988686	18.468672	46		3.52	21.6	5.69	0.38	-2.59	-10.0	10.75
125	Claremont	groundwater	33.992906	18.456642	116		3.15	24.7	6.54	0.44	-2.44	-10.0	9.48
126	Claremont	groundwater	33.981444	18.470650	23	28	3.53	22.4	5.98	1.39	-2.26	-7.9	10.20
127	Claremont	groundwater	33.982886	18.459864	44		2.68	22.3	6.16	0.21	-2.49	-11.4	8.49
128	Rondebosch	groundwater	33.964133	18.491517	13	60	3.75	21.9	5.88	0.69	-2.81	-11.0	11.48
129	Newlands	groundwater	33.980606	18.448028	55		1.53	22.4	6.18	0.18	-2.67	-8.6	12.74
130	Mowbray	river	33.946981	18.478081	5		2.48	22.6	6.54	0.24	-2.16	-5.9	11.37
131	Claremont	groundwater	33.988972	18.464472	50	100	3.40	22.4	5.91	0.20	-2.13	-10.4	6.60
132	Rondebosch	groundwater	33.976722	18.482747	25	55	4.23	21.6	5.18	0.98	-1.97	-8.5	7.27
133	Mowbray	groundwater	33.947128	18.493586	11	30	3.96	20.7	6.06	1.28	-2.61	-12.2	8.64
134	Rondebosch	groundwater	33.961942	18.488808	9		3.92	22.5	4.30	1.10	-2.53	-9.4	10.84
135	Observatory	groundwater	33.940519	18.460189	70	200	1.45	29.3	7.93	1.53	-2.02	-6.0	10.18
136	Observatory	groundwater	33.934711	18.471081	8	>50	2.54	22.9	6.63	1.81	-2.32	-9.6	8.95
137	Rondebosch	groundwater	33.975064	18.488764	22	3	4.42	22.1	6.63	0.59	-1.50	-3.5	8.54
138	Bergvliet	groundwater	34.049250	18.460269	14	12	6.94	21.3	4.91	1.23	-2.29	-9.9	8.39
139	Lansdowne	groundwater	33.982986	18.494222	20	10	5.41	22.8	5.43	0.35	-2.05	-6.4	9.97
140	Lansdowne	groundwater	33.996806	18.505672	21		7.12	21.7	5.49	0.43	-2.37	-9.7	9.27
141	Lansdowne	groundwater	33.987397	18.500719	19		6.32	21.2	5.45	0.97	-2.27	-8.5	9.63
142	Rondebosch East	groundwater	33.976461	18.497931	17		5.18	22.2	6.20	3.07	-2.31	-10.3	8.14
143	Rondebosch East	groundwater	33.979372	18.494300	19	~60	5.08	22.2	6.11	1.32	-2.33	-9.9	8.74
144	Belthorn Estate	groundwater	33.987283	18.513567	17		7.08	24.1	6.44	1.05	-2.30	-8.1	10.30
145	Silvertown	groundwater	33.964633	18.521894	10		6.81	22.4	6.33	1.69	-2.44	-8.9	10.62
146	Hazendal	groundwater	33.958756	18.507589	9	17	5.41	24.6	7.14	1.59	-2.38	-8.8	10.21
147	Rondebosch	groundwater	33.953344	18.486478	22	~35	3.39	23.7	7.87	1.16	-2.59	-10.9	9.78
148	Belthorn	groundwater	33.982742	18.514058	16	6	7.50	23.3	5.82	0.75	-2.19	-8.0	9.57
149	Rustdale	groundwater	33.974736	18.513458	14		6.32	21.0	5.63	0.70	-2.10	-7.2	9.64
150	Nerissa Estate	groundwater	33.991281	18.510742	20	10	7.10	25.6	6.13	1.24	-2.03	-5.8	10.47
151	Mowbray	groundwater	33.953542	18.492000	12	75	3.92	21.5	6.09	2.53	-3.01	-12.8	11.25
152	Athlone	groundwater	33.969717	18.499431	17		4.99	23.9	6.19	0.19	-0.45	4.2	7.79
153	Belgravia	groundwater	33.972444	18.518969	11		6.78	25.2	5.93	0.51	-2.27	-7.6	10.53
154	Mowbray	groundwater	33.947703	18.493053	10		4.06	21.1	6.07	1.56	-2.61	-11.5	9.38
155	Rondebosch	groundwater	33.960050	18.477689	23		2.82	25.3	6.26	0.46	-2.34	-8.8	9.91
156	Claremont	groundwater	33.988953	18.484431	23		5.15	37.1	7.34	0.21	-1.32	-2.0	8.55

Sample #	Location	Sample type	Latitude S	Longitude E	Altitude (mamsl)	Depth (m)	Distance from unconformity (km)	Temp (℃)	pH	EC (mS/cm)	$\delta^{18}O$ (‰)	δD (‰)	d-excess (‰)
157	Wynberg	groundwater	34.009925	18.480964	26		5.83	25.6	7.12	0.97	-1.81	-7.4	7.10
158	Kenilworth	groundwater	34.002049	18.473064	48	10	4.93	22.9	5.22	0.41	-2.35	-9.1	9.66
159	Kenilworth	groundwater	33.998853	18.478147	33		5.13	23.8	6.63	0.64	-2.43	-9.0	10.40
160	Kenilworth	groundwater	33.994011	18.465244	56		3.03	21.0	6.12	0.33	-2.46	-11.4	8.32
161	Kenilworth	groundwater	33.996256	18.473989	43	35	4.66	26.1	6.18	0.55	-2.52	-10.9	9.27
162	Rondebosch	groundwater	33.961161	18.470897	11		2.21	23.6	7.87	1.11	-2.75	-11.4	10.57
163	Rondebosch	groundwater	33.969481	18.471883	19		2.81	22.1	6.85	0.53	-2.69	-11.6	9.93
164	Claremont	groundwater	33.977083	18.485019	26		4.12	23.7	6.41	0.46	-2.47	-11.0	8.80
165	Newlands	groundwater	33.972183	18.460675	36		2.10	22.3	5.73	0.25	-2.54	-8.5	11.80
166	Newlands	groundwater	33.973553	18.470906	26		2.95	27.4	6.34	0.58	-2.15	-8.0	9.23
167	V&A Waterfront	groundwater	33.911036	18.421792	12	70	3.93	24.0	6.91	1.09	-2.27	-7.6	10.58
168	V&A Waterfront	groundwater	33.911558	18.419989	15	60	3.75	25.2	7.17	1.33	-1.94	-7.0	8.55
169	Woodstock	groundwater	33.924858	18.448833	4		2.37	23.1	7.08	3.32	-2.24	-8.3	9.62
170	Foreshore	groundwater	33.926175	18.442175	5		2.27	24.4	6.55	2.13	-2.54	-9.7	10.66
171	Woodstock	groundwater	33.927156	18.449506	7	55	2.41	22.2	6.60	1.43	-2.29	-8.8	9.53
172	Salt River	groundwater	33.929106	18.459169	10		2.53	29.7	7.65	0.68	-1.79	-1.9	12.41
173	Salt River	groundwater	33.935658	18.457703	39		1.84	21.8	6.21	1.62	-2.69	-10.9	10.61
174	University Estate	groundwater	33.937339	18.451900	75	112	1.41	24.3	5.81	1.18	-2.78	-11.1	11.16
175	University Estate	groundwater	33.937214	18.450978	80	110	1.44	21.9	5.95	0.85	-2.96	-11.8	11.92
176	University Estate	groundwater	33.939678	18.448850	118		1.13	24.8	6.55	1.57	-3.01	-11.7	12.34
177	Walmer Estate	groundwater	33.934392	18.444669	74	100	1.61	25.1	6.10	0.99	-2.57	-10.2	10.38
178	Oranjezicht	groundwater	33.942717	18.416522	116	82	1.22	21.1	6.38	0.42	-3.31	-13.3	13.18
179	Camps Bay	groundwater	33.952267	18.379153	6	12	1.64	22.2	6.41	0.50	-3.22	-13.1	12.67
180	Camps Bay	groundwater	33.944381	18.379189	46		1.24	21.5	6.23	1.35	-2.69	-11.8	9.70
181**	Camps Bay	groundwater	33.949	18.384	82	120	1.30	25.1	6.61	0.43	-3.67	-13.6	15.73
182	Zonnebloem	groundwater	33.928378	18.443228	13		2.16	24.6	6.21	1.23	-3.04	-11.8	12.51
183	Vredehoek	groundwater	33.942453	18.421450	128		0.90	18.2	6.23	0.11	-1.77	-4.6	9.56
184	Gardens	groundwater	33.934158	18.409008	59		1.70	20.8	7.47	0.73	-2.32	-8.6	9.98
185	Oranjezicht	groundwater	33.944211	18.413511	144		1.23	19.0	6.86	0.13	-2.91	-11.8	11.52
186	Gardens	groundwater	33.929222	18.409697	49		1.88	23.1	7.14	1.04	-2.23	-8.0	9.80
187	Tamboerskloof	groundwater	33.933514	18.399994	157		0.87	21.4	7.21	2.17	-2.98	-11.9	11.97
188**	Bergvliet	groundwater	34.047	18.446	15	8	4.74	20.8	6.36	0.89	-2.23	-8.4	9.46
189	Constantia	groundwater	34.030414	18.457536	30		5.22	23.4	7.23	0.78	-2.38	-12.6	6.41
190	Bergvliet	groundwater	34.043850	18.449336	29		4.76	24.5	6.48	0.49	-2.16	-10.2	7.13
191	Bergvliet	groundwater	34.053519	18.459231	14		5.94	20.2	6.56	0.92	-2.58	-12.0	8.62
192	Bergvliet	groundwater	34.048672	18.459081	16	80	5.91	23.4	6.52	1.47	-3.01	-14.5	9.61
193	Bergvliet	groundwater	34.045631	18.460297	14	9	5.74	20.6	4.00	0.88	-2.49	-10.5	9.46
194	Bergvliet	groundwater	34.046172	18.447303	21	16	4.65		4.54	1.10	-2.53	-10.1	10.19
195	Bergvliet	groundwater	34.045897	18.445642	19	40	4.40	19.8	5.56	0.81	-2.73	-11.8	10.05
196**	Constantia	groundwater	34.022	18.451	48	25	4.37	22.6	6.48	0.55	-2.18	-9.8	7.64

Sample #	Location	Sample type	Latitude S	Longitude E	Altitude (mamsl)	Depth (m)	Distance from unconformity (km)	Temp (℃)	pH	EC (mS/cm)	$\delta^{18}O$ (‰)	δD (‰)	d-excess (‰)
197	Kirstenhof	groundwater	34.073344	18.447447	10	4	2.42	21.9	7.19	0.68	-1.44	-5.5	6.07
198	Lakeside	groundwater	34.092092	18.465281	4	10	0.73	21.6	7.14	0.83	-2.38	-9.5	9.55
199	Westlake	groundwater	34.082294	18.442681	44	90	0.91	20.8	7.08	0.71	-2.43	-10.9	8.53
200	Westlake	groundwater	34.076292	18.437789	29	45	1.32	21.3	6.65	0.29	-3.12	-13.7	11.22
201	Westlake	groundwater	34.078514	18.441192	28		1.34	23.3	6.63	0.38	-2.72	-10.6	11.21
202	Dreyersdal	groundwater	34.052078	18.454525	16		5.00	20.4	4.04	0.57	-2.52	-10.9	9.25
203	Kirstenhof	groundwater	34.068997	18.454922	9	35	2.57	24.7	5.92	0.57	-2.87	-12.9	10.11
204	Kirstenhof	groundwater	34.070044	18.455233	8	35	2.28	21.2	5.99	0.45	-2.89	-12.4	10.77
205	Kirstenhof	groundwater	34.070139	18.456214	8	35	2.24	23.9	6.01	0.47	-2.96	-13.5	10.20
206	Steenberg Estate	groundwater	34.062764	18.432361	32		2.55	23.9	6.18	0.60	-1.13	-5.3	3.72
207	Kirstenhof	groundwater	34.068347	18.453189	9	18	2.44	20.2	6.35	0.45	-2.94	-13.5	10.00
208**	Tokai	groundwater	34.061	18.444	15	12	3.05	21.0	5.24	1.01	-2.03	-8.3	7.90
209	Bergvliet	groundwater	34.042928	18.447294	31	23	4.24	20.0	4.22	0.53	-2.57	-11.0	9.57
210	Marina Da Gama	groundwater	34.091275	18.475667	5	3	1.49	22.7	7.38	2.79	-1.69	-6.6	6.96
211	Muizenberg	groundwater	34.104617	18.467597	9	9	0.41	20.7	6.24	0.55	-2.93	-11.6	11.84
212	Fish Hoek	groundwater	34.131469	18.424308	12	<10	1.10	20.8	6.47	0.64	-2.79	-11.5	10.86
213	Fish Hoek	groundwater	34.130650	18.424856	9	<10	1.05	21.2	6.69	0.89	-3.28	-14.6	11.60
214	Muizenberg	groundwater	34.110903	18.466425	15		0.25	28.4	6.18	0.30	-4.06	-17.5	14.97
215	Muizenberg	spring	34.107086	18.468378	9		0.42	24.2	6.78	0.17	-1.83	-3.7	10.96
216	Westlake	groundwater	34.087119	18.446622	71		0.38	23.3	6.51	0.56	-3.62	-16.1	12.90
217	Wynberg	groundwater	33.998150	18.463281	76	50	4.04	20.0	6.00	0.16	-2.50	-9.3	10.66
218	Silverglade	groundwater	34.126589	18.413081	20	18	0.39	21.9	6.66	1.43	-3.10	-13.7	11.13
219	Clovelly	river	34.118553	18.417653			0.41	19.8	7.17	0.56	-3.19	-12.0	13.51
220	Clovelly	groundwater	34.122447	18.425150	21	18	0.50	21.9	7.16	0.93	-2.22	-8.5	9.23
221	Fish Hoek	groundwater	34.133022	18.432125	4		0.64	22.2	7.12	0.77	-3.14	-12.8	12.36
222	Fish Hoek	groundwater	34.131986	18.428625	7		0.74	22.0	7.13	1.45	-3.57	-15.8	12.79
223	Fish Hoek	groundwater	34.135978	18.427161	10		0.84	22.6	6.77	1.75	-3.41	-14.,9	12.40
224	Fish Hoek	groundwater	34.135125	18.429053	10		0.98	23.4	6.74	1.16	-3.24	-13.7	12.21
225	Simon’s Town	groundwater	34.203914	18.454131	45	70	0.56	22.0	6.80	1.38	-4.37	-19.9	15.04
226	Pinelands	groundwater	33.936361	18.507317	7	4	5.67	21.0	6.86	2.93	0.24	1.5	-0.38
227	Pinelands	groundwater	33.937328	18.507692	7	20	5.61	20.2	6.25	51.30	-2.79	-13.6	8.70
228	Pinelands	groundwater	33.937328	18.507692	7	35	5.61	20.4	6.18	58.70	-2.41	-13.6	5.67
229	Pinelands	groundwater	33.940869	18.515664	9	4	6.24	22.3	7.07	10.50	-2.79	-12.0	10.33
230	Kensington	groundwater	33.910700	18.505789	15	3	6.89	21.5	6.95	1.25	-2.97	-12.2	11.53
231	Pinelands	groundwater	33.940294	18.499025	15		4.74	24.8	6.86	2.54	-3.73	-16.2	13.67
232	Pinelands	groundwater	33.925497	18.511819	12	6	6.45	23.3	6.84	1.04	-1.99	-7.1	8.81
233	Pinelands	groundwater	33.929950	18.504483	9	8	5.60	29.8	7.44	1.15	-2.32	-7.6	10.95
234	Mowbray	groundwater	33.947256	18.468517	29	100	1.77	20.3	6.89	0.95	-3.20	-11.6	13.98
235	Woodstock	groundwater	33.927528	18.453503	10		2.61	22.8	7.25	1.61	-2.64	-10.4	10.75
236	City Bowl	groundwater	33.932447	18.422106	38		1.89	23.0	6.86	0.71	-2.72	-10.7	11.04

Sample #	Location	Sample type	Latitude S	Longitude E	Altitude (mamsl)	Depth (m)	Distance from unconformity (km)	Temp (℃)	pH	EC (mS/cm)	$\delta^{18}O$ (‰)	δD (‰)	d-excess (‰)
237	Bakoven	groundwater	33.962456	18.379314	72	4	1.20	24.8	7.09	0.40	-3.28	-13.1	13.18
238	Seapoint	groundwater	33.912472	18.389061	7		2.39	26.3	6.78	0.26	-1.31	-1,5	9.00
239	Three Anchor Bay	groundwater	33.908403	18.395914	12		2.86	22.5	7.04	6.60	-2.99	-12.3	11.67
240	Greenpoint	spring	33.904714	18.402278	8		3.46	26.6	7.41	0.19	-2.17	-7.2	10.17
241	Westlake	groundwater	34.075658	18.433253	41	50	1.30	21.0	6.93	0.63	-2.94	-12.3	11.23
242	Muizenberg	groundwater	34.116306	18.461644	12		0.27	19.0	6.92	0.39	-3.91	-16.9	14.40
243	Fish Hoek	groundwater	34.130847	18.421717	16	60	1.23	21.6	6.83	1.15	-3.26	-14.8	11.31
244	Glencairn	groundwater	34.154600	18.418219	33	6	0.34	24.6	6.65	2.02	-3.53	-15.3	12.91
245	Murdock Valley	groundwater	34.219544	18.461619	82		0.33	18.9	5.23	0.17	-3.94	-15.2	16.32
246	Simon’s Town	groundwater	34.193272	18.429286	26		0.62	24.9	5.75	0.99	-3.87	-16.5	14.42
247	Glencairn Heights	river	34.153075	18.430547	86		0.16	20.4	5.34	1.21	-4.06	-18.6	13.85
248	Lakeside	spring	34.090161	18.454056	58		0.05	24.2	4.30	0.56	-3.86	-16.8	14.08
249	Tokai	groundwater	34.063367	18.439936	22	5	2.79	22.2	5.94	0.96	-2.59	-10.7	10.00
250	Wynberg	groundwater	34.003011	18.463681	57	40	4.25	23.6	6.67	0.13	-1.68	-3.0	10.41
251	Plumstead	groundwater	34.019436	18.480608	20	11	6.46	20.7	6.24	1.18	-1.95	-7.6	7.99
252	Kenwyn	groundwater	33.997194	18.493528	23		6.37	22.3	6.12	0.46	-2.65	-11.5	9.72
253*	Rondebosch	groundwater	33.962181	18.478608	23		2.93		6.07	0.71	-3.31	-12.0	14.46
254*	Rondebosch	groundwater	33.962181	18.478608	23		2.93		6.44	0.68	-3.23	-12.1	13.76
255*	Muizenberg	groundwater	34.117528	18.459925	14		0.30		4.55	0.44	-4.02	-16.7	15.49
256*	Ottery	groundwater	34.022486	18.512589	15		10.10		6.29	0.64	-2.37	-8.2	10.73

* sample site uncertain
** not divulged at request of the owner

The EC of the water samples ranges between 0.11 mS/cm and 58.70 mS/cm and the median EC for the 256 samples is 0.72 mS/cm (Table 4.2). The δD values range from -19.9‰ to +13.7‰, whereas the $\delta^{18}O$ values range from -4.37‰ to +2.35‰. The spring water samples have average δD and δ $\delta^{18}O$ values of -10.6‰ and -2.85‰, respectively, and the river water samples have average δD and $\delta^{18}O$ values of -10.0‰ and -2.61‰, respectively. The average δD and $\delta^{18}O$ values for the groundwater samples are -10.2‰ and -2.57‰, respectively. By comparison, the average δD and $\delta^{18}O$ values for the stagnant surface water samples 39, 40 and 41 are +10.9‰ and +1.95‰, respectively. The d-excess of the groundwater ranges from -0.38‰ to +16.32‰ and the average d-excess is +10.44‰, whereas the stagnant surface samples 39, 40 and 41 have d-excess values of -4.57‰, -4.54‰ and -5.10‰ respectively. The pH ranges from a minimum of 4.00 to a maximum of 7.93 with an average of 6.44.

Table 4.2: Summary statistics of the raw dataset contained in Table 4.1.

Sample type		Temp (℃)	pH	EC (mS/cm)	$\delta^{18}O$ (‰)	δD (‰)	d-excess (‰)
All	Min	18.2	4.00	0.11	-4.37	-19.9	-0.38
	Max	37.1	7.93	58.70	2.35	13.7	16.32
	Median	22.2	6.52	0.72	-2.59	-10.6	10.47
	Average	22.5	6.44	1.75	-2.53	-10.2	10.48
	SD	2.5	0.78	5.83	0.76	4.0	2.56
Groundwater	Min	18.2	4.00	0.11	-4.37	-19.9	-0.38
	Max	37.1	7.93	58.70	0.24	4.2	16.32
	Median	22.2	6.48	0.72	-2.60	-10.6	10.44
	Average	22.5	6.44	1.52	-2.58	-10.2	10.44
	SD	2.5	0.76	5.11	0.57	3.2	1.93
River	Min	19.8	5.34	0.24	-4.06	-18.6	4.94
	Max	22.6	7.17	1.21	-1.05	-3.4	13.85
	Median	20.4	6.54	0.67	-2.68	-9.0	12.44
	Average	20.9	6.35	0.69	-2.61	-10.0	10.92
	SD	1.5	0.93	0.41	1.30	6.8	4.14
Spring	Min	19.0	4.30	0.17	-3.91	-16.9	10.17
	Max	26.6	7.41	0.56	-1.83	-3.7	14.40
	Median	24.2	6.92	0.39	-2.47	-8.3	11.51
	Average	23.5	6.52	0.35	-2.85	-10.6	12.22
	SD	3.2	1.26	0.16	0.97	6.0	1.90
Stagnant surface water	Min	23.5		1.74	1.38	6.5	-5.10
	Max	24.0		35.70	2.35	13.7	-4.54
	Median	23.8		35.20	2.13	12.5	-4.57
	Average	23.8		24.21	1.95	10.9	-4.74
	SD	0.3		19.46	0.51	3.8	0.32

4.1 pH

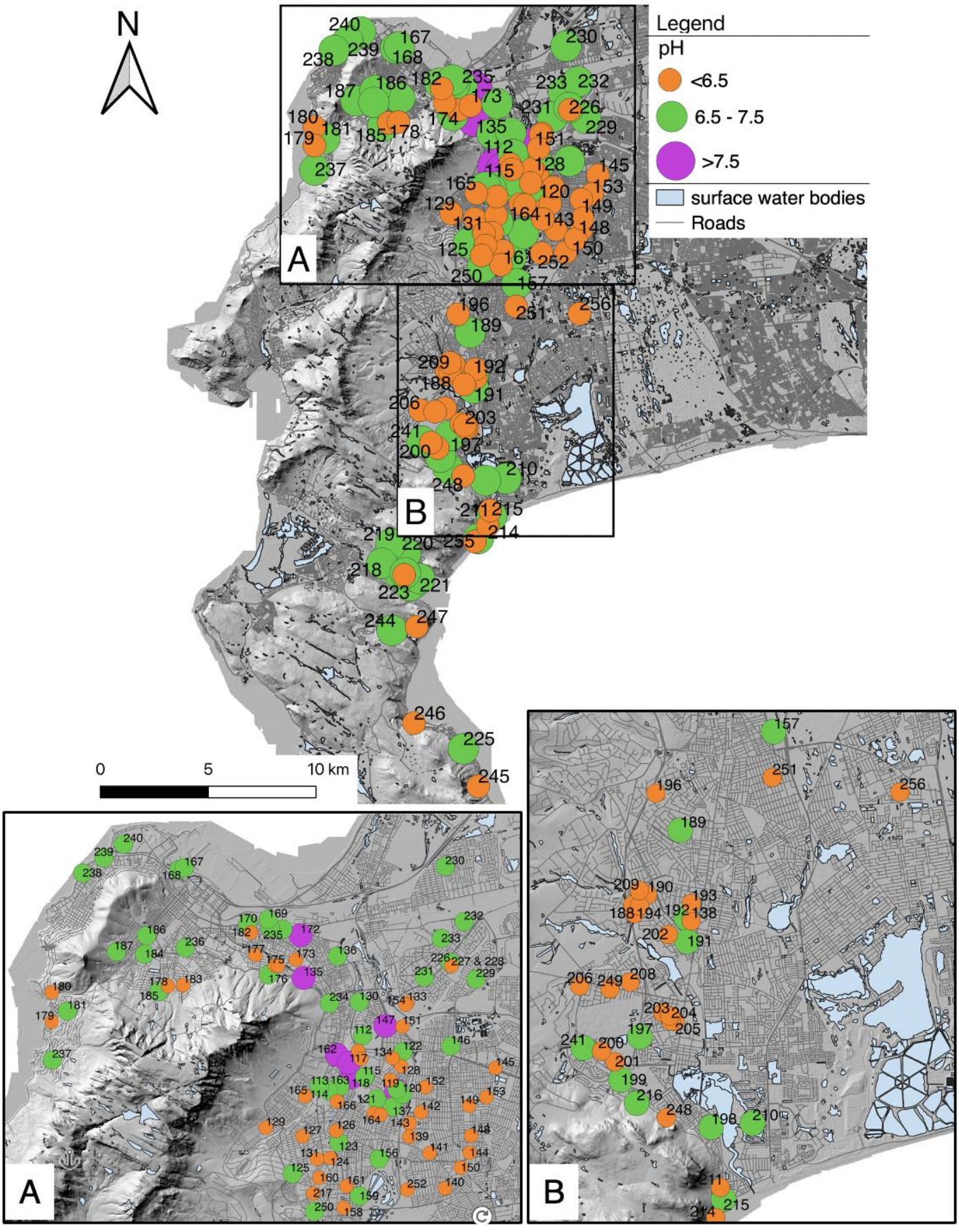

Figure 4.1: The spatial distribution of the water samples with pH measurements (where the number refers to the sample number)(adapted from the City of Cape Town Open Data Portal [CoCT ODP], 2015a; City of Cape Town Open Data Portal [CoCT ODP], 2015b; City of Cape Town. Open Data Portal [CoCT ODP], 2016).

The majority of the water samples have an acidic or neutral pH. However, a number of samples, including samples 116, 117, 118, 135, 147, 162 and 172, have pH readings >7.5 i.e. they are alkaline. These samples predominantly occur towards the northeast of the map (Figure 4.1).

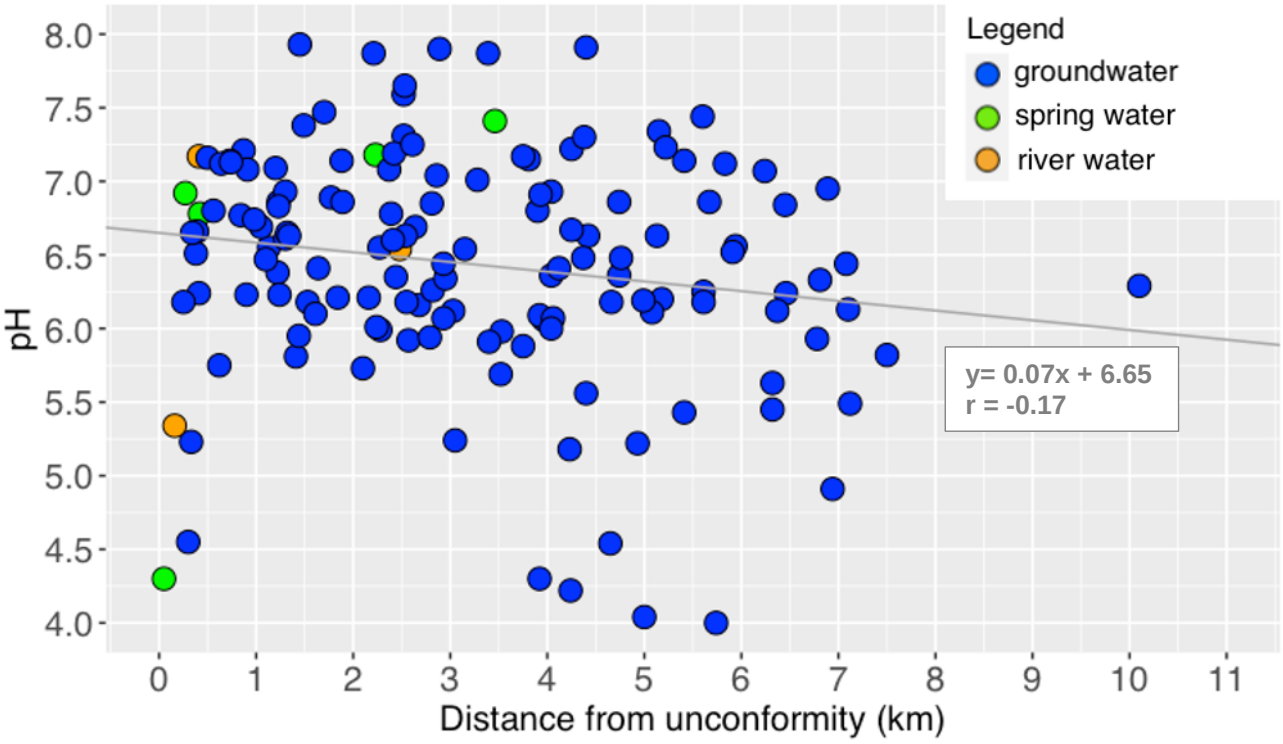

Figure 4.2: The relationship between the water samples with pH measurements and their distance from the TMG and Malmesbury Group unconformity.

The distance from the TMG and Malmesbury Group unconformity ranges from 0.05 km to 10.10 km for the water samples presented above (Figure 4.2). The data appears to be relatively scattered, however there is a minor but discernable pattern for the pH to decrease with increasing distance from the unconformity. The correlation coefficient for the pH and the distance from the TMG and Malmesbury Group unconformity of the water samples is low (r = -0.17).

4.2 Electrical conductivity (EC)

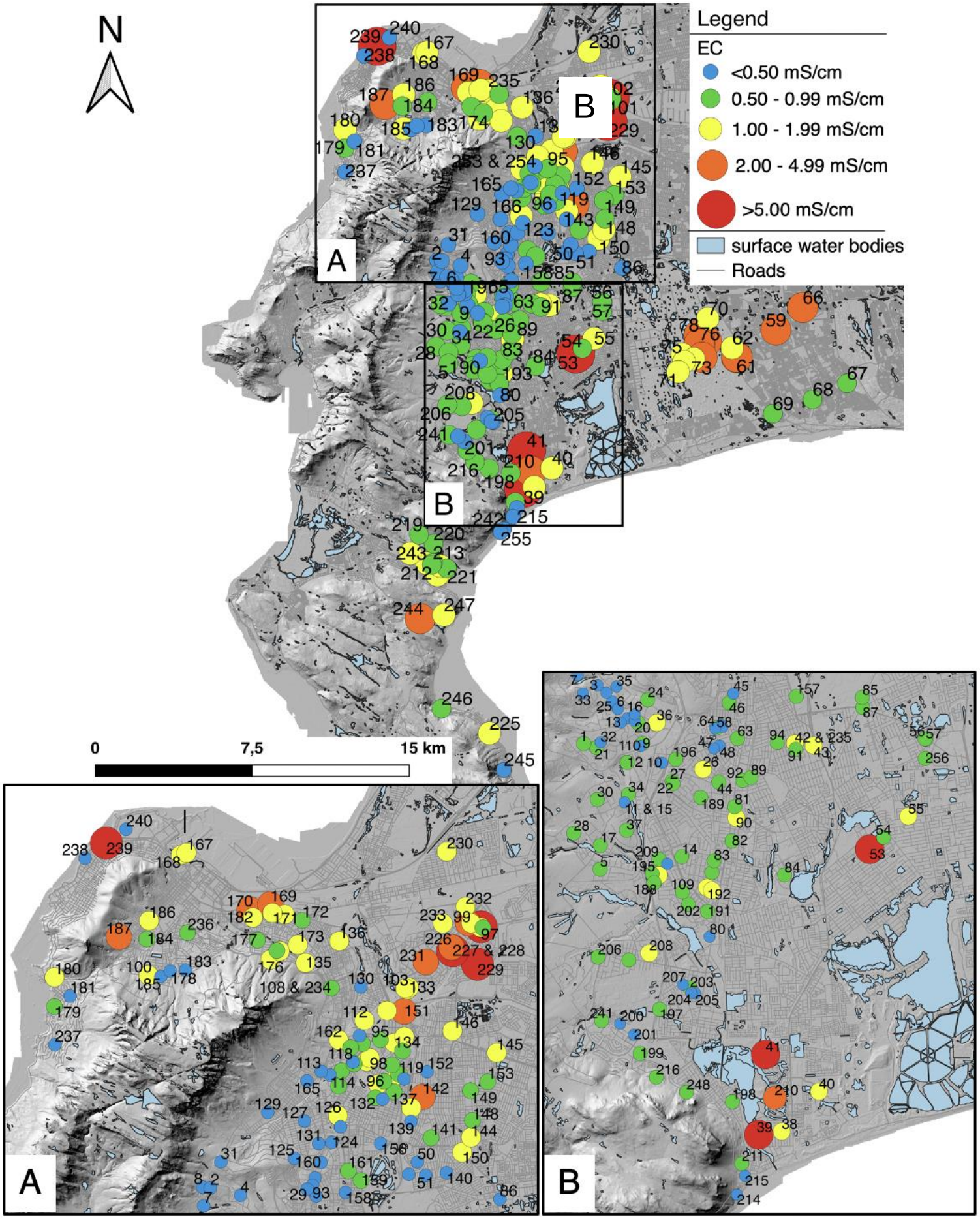

Figure 4.3: The spatial distribution of the water samples with EC measurements (where the number refers to the sample number) (adapted from CoCT ODP, 2015a; CoCT ODP, 2015b; CoCT ODP, 2016).

Seawater has an EC of approximately 50.00 mS/cm (Mary River Catchment Coordinating Committee, 2013). The surface water samples, from Sandvlei estuary, samples 39 and 41, have relatively elevated EC measurements of 35.70 mS/cm and 35.20 mS/cm, respectively. In contrast, the Capricorn Park lake sample (sample 40) has a relatively low EC of 1.74 mS/cm, and the river samples (samples 101, 130, 219 and 247) collected from Elsieskraalrivier in Pinelands, the Black River from Rhodes High School, the Silvermynrivier from the Clovelly Country Club, and a stream in Glencairn Heights have even lower EC values of 0.77 mS/cm, 0.24 mS/cm, 0.56 mS/cm and 1.21 mS/cm, respectively. The spring water samples (samples 113, 215, 240, 242 and 248) collected from Westerford High School in Rondebosch, False Bay College in Muizenberg, Greenpoint Urban Park, St. James and Boyes Drive have EC measurements of 0.42 mS/cm, 0.17 mS/cm, 0.19 mS/cm, 0.39 mS/cm and 0.56 mS/cm, respectively.

There appears to be a pattern in the EC measurements of the groundwater samples across the study area. The majority of the groundwater samples that were collected at higher altitudes (>30 mamsl), on the eastern slopes of Table Mountain and Constantiaberg have EC measurements of <1 mS/cm. At lower altitudes (<30 mamsl) the EC measurements are generally higher. For example, Philippi Farmlands and Mitchells Plain have higher EC measurements than those in Wynberg and Retreat. The suburbs of Newlands, Bishopscourt and Constantia have particularly low EC measurements of <0.5 mS/cm. Pinelands, which is located at relatively low altitudes of 7 - 16 mamsl, has groundwater with especially high EC measurements of up to 58.70 mS/cm. Samples 53 and 239, collected from the SPCA located in Grassy Park and in Three Anchor Bay, both located at relatively low altitudes of 12 mamsl also have comparatively high EC measurements of 5.53 mS/cm and 6.60 mS/cm, respectively.

However, there are a number of exceptions to this pattern of lower EC at higher altitudes and higher EC at lower altitudes. There are a number of samples which have comparatively high isotopic values even though they are located at relatively high altitudes such as samples 36, 112, 126, 135, 147, 162, 173, 174, 176, 180, 186 and 187. Many of these samples occur towards the north and northeast of the study area. In addition, the samples collected along the coast of Mitchells Plain (samples 67, 68 and 69) have lower EC measurements than expected for the low-lying area with values of 0.67 mS/cm, 0.76 mS/cm and 0.71 mS/cm, respectively. A plot of EC vs. altitude was not included because the range in altitude is not great enough across the study area to show a statistically significant relationship.

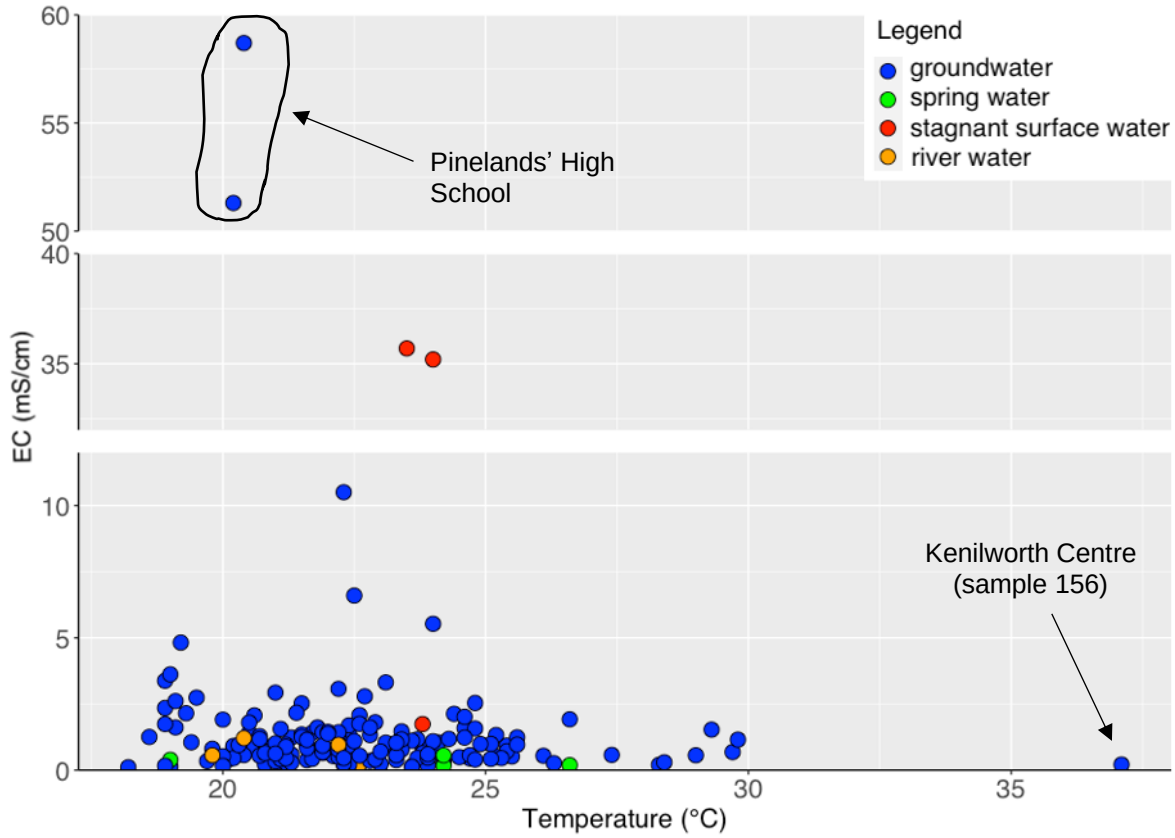

Figure 4.4: The relationship between the water samples with temperature measurements and their EC.

Overall, it appears that the groundwater samples have low EC and temperature measurements in comparison to the stagnant surface water samples, and similar EC and temperature measurements to the spring and river water samples. There are, however, several groundwater samples that deviate from this pattern and have higher EC and temperature measurements than the stagnant surface samples. For example, samples 227 and 228, collected from Pinelands High School have much higher EC measurements than the stagnant surface water samples, and sample 156 collected from Kenilworth Centre has a much higher temperature than the stagnant surface water samples. The groundwater samples with relatively high temperatures may be warmer than expected because they may not have been pumped for long enough i.e., the water may have been sitting in a tank or pipe above the ground. For example, sample 156 has a very high temperature of 37.1 ℃ because it was collected from a tank that was supplied water by a dark-coloured pipe connected to the borehole, which runs along the roof of the shopping centre, and lies in the sun. There was no way to directly sample the freshly pumped borehole water.

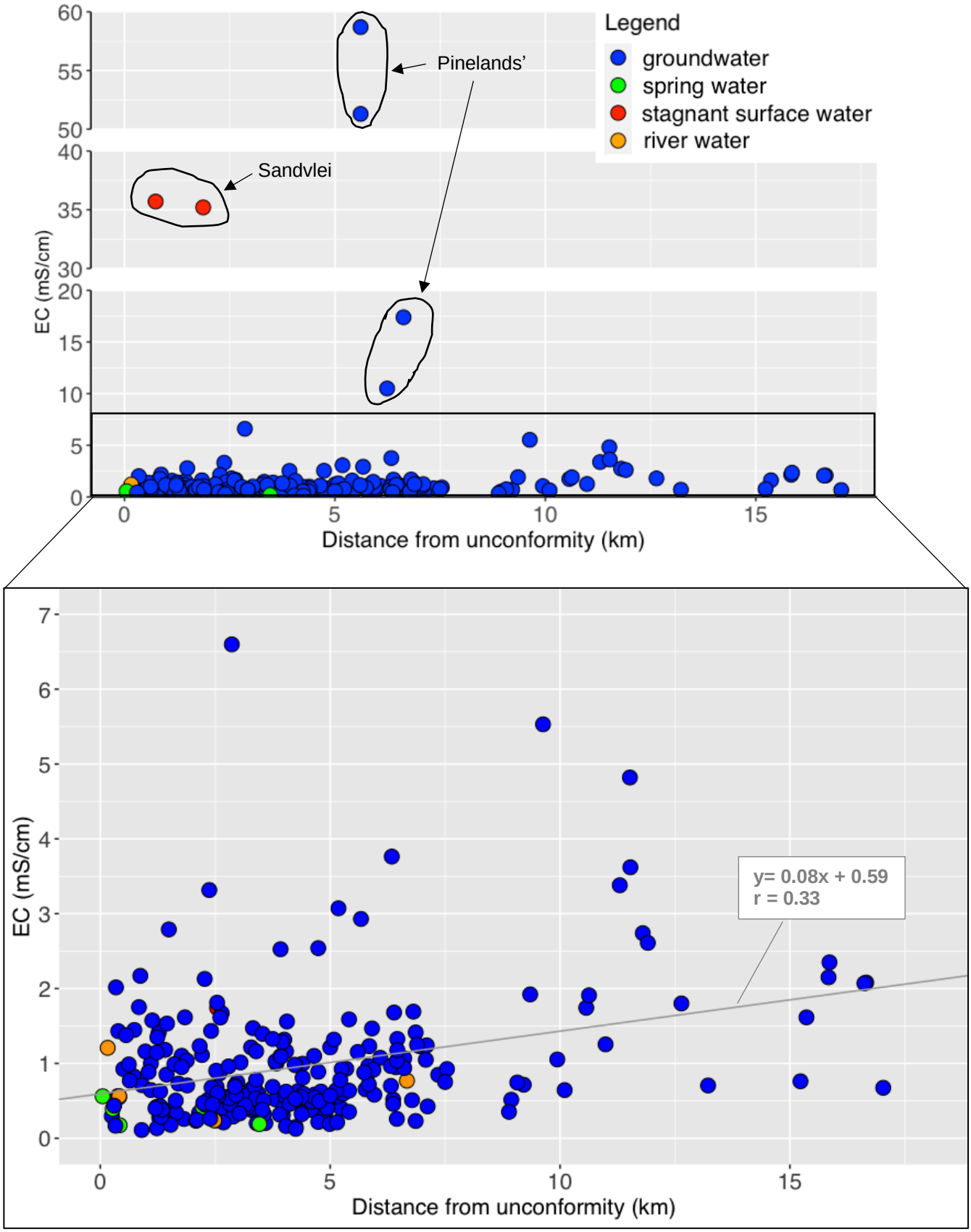

Figure 4.5: The relationship between the water samples with EC measurements and their distance from the TMG and Malmesbury Group unconformity (where r= 0.33 when omitting the outliers).

The distance from the unconformity ranges from 0.05 km to 17.03 km for the data presented above (Figure 4.5). There are 6 samples that are clear outliers in the dataset. They are located relatively close to the unconformity, but they have very high EC values (>10 mS/cm). These samples (samples 39, 41, 97, 227, 228 and 229) were collected from Sandvlei and the suburb of Pinelands (a household, Pinelands High School and the Grace School). The correlation coefficient of the EC and the distance from the TMG and Malmesbury Group unconformity of the water samples is 0.33 when omitting the outliers (samples 39, 41, 97, 227, 228 and 229).

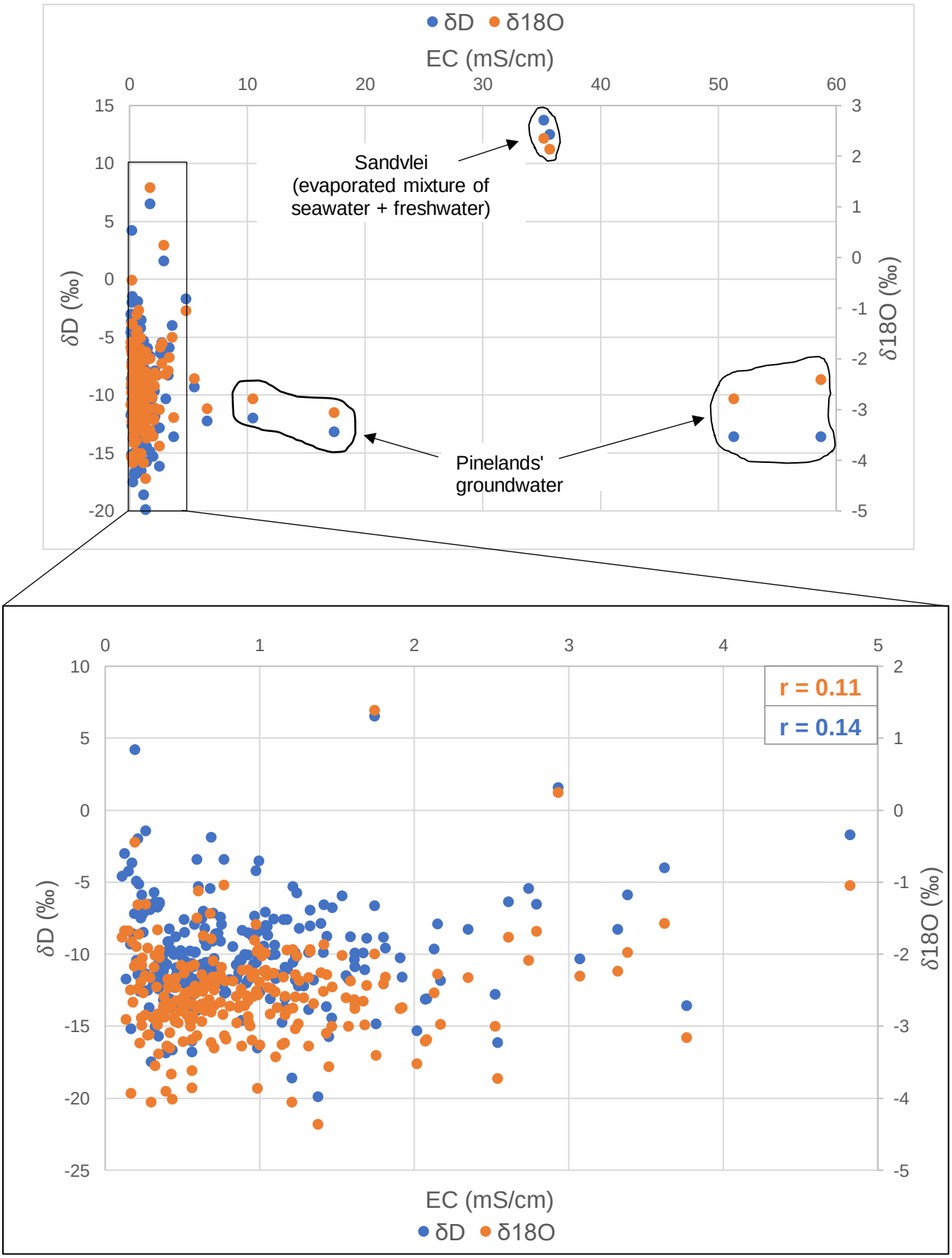

Figure 4.6: The relationship between the water samples with EC measurements and their δD and δ^{18}O values (where the Pearson r values are calculated for the inset data only).

There are 4 clusters of data points: 3 clusters with EC values of >15 mS/cm and 1 large cluster of data points with EC values of <10 mS/cm (Figure 4.6). The 3 clusters of data points with EC values of >15 mS/cm are the surface water samples collected from Sandvlei (samples 39 and 41) with positive isotopic values, and the groundwater samples collected from Pinelands (samples 97, 227, 228 and 229) with negative isotopic values, whereas the large cluster of data points with EC values of <10 mS/cm consists of the rest of the water samples (including the groundwater, the spring water, river samples and the stagnant surface water sample collected from the Capricorn Park lake). Overall, there does not appear to be an obvious relationship between the EC measurements of the water samples and their δD and $\delta^{18}O$ values.

4.3 Stable isotope composition of all the water samples

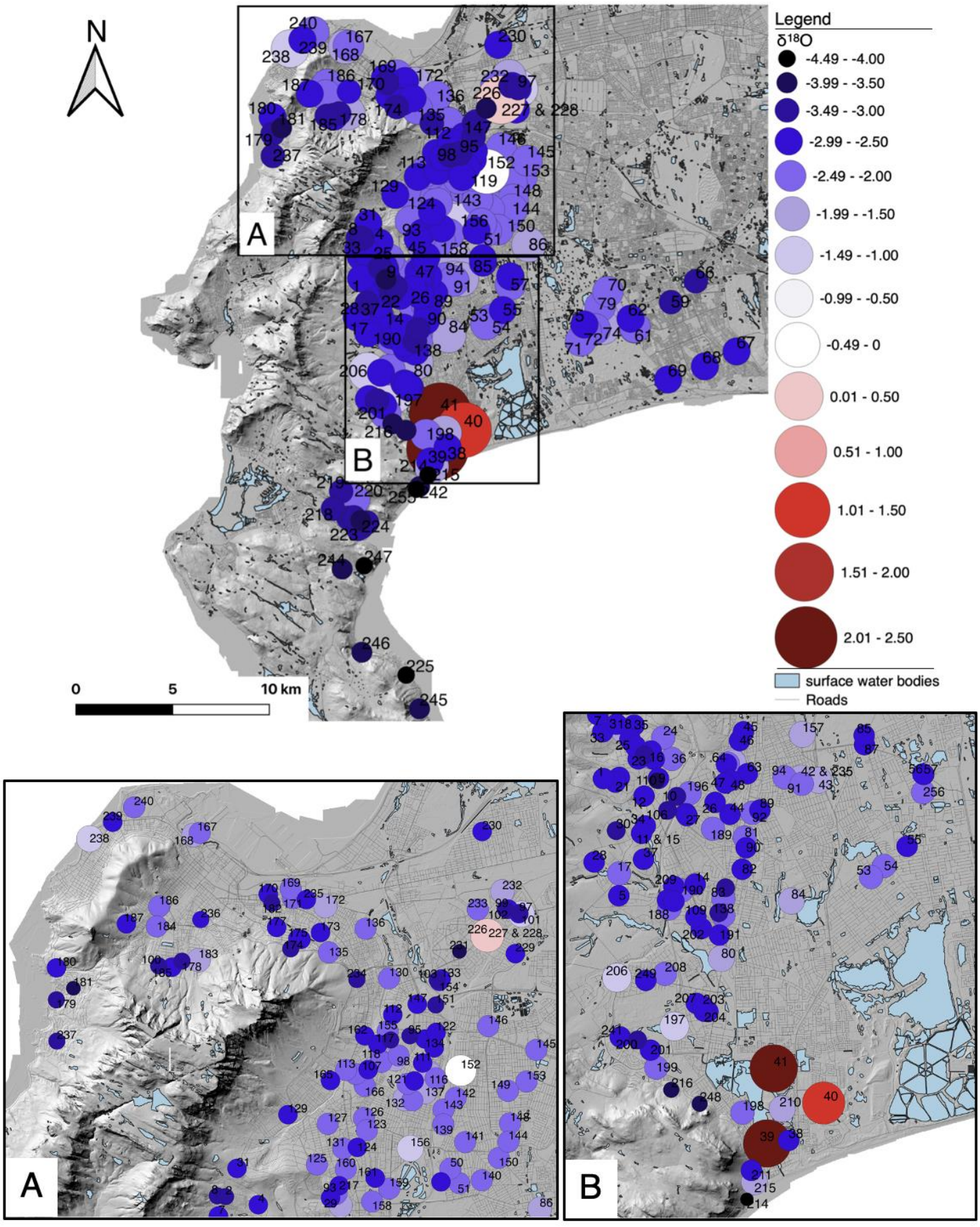

Figure 4.7: The spatial distribution of the water samples with measured $\delta^{18}O$ values (where the number refers to the sample number) (adapted from CoCT ODP, 2015a; CoCT ODP, 2015b; CoCT ODP, 2016).

The surface water samples collected at Sandvlei estuary and Capricorn Park lake are clearly visible on the map due to their positive $\delta^{18}O$ values (shown in red; Figure 4.7). Sample 226, which was collected from a shallow wellpoint in Pinelands, is also apparent due its positive $\delta^{18}O$ value (shown in pink; Figure 4.7). There is not a very clear spatial pattern for the $\delta^{18}O$ values of the groundwater samples across the study area. However, in general, it appears that the $\delta^{18}O$ values are more negative at higher altitudes (>30 m), and less negative at lower altitudes in areas such as Philippi Farmlands and the suburb of Pinelands (Figure 4.7). The samples collected towards the south of the study area, along the eastern slopes of Swartkop, have particularly low $\delta^{18}O$ values (Figure 4.7).

There are a number of outliers to this relationship. Several groundwater samples that are located along the eastern slopes of Table Mountain and Constantiaberg have less negative $\delta^{18}O$ values than expected, for example samples 49 & 250, 197 and 206 (Figure 4.7). In addition, the samples collected in Mitchells Plain (samples 59, 66, 67, 68 and 69) also deviate from the relationship between the $\delta^{18}O$ values and the altitude (Figure 4.7). These samples have more negative $\delta^{18}O$ values than expected. The distribution of the water samples and their δD values is not shown because oxygen and hydrogen are highly correlated.

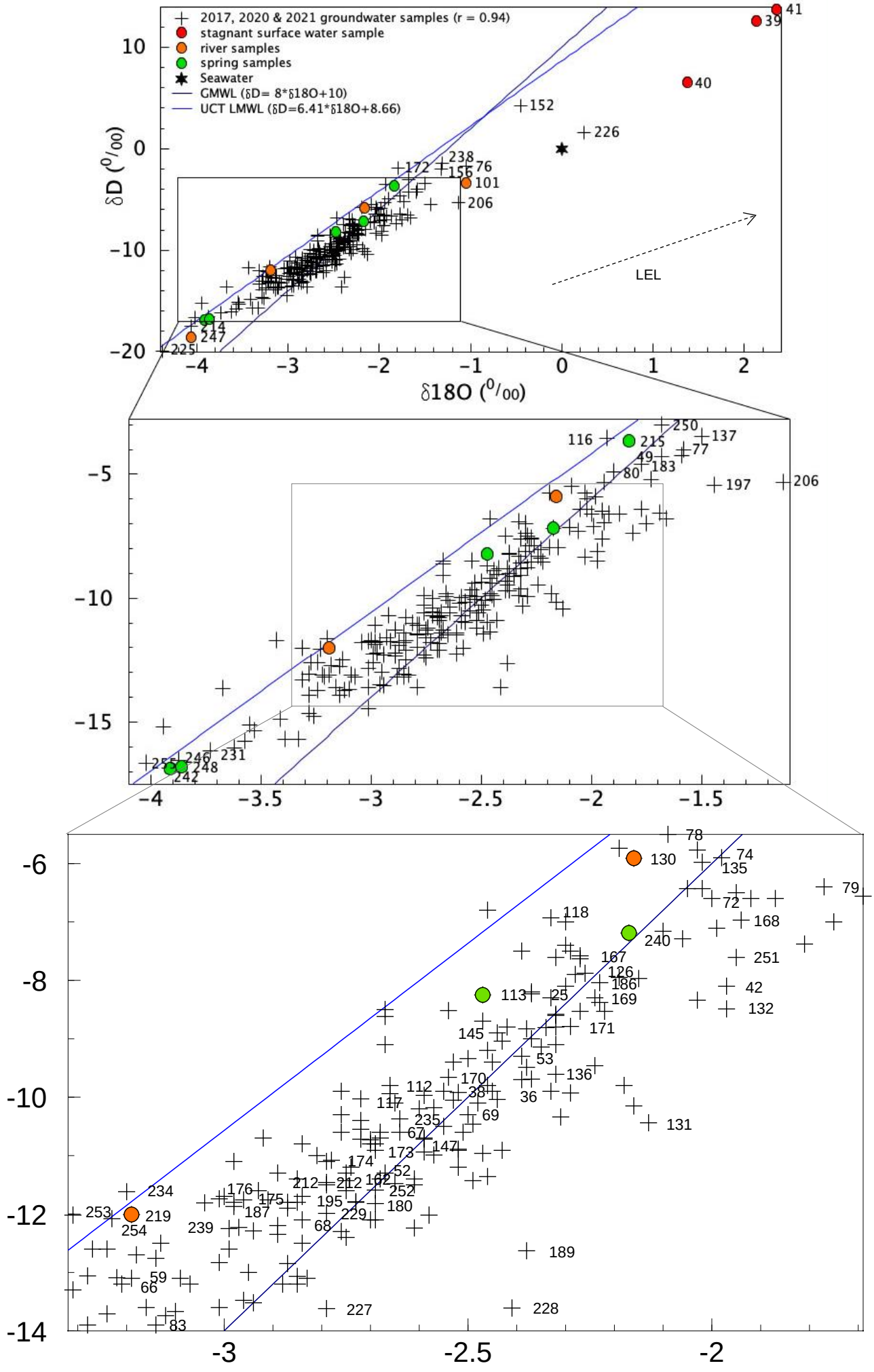

Figure 4.8: δD vs. δ^{18}O values of the water samples compared to the GMWL, the LMWL defined by Harris et al. (2010) using the RMA method, the LEL and seawater isotope data.

The surface water samples 39, 40 and 41, generally, have much higher δD and $\delta^{18}O$ values than the rest of the water samples, as discussed previously. They plot significantly below the GMWL and LMWL. In comparison, the groundwater, spring and river samples generally have much lower δD and $\delta^{18}O$ values and they mostly plot near or on the GMWL and below the LMWL, except for sample 101 which is shifted slightly to the right of the GMWL and the LMWL.

The δD and $\delta^{18}O$ values of the groundwater data are well-correlated with a correlation coefficient of 0.94. The groundwater samples 152 and 226 have elevated δD and $\delta^{18}O$ values in comparison to the rest of the groundwater dataset. Sample 226 appears to have been shifted significantly to the right of the LMWL and GMWL. It plots relatively close to the stable isotope value of seawater, with δD and $\delta^{18}O$ values of +1.54‰ and +0.24‰, respectively. Samples 49 & 250, 137, 156, 172, 197, 206 and 238 also have relatively high δD and $\delta^{18}O$ values. In contrast, samples 214, 225, 242, 246, 247, 248 and 255 have the lowest δD and $\delta^{18}O$ measurements with δD and $\delta^{18}O$ values that range from -19.91‰ to -16.54‰, and from -4.37‰ to -3.86‰, respectively. These samples have been collected from the eastern slopes of the Cape Peninsula mountains towards the southern extent of the study area (Figure 4.8).

The majority of the samples from Philippi Farmlands (samples 72, 74, 76, 77, 78, 79 and 80) have relatively high δD and $\delta^{18}O$ values and plot slightly towards the right of the LMWL and the GMWL. A number of other samples plot towards the right of the LMWL and the GMWL such as samples 228 and 189. In comparison, the samples collected at higher altitudes, along the eastern slopes of the Cape Peninsula mountain range, generally have lower δD and $\delta^{18}O$ values and mostly plot in between the LMWL and the GMWL.

4.4 Stable isotope composition of the groundwater samples

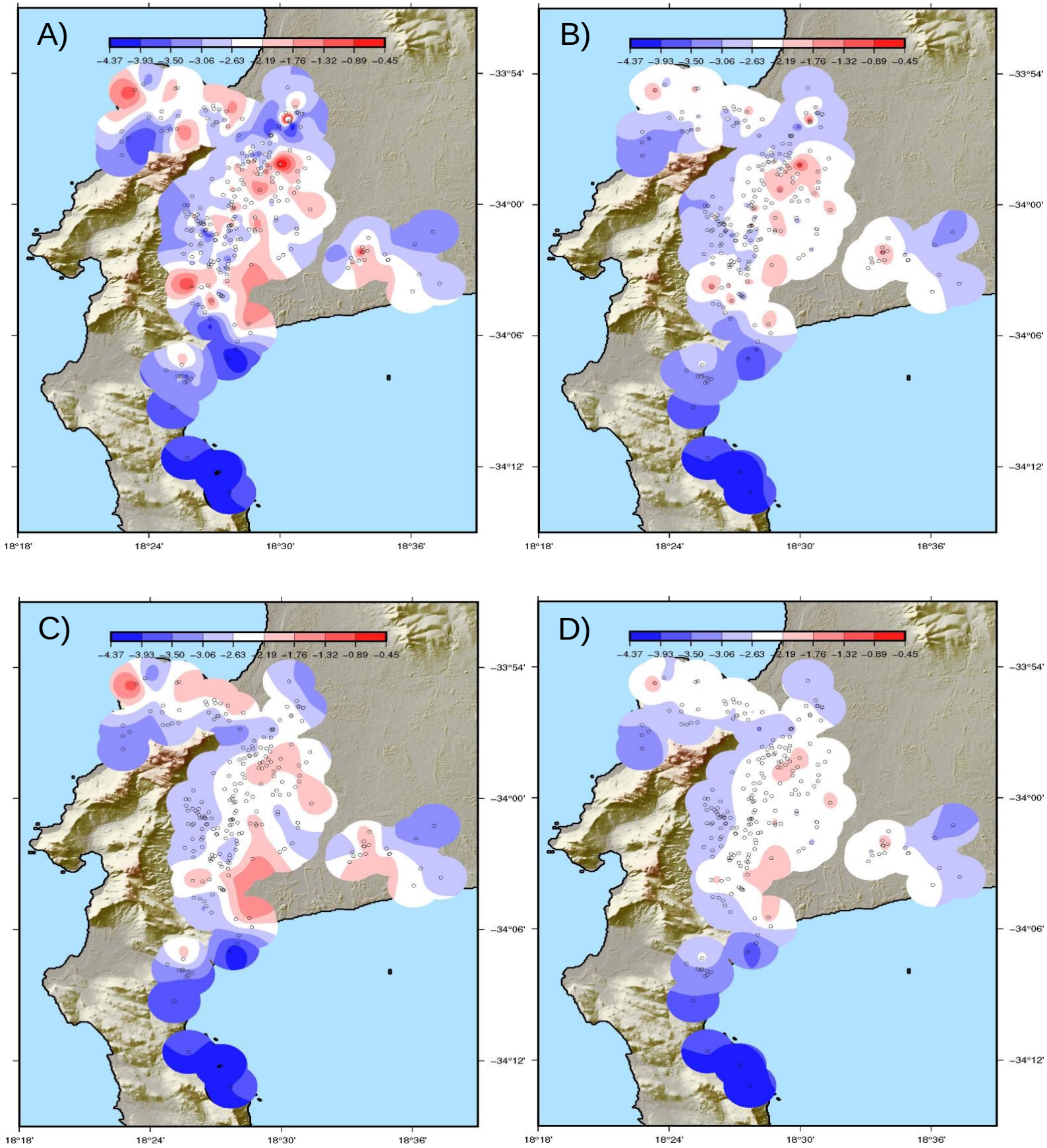

Figure 4.9: Oxygen isoscapes of the groundwater data produced using the A) *surface* command with minimum curvature, B) *surface* command with a tension factor of 0.25, C) *blockmean* command with minimum curvature and D) *blockmean* command with a tension factor of 0.25 in GMT (DEM from Copernicus, 2021).

Two methods were used to produce these isoscapes: 1) in Figure 4.9A and Figure 4.9B the raw data were simply interpolated using continuous curved splines using the *surface* command. The grid was masked everywhere >1 arcminute away from a data point. In Figure 4.9A the minimum curvature (smoothest) solution was found, but in Figure 4.9B the tension factor was increased to 0.25. The grid was masked everywhere more than 1 arcminute away from a data point.

In Figure 4.9C and Figure 4.9D the original point data were first averaged within 1 arcminute blocks using the *blockmean* command. This resulted in a new set of point data with each point having the mean value and location of all of the original data points within that block. This technique reduces the effect of individual anomalous points which may have been affected by processes such as evaporation. These data were then interpolated using the *surface* command as described above.

The isoscapes do not show a very clear pattern in the $\delta^{18}O$ values across the study area. In general, the isoscapes display a narrow band of relatively low oxygen isotope values surrounding the mountain ranges (at higher altitudes), while in areas located further from the mountain (at lower altitudes), the oxygen isotope values are more positive and variable.

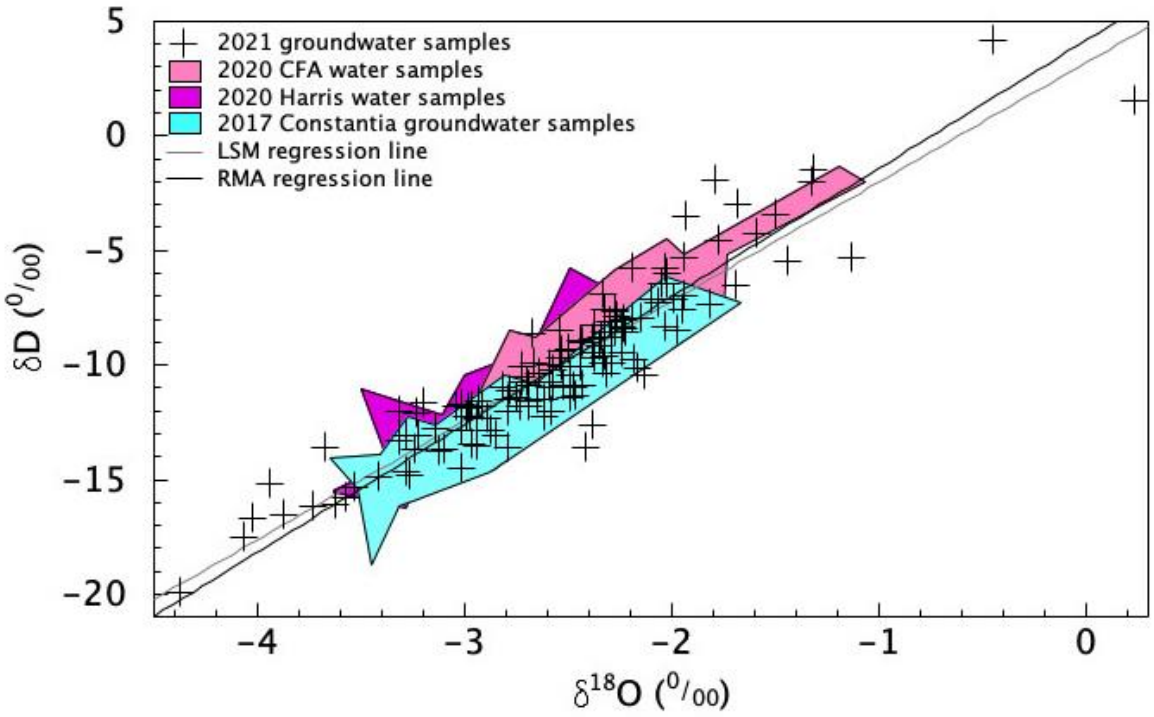

Figure 4.10: Comparison of the δD vs. δ^{18}O values of the 2021 groundwater samples and their lines of best fit with the 2017 Constantia groundwater, the 2020 Cape Flats Aquifer (CFA) samples and the water samples collected by Harris (2020).

Two methods were used to determine the line of best fit of the 2021 groundwater samples: 1) the LSM and 2) the RMA method. The LSM generated the following equation for the line of best fit: $\delta D = 5.20*\delta^{18}O + 3.17$, whereas the RMA method calculated the line of best fit as: $\delta D = 5.58*\delta^{18}O + 4.14$. Both of these lines of best fit have lower y-intercept values than the GMWL ($\delta D = 8*\delta^{18}O + 10$) and the LMWLs (LSM: $\delta D = 5.55*\delta^{18}O + 6.11$; RMA method: $\delta D = 6.41*\delta^{18}O + 8.66$) defined by Harris et al. (2010) at UCT. The lines of best fit for the groundwater have y-intercept values that are much more similar to the recent LMWL calculated (LSM: δD = 5.15* δ18O + 5.05 and the RMA method: δD = 5.90* δ18O + 6.84), based on 12 years of rainfall data collected between 2009 – 2020 (Kasolo, 2020).

In general, the Constantia groundwater, collected in 2017, has slightly more negative δD and δ^{18}O values than the CFA groundwater samples, that were collected in 2020. The groundwater collected in 2021 overlaps with the groundwater data from Constantia, and the groundwater data from the Cape Flats and Southern Suburbs, and data collected by Harris (2020). However, the 2021 samples have a broader isotopic range than the Constantia, CFA and Harris' (2020) groundwater samples (Figure 4.10).

4.4.1 Comparison with UCT precipitation dataset

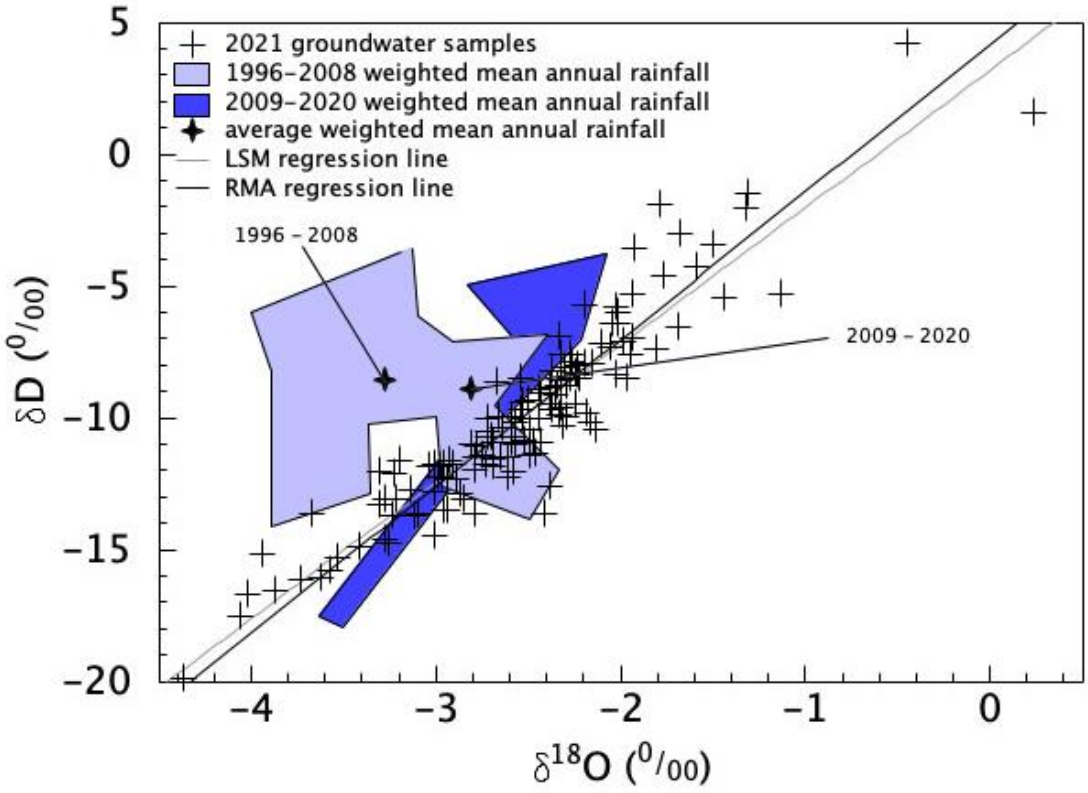

Figure 4.11: Comparison of the δD and δ^{18}O values of the 2021 groundwater samples and their lines of best fit with the weighted mean annual rainfall for 1996 – 2008 and 2009 – 2020.

The average δD and δ^{18}O values of the weighted mean annual rainfall experienced from 1996 – 2008 is -8.6‰ and -3.28‰, and the average δD and δ^{18}O values of the weighted mean annual rainfall experienced from 2009 – 2020 is -8.9‰ and -2.81‰. Majority of the groundwater samples collected in 2021 plot closer to the field of the weighted mean annual rainfall for 2009 – 2020 than the field of the weighted mean annual rainfall for 1996 – 2008.

4.4.2 Comparison with the Table Mountain spring dataset

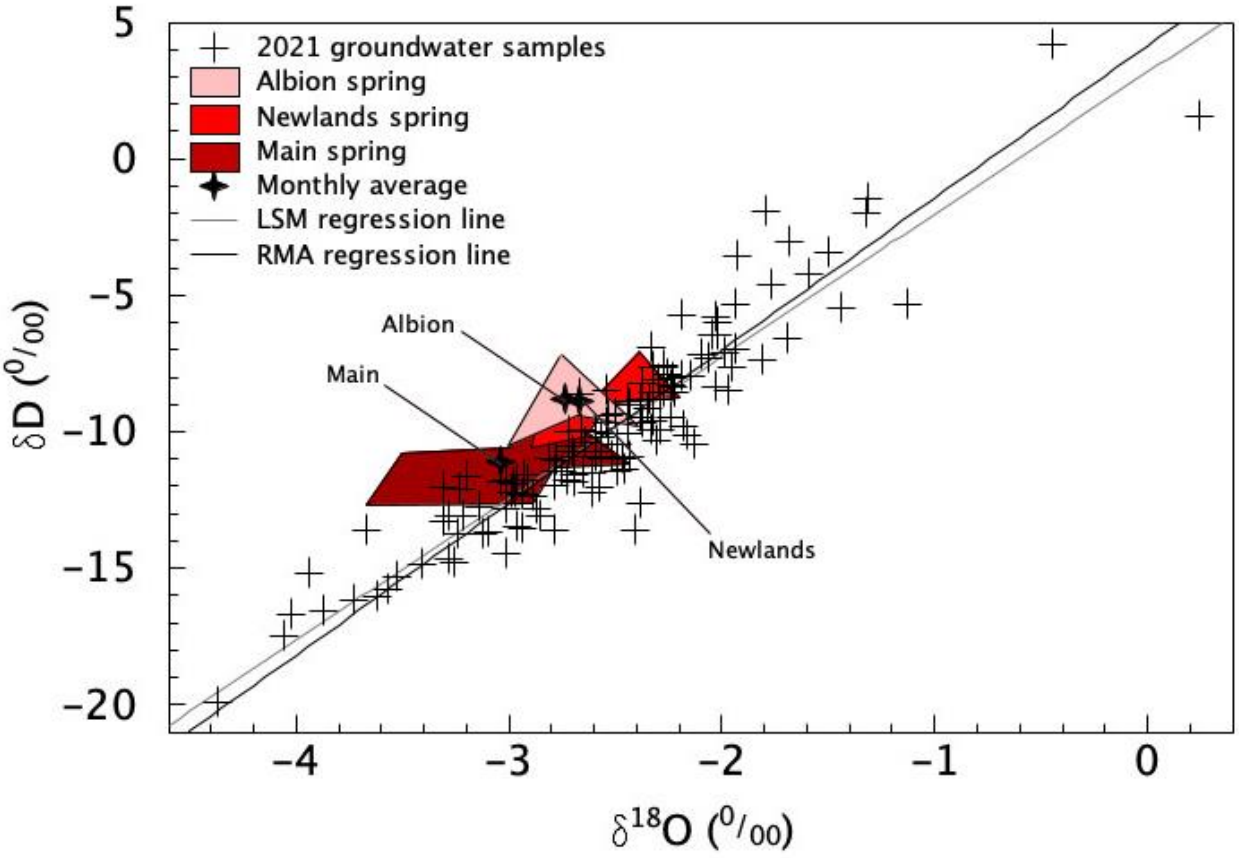

Figure 4.12: Comparison of the δD and δ^{18}O values of the 2021 groundwater samples and their lines of best fit with the Table Mountain spring water data.

The Main, Newlands and Albion spring have monthly average δD values of -11.1‰, -8.9‰, and -8.8‰, respectively, and monthly average δ^{18}O values of -3.04‰, -2.67‰ and -2.74‰, respectively, for the months of September 2019, October 2019 and November 2019, as well as January 2020 for the Main spring. The data fields of the Main and Albion springs plot slightly beyond the range of the 2021 groundwater samples. They have slightly higher δD values at given δ^{18}O values of the groundwater samples collected in 2021 from predominantly the eastern slopes of the Cape Peninsula mountain range.

4.4.3 Comparison with Daws' dataset

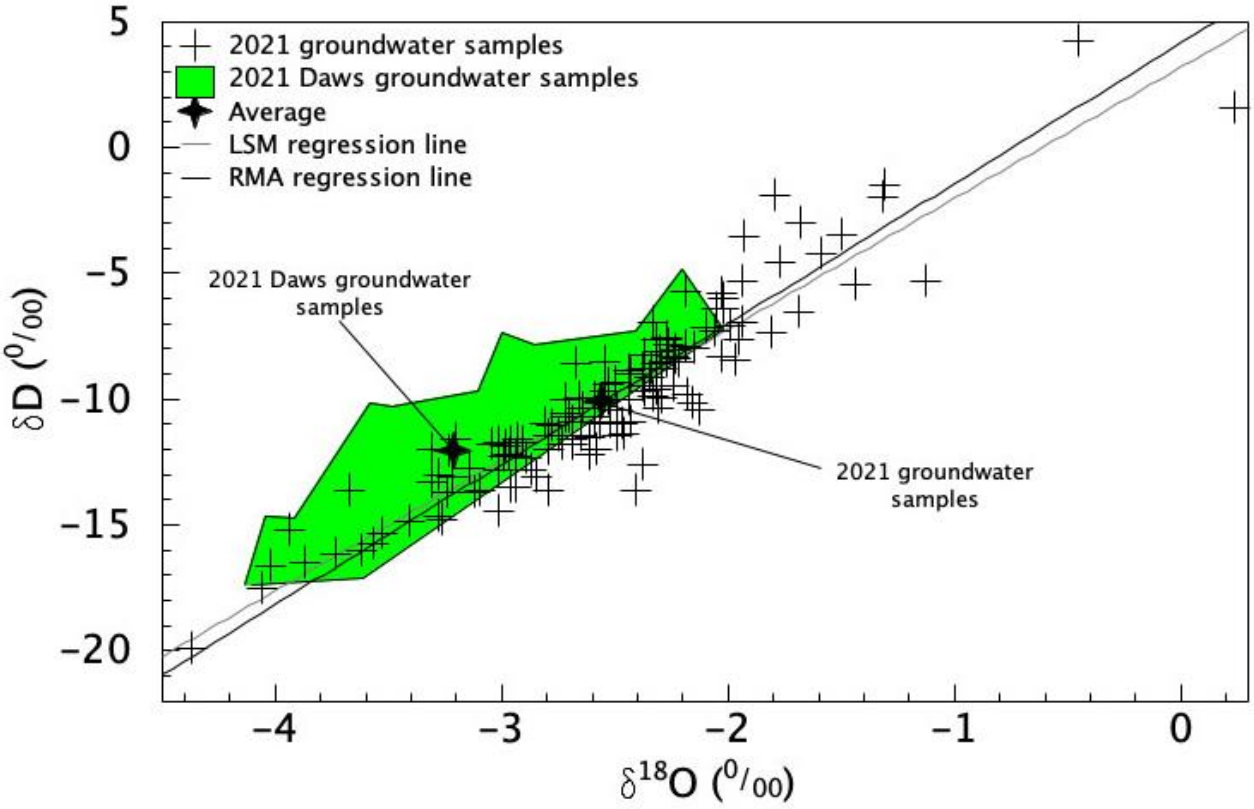

Figure 4.13: Comparison of the δD and δ^{18}O values of the 2021 groundwater samples and their lines of best fit with the groundwater samples collected by Daws (2021).

A comparison of the δD and δ^{18}O values of the 2021 groundwater samples collected in this study is made with the δD and δ^{18}O values of the groundwater samples collected by Daws (2021). The δD and δ^{18}O values for the groundwater samples collected by Daws (2021) is generally more negative with average values of -12.1‰ and -3.21‰ in comparison to the groundwater samples collected from predominantly the eastern slopes of the Cape Peninsula mountain range with average δD and δ^{18}O values of -10.1‰ and -2.56‰, respectively (Figure 4.13). In addition, the groundwater samples collected by Daws (2021) have a narrower range of δD and δ^{18}O values of -16.5‰ to -6.4‰ and -4.04‰ to -2.19‰ in comparison the groundwater samples collected in this study with δD and δ^{18}O values that range from -19.9‰ to +4.2‰ and -4.37‰ to +0.24‰, respectively (Figure 4.13). Furthermore, the groundwater samples collected by Daws (2021) appear to plot with a more gradual slope than the groundwater samples collected in this study (Figure 4.13).

The results from Daws (2021) form part of a MSc that is in preparation, therefore the raw data has not been presented. The spring and autumn datasets collected by Daws (2021) have very similar stable isotope values to each other. The mean spring δD and δ^{18}O values are -12.4‰ and -3.33‰, respectively, whereas the mean autumn δD and δ^{18}O values are -12.1‰ and -3.21‰, respectively. The δD and δ^{18}O values range from a minimum of -16.5‰ and -4.04‰ to a maximum of -6.4‰ and -2.19‰, respectively, in spring. In comparison, the δD and δ^{18}O values range from a minimum of -16.5‰ and -4.00‰ to a maximum of -7.0‰ and -2.14‰, respectively, in autumn.

4.5 Depth

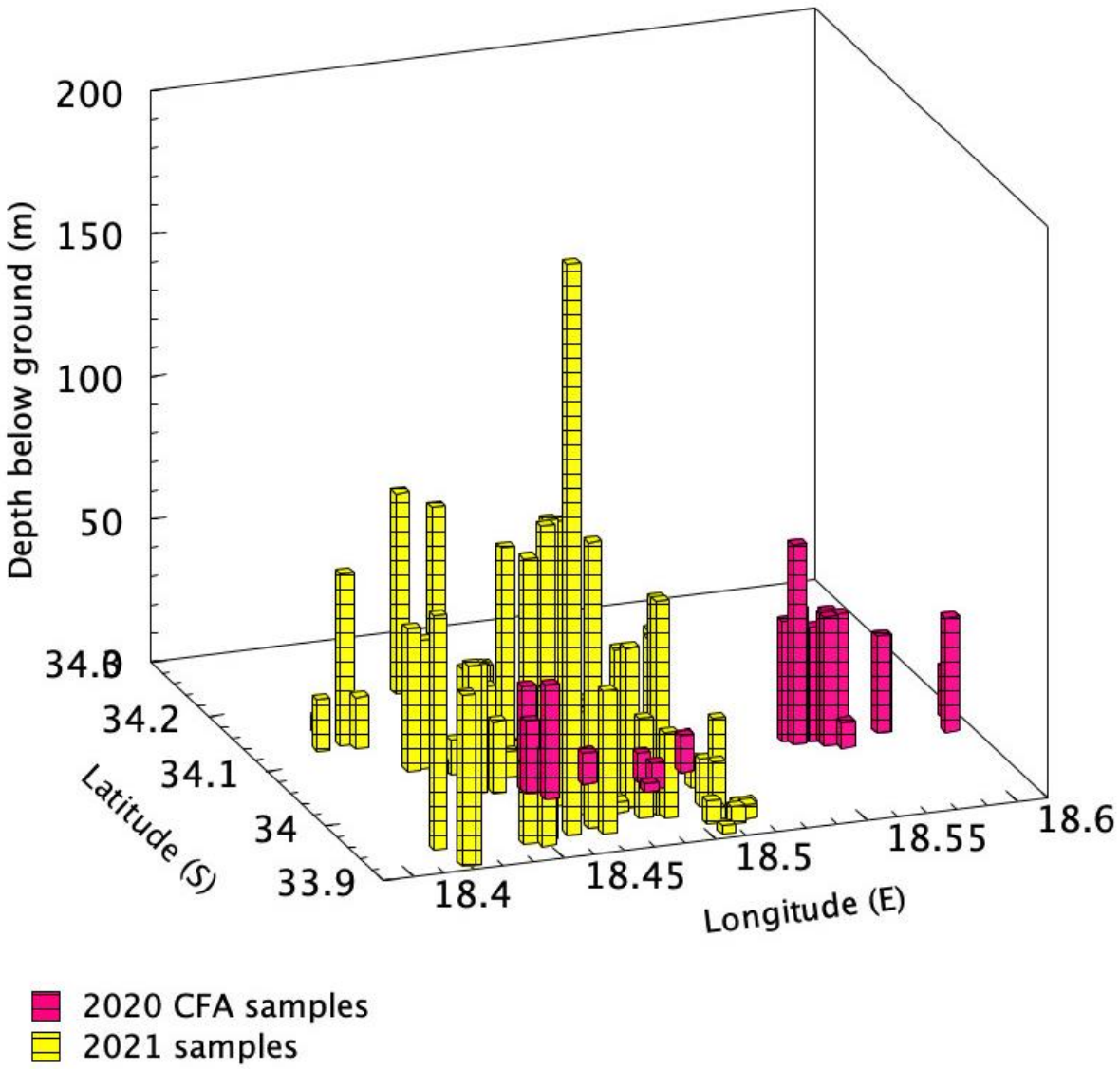

Figure 4.14: Plot of the GPS coordinates of the groundwater samples and their borehole and wellpoint depth data.

The depth of commercial boreholes is usually drilled to at least a few m below the water table. The range in the depth is much greater for the groundwater samples collected in 2021 than in 2020. In 2021, majority of the samples occur within the range of 0 m to 120 m but it extends to 200 m (Figure 4.14). In 2020, majority of the samples occur within the range of 0 m to 47 m but it extends to 70 m (Figure 4.14). In the 2020 CFA groundwater dataset, there are 2 main clusters of δD and $\delta^{18}O$ values at borehole or wellpoint depths of 10 m and 45 m.

The average δD and δ^{18}O values of the groundwater samples have been presented below at given depth intervals (Table 4.3). The 2020 groundwater samples collected from boreholes or wellpoints drilled to depths of <20 m appear to show an increase in the average δD and δ^{18}O values with an increase in depth to 20 – 60 m, while the samples collected from boreholes drilled to depths of 20 – 60 m show a decrease in the δD and δ^{18}O values with an increase in depth to >60 m (Table 4.3). In comparison, the δD and δ^{18}O values of the 2021 groundwater samples generally decrease with increasing depth (Table 4.3).

Table 4.3: Average δD and δ^{18}O values of the groundwater samples at given borehole and wellpoint depth intervals.

Depth intervals	**2020**		**2021**	
	δ^{18}O	**δD**	**δ^{18}O**	**δD**
<20 m	-2.51	-9.4	-2.36	-9.2
20 - 60 m	-2.38	-8.6	-2.53	-10.6
>60 m	-3.09	-11.0	-2.90	-11.8

The average EC measurements of the groundwater samples have been presented below at given depth intervals (Table 4.4). Both the 2020 and 2021 groundwater samples show a similar pattern in the variation of EC with the depth of the boreholes and wellpoints. The EC measurements of groundwater collected from boreholes or wellpoints drilled to depths of <20 m is lower than the EC measurements of boreholes drilled to depths of 20 m – 60 m, and the EC measurements of the groundwater collected from boreholes drilled to depths >60 m have lower EC measurements than the groundwater collected from boreholes drilled to depths of 20 – 60 m. The boreholes drilled to depths of 20 m – 60 m contain numerous groundwater samples with relatively high EC measurements collected from Phillipi farmlands and Mitchelles Plain in the 2020 dataset, and groundwater samples collected from Pinelands with high EC values (samples 97, 227, 228 and 229) in the 2021 dataset. Samples 227 and 228, collected from Pinelands High School have particularly high EC measurements of 51.30 mS/cm and 58.70 mS/cm, respectively. They were collected from different depths within a single borehole at Pinelands High School. This was done by pumping the water up to the surface through a pipe that was placed at depths of 20 m and 35 m within the borehole. Sample 227 was collected from a depth of 20 m, whereas sample 228 was collected from a depth of 35 m. A third sample (sample 226) was collected at Pinelands High School from a wellpoint located ~10 – 15 m

away from the borehole. The water collected from the wellpoint (4 m deep) had a much lower EC measurement of 2.96 mS/cm.

Table 4.4: Average EC measurements of the groundwater samples at given borehole and wellpoint depth intervals.

Depth intervals	2020	2021
<20 m	1.38	1.33
20 - 60 m	2.53	5.15
>60 m	1.84	1.06

The 10 samples that were chosen for strontium analysis out of the 256 water samples collected in this study are presented below (Table 4.5). The $^{87}Sr/^{86}Sr$ ratios range from a minimum value of 0.70935 (sample 213) to a maximum value of 0.73023 (sample 181). The average $^{87}Sr/^{86}Sr$ ratio is 0.71417. The concentration of strontium in the water samples was not measured because it was beyond the scope of this study.

4.6 Strontium isotopes

Table 4.5: The $^{87}Sr/^{86}Sr$ ratios of the groundwater samples in comparison to their location, altitude, distance from the Malmesbury Group and TMG unconformity, EC, $\delta^{18}O$ value and depth.

Sample #	Location	Altitude (mamsl)	Distance from unconformity (km)	EC (mS/cm)	$^{87}Sr/^{86}Sr$	$\delta^{18}O$ (‰)	Depth (m)
135	Observatory	70	1.45	1.53	0.72054	-2.02	200
145	Silvertown	10	6.81	1.69	0.71426	-2.44	
152	Athlone	17	4.99	0.19	0.70985	-0.45	
167	V&A Waterfront	12	3.93	1.09	0.71171	-2.27	70
181	Camps Bay	82	1.30	0.43	0.73023	-3.67	120
183	Vredehoek	128	0.90	0.11	0.71058	-1.77	
195	Bergvliet	19	4.40	0.81	0.71350	-2.73	40
213	Fish Hoek	9	1.05	0.89	0.70935	-3.28	
227	Pinelands	7	5.61	51.3	0.71131	-2.79	20
242	Muizenberg	12	0.27	0.39	0.71036	-3.91	

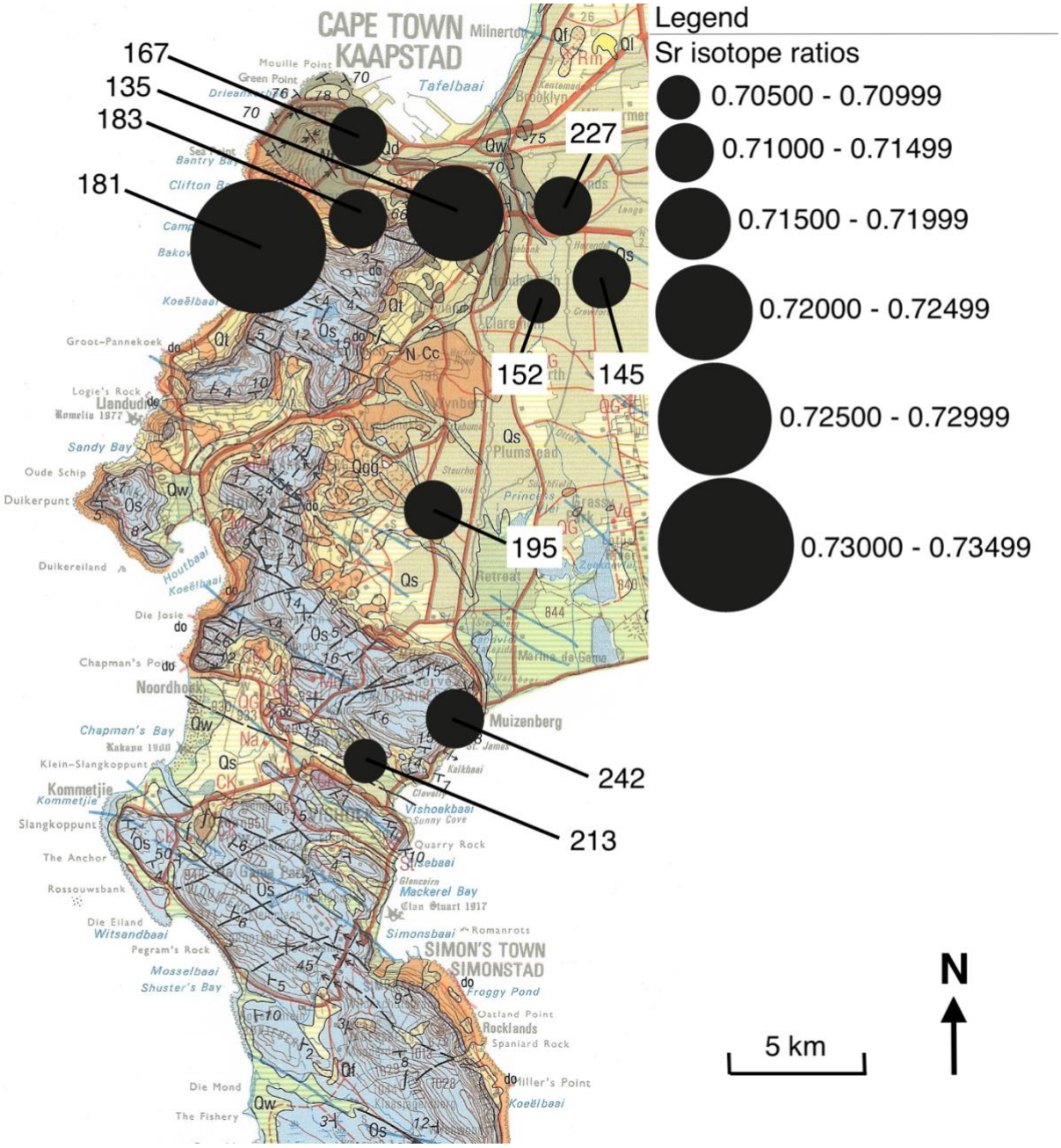

Figure 4.15: The spatial distribution groundwater samples with $^{87}Sr/^{86}Sr$ ratios in relation the local geology of the study area (where the number refers to the sample number; adapted from the CGS, 1990).

The strontium isotope ratios of the water samples appear to be related to the substrate lithology. The strontium isotope ratios seem to be higher for the samples collected in closer proximity to the Malmesbury Group and the Cape Granite Suite (e.g. samples 135 and 181) than the samples collected from areas covered by Quaternary deposits (e.g. 145, 152, 195, 213, 227, 242).

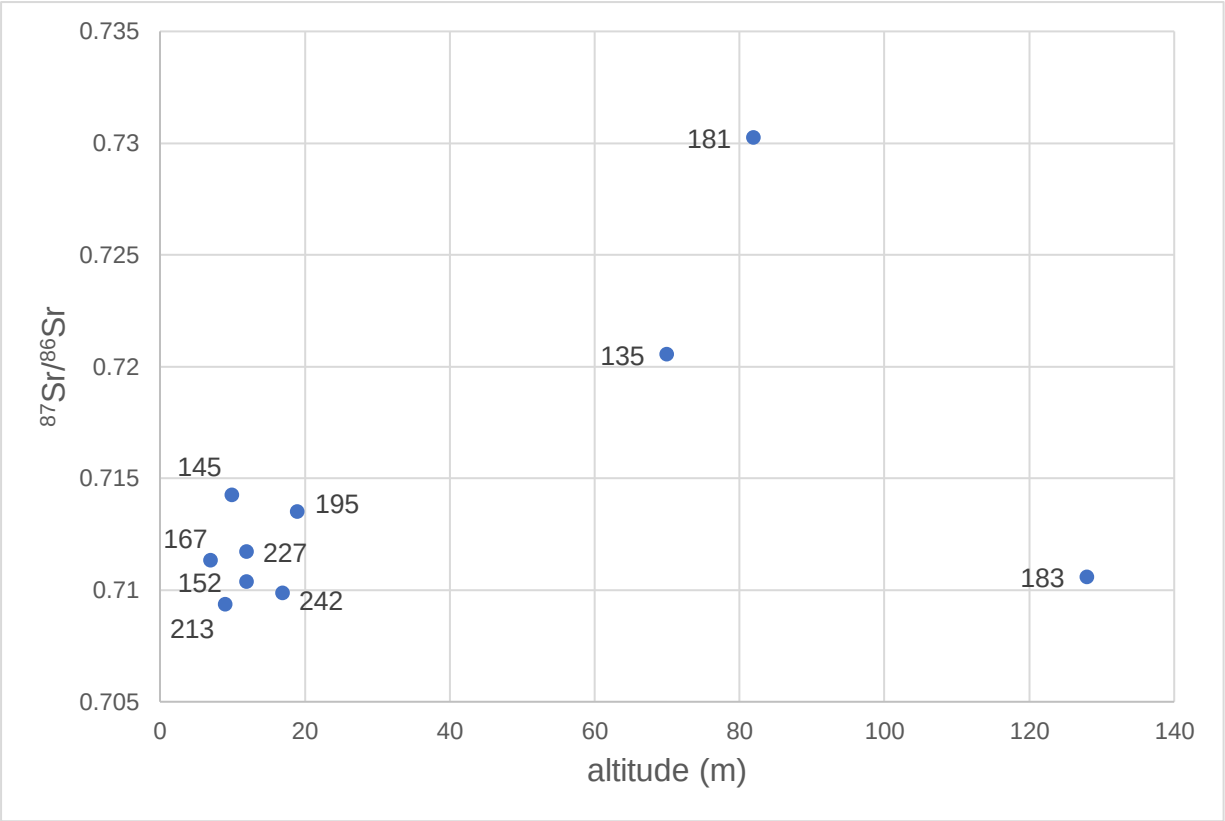

Figure 4.16: $^{87}Sr/^{86}Sr$ ratios vs. altitude of the groundwater samples.

The samples located at lower altitudes (<20 m) all have relatively low $^{87}Sr/^{86}Sr$ ratios of between 0.70935 and 0.71426 with an average of 0.71148, whereas the samples collected from higher altitudes (>60 m) have a fairly wide range in $^{87}Sr/^{86}Sr$ ratios of between 0.71958 and 0.73023 with an average of 0.72045. It would have been beneficial to determine the relationship of the strontium isotope ratios vs. the concentration of strontium within the water samples, however this was not possible as previously mentioned.

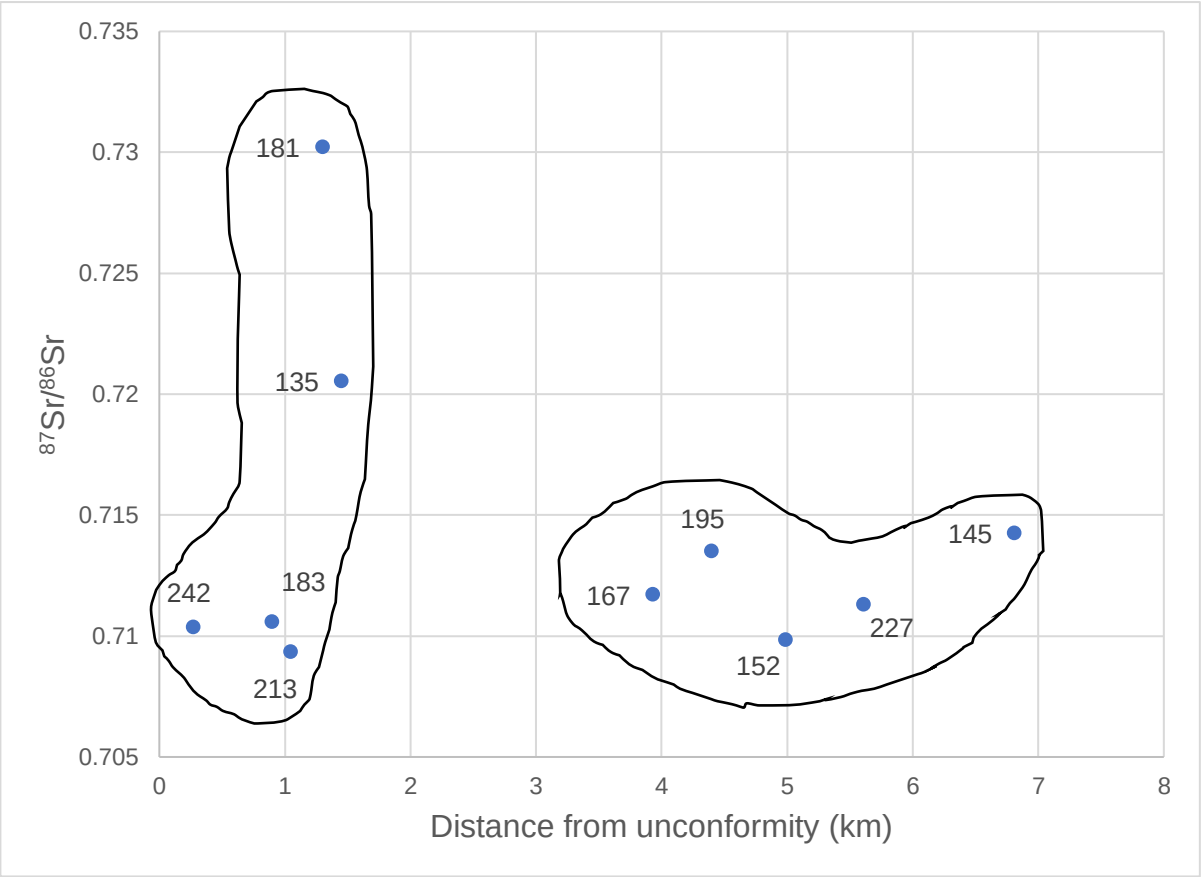

Figure 4.17: $^{87}Sr/^{86}Sr$ ratios vs. distance from the TMG and Malmesbury Group unconformity of the groundwater samples.

The data is relatively scattered, however there do appear to be 2 clusters of datapoints. There is a tabular cluster of datapoints with a broad range of $^{87}Sr/^{86}Sr$ ratios with an average of 0.71621 that are located <2 km from the TMG and Malmesbury Group unconformity, and a concave oval shaped cluster of datapoints with a narrower range of $^{87}Sr/^{86}Sr$ ratios with an average of 0.71213 that are located >3 km from the TMG and Malmesbury Group unconformity.

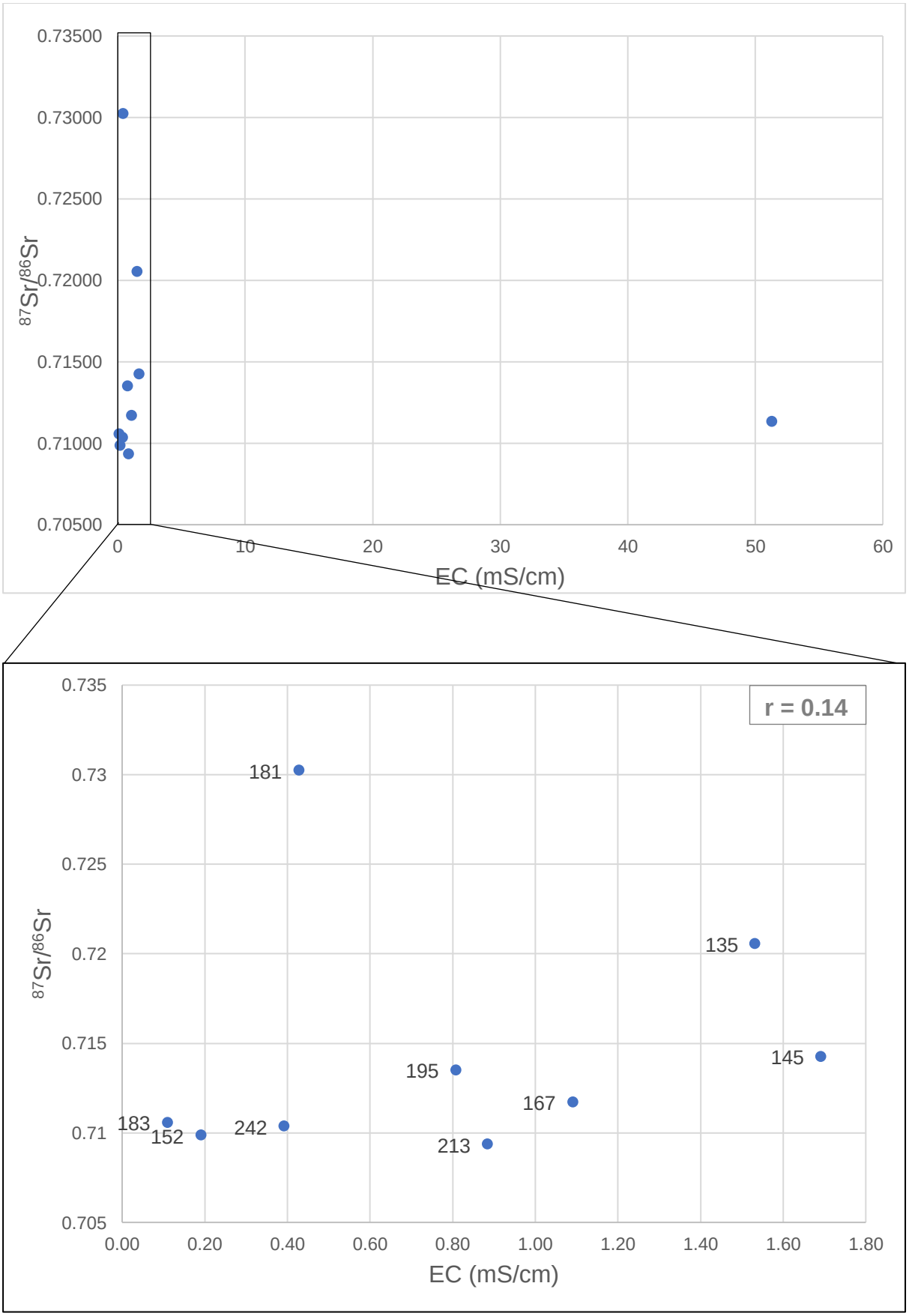

Figure 4.18: $^{87}Sr/^{86}Sr$ ratios vs. EC of the groundwater samples.

There does not appear to be an obvious relationship between the EC measurements of the water samples and their $^{87}Sr/^{86}Sr$ ratios. The correlation coefficient for the $^{87}Sr/^{86}Sr$ ratios and the EC is low with a value of 0.14 when omitting sample 227.

4.6.1 Comparison with Daws' dataset

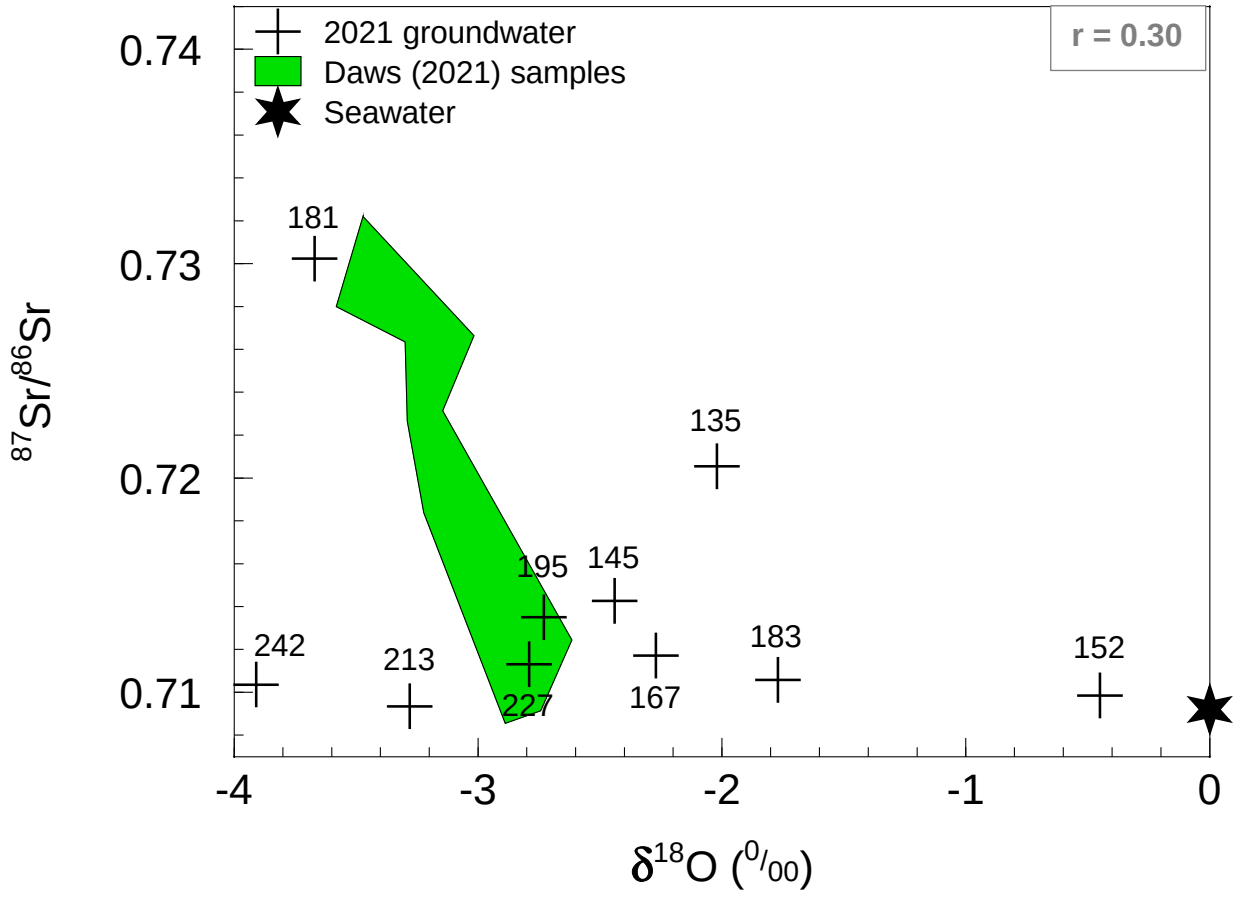

Figure 4.19: $^{87}Sr/^{86}Sr$ ratios vs. $\delta^{18}O$ values of the groundwater samples (where r= 0.30 for 2021 groundwater).

The $^{87}Sr/^{86}Sr$ ratios and the average $\delta^{18}O$ values of the spring and autumn samples, collected by Daws (2021), have been plotted as a field. Daws' (2021) samples have a similar range in the $^{87}Sr/^{86}Sr$ ratios as the 2021 groundwater samples collected in this study, but a much narrower range in the $\delta^{18}O$ values. The $^{87}Sr/^{86}Sr$ ratios of Daws' (2021) dataset ranges from a minimum value of 0.709507 (sample HB49) to a maximum value of 0.731182 (sample HB28). The average $^{87}Sr/^{86}Sr$ ratio for Daws' (2021) samples is 0.71917. The correlation coefficient between the $^{87}Sr/^{86}Sr$ and the $\delta^{18}O$ values of the 2021 water samples collected in this study is relatively low (r= 0.30).

Chapter 5: Discussion

This chapter aims to explain the spatial variation of the physiochemical characteristics (EC, pH, and isotopic values) with respect to previous research, to address questions such as the influx of seawater, recharge, and systemic changes with time. The causes of the groundwater quality and the factors that affect the stable isotope composition of water such as altitude and amount effects as well as evaporation, are discussed. In addition, the primary influence of the strontium isotope ratios of the Cape Town groundwater is determined.

5.1 pH

Natural waters that are not contaminated typically have a pH range of 6.5 – 8 with seawater on the upper end of the scale with a value of ~8 (United States Geological Survey, 2021). The majority of the water samples collected in this study occur within this range, however there are a number of water samples that have a pH of <6.5 (Figure 4.1). Groundwater from the TMG Aquifer is characteristically acidic (Brown et al., 2003). Unbuffered water from the TMG Aquifer has been found to have a pH as low as 3 in inter-montane domains (Rosewarne, 2002). The groundwater samples with relatively low pH values that were collected along the eastern slopes of the Cape Peninsula mountain range occur in a relatively steep area that lacks sources of anthropogenic contamination such as fertilizers and sewage because they occur on the outer edge of the urban area. The relatively low pH readings could reflect dissolution of the local rocks, influence of the catchment vegetation or the nature of the rainfall. The dissolution of quartz in water produces silicic acid, which could be an explanation for the low pH measurements of the samples located along the eastern slopes of the Cape Peninsula mountains where the TMG outcrops (Wolfgang, 2003). Alternatively, the pH may be influenced by organic acids which are released from the decay of certain vegetation types present in the catchment area, such as fynbos and some tree species (Day et al., 2020). Rainfall could also be the cause of the relatively low pH measurements. Rainfall naturally has a slightly acidic pH of 5.6 due to carbon dioxide reacting with water in the atmosphere to form carbonic acid (United States Geological Survey, 1997). The formation of acid rain can also further lower the pH of the rainwater. Acid rain is formed due to air pollution being higher than deemed safe for human health (Tshehla and Wright, 2019). Particles such as nitrogen oxides and sulphur oxides, associated with industrial activities, mix and react chemically with water and oxygen in the atmosphere to form acid rain (Tshehla and Wright, 2019). However, acid rain is unlikely

to be a major contributor to the acidity of the groundwater because there is a lack of industrial activity in the high-income residential areas such as Constantia and Newlands, that occur along the lower eastern slopes of the Cape Peninsula mountain range. Therefore, the relatively low pH readings are most probably a function of the natural acidity of rainfall and/or the dissolution of the TMG quartzite and/or the acidic leachate associated with the local vegetation.

The occurrence of acidic groundwater along the slopes of eastern slopes of the Cape Peninsula mountains is likely related to the groundwater remaining unbuffered because the TMG lacks carbonate, clay and mafic minerals (Gomo, 2018). Carbonate, clay and mafic minerals increase the buffering capacity of groundwater by releasing ions, which combine with hydrogen ions, resulting in a neutralisation of pH (Wolfgang, 2003). The Sandveld Group, which contains calcareous rich lenses, and shell material, on modern and ancient beaches such as the Cape Flats, may neutralise the groundwater in some areas. Aza-Gnanji et al. (2013) states that groundwater from the CFA is predominantly alkaline due to the dissolution of carbonate and calcrete. Unfortunately, the pH of the water samples collected from the CFA in 2020 was not measured so no comparison can be made.

The water samples towards the northeast of the study area (located around Observatory) with relatively high pH readings could be the result of the presence of carbonate minerals in the Quaternary deposits (Sandveld Group) in the area or the Malmesbury Group which is the bedrock lithology (Figure 4.1). When investigating the joints in the Malmesbury Group at the old oil storage quarry site at Cape Town Harbour, Stowe (1995) found that the joints were filled with carbonate and/or grey-green coloured clay. The presence of carbonate in the joints may be prevalent in the area of the Cape Town Harbour, which is located in the northeast of the study area. Otherwise, these samples could be affected by a local source of anthropogenic contaminants that are highly alkaline. Halenyane (2017) found that Albion spring, located ~6 km from Observatory, had the highest trace element concentrations in a study conducted on the Albion, De Waal, Main, and Newlands springs. Albion spring had higher Ba, Ga, Sc, Sr, Zr and significantly higher Pb, Zn and Cu concentrations over the months of January – February 2017 in comparison to the other springs which are located further away from Observatory. Heavy metal elements such as Pb, Se and Zn are more mobile in alkaline solutions and can be released through activities associated with mining and industrial processes as well as coal combustion (Moorcroft, 2019). The relatively high alkalinity of the groundwater samples collected in this study is probably associated with light industry activities or the

dumping of ash, furnace and coal waste in the observatory area (HKS LAWGIBB, 1995). Alternatively, the relatively high pH values of the groundwater samples collected in this study could be associated with contamination from the drilling of deep boreholes. Drilling mud has a pH of >8. (Gamal et al., 2019). Therefore, deeper boreholes, such as the Groote Schuur Hospital borehole (200 m deep), may have required more drilling mud which could have resulted in it being contaminated to a greater extent than wellpoints located in areas with a shallower water table that did not require as much drilling mud. Localised seawater ingress associated with over-abstraction of groundwater related to anthropogenic activities, is another possible explanation for the high pH readings because, although these groundwater samples are alkaline, they have pH values of <8. These are just a few examples of anthropogenic contaminants that could possibly be increasing the pH of the groundwater in the northeast of the study area. The low correlation coefficient between the pH and the distance from the TMG and Malmesbury Group unconformity indicates that there is no relationship (Figure 4.2).

5.2 Electrical conductivity (EC)

Cape Town tap water usually has an EC of ~0.15 mS/cm (Harris, 2017), but water with EC measurements of <0.70 mS/cm is considered potable (South African National Standards, 2015). In comparison, seawater has an EC of about 50.00 mS/cm (Mary River Catchment Coordinating Committee, 2013). Sandvlei estuary is temporarily open to the ocean. Therefore, the samples (sample 39 and 41) collected from it have relatively high salinities of 35.70 mS/cm and 35.20 mS/cm, respectively, because they probably consist of a mixture of freshwater and seawater (Figure 4.3). The lake in Capricorn Park is an artificial water body that was constructed to drain stormwater. The relatively low to moderate EC (1.74 mS/cm) of sample 40, collected from it, could therefore reflect natural causes such as rainwater dissolving marine aerosols deposited on the vegetation or soil and/or it could be affected by anthropogenic activities such as contamination of the natural groundwater by pollution (Figure 4.3). Records from between 1 May - 30 June 2013 reveal that the quality of water in the Capricorn Park lake deteriorated due to the influx of oil, litter, cigarette butts, chemicals associated with detergents and other anthropogenic pollutants (Mugabe, 2013). Contamination of surface water bodies has been found to be widespread across the CoCT. The river samples (samples 101, 130, 219 and 247) have relatively low to moderate EC measurements ranging from 0.24 mS/cm to 1.21 mS/cm. They are assumed to have been altered by anthropogenic effects because a study conducted by Day et al. (2020) revealed that the river systems within every one of Cape Town's

sub-catchments have higher EC readings than the natural EC reference measured in the 1980s. Sewage effluent, and surface run-off from urbanized and agricultural land were identified as the main culprits (Day et al., 2020).

The very low EC readings of groundwater from Newlands, Bishopscourt and Constantia appears to be related to the topography. The presence of dolerite dykes and faults in the area may have resulted in preferential fluid conduits along the contacts or fault zones, which eventually eroded to form valleys (such as Newlands Ravine and Nursery Ravine) with well-established flow pathways. The steep valley slopes result in the groundwater moving relatively rapidly and therefore having a relatively short residence time, which prevents particles such as salts from dissolving and accumulating in the groundwater (Hariall, 2020). Similarly, the spring water samples (samples 113, 215, 240, 242 and 248) are thought to have relatively low ECs, ranging from 0.17 mS/cm to 0.56 mS/cm, because they are located close to the mountains. The overall increase in EC of the groundwater samples towards lower altitudes may be due to the accumulation of dissolved chemicals from fertilizers (Harris, 2017; Figure 4.3). Harris (2017) suggested that this was the case when interpreting data from the 2017 Constantia water samples. This could also explain why Philippi, which is a horticultural area, has relatively moderate to high EC measurements ranging from 1.05 mS/cm to 4.82 mS/cm. Extraction of the groundwater for irrigation could also increase the salinity of the return flow of the abstracted water due to evaporation (Aza-Gnandji et al., 2013). The relatively moderate EC values of 2.08 mS/cm and 2.07 mS/cm of samples 59 and 66, respectively, collected from Mitchells Plain, may be associated with pollution because of poor sanitation and waste disposal in the densely populated area (Adelana and Xu, 2006). Alternatively, the relatively moderate EC measurements (ranging from 1.05 mS/cm to 4.82 mS/cm) of the water samples collected inland in Philippi and Mitchells Plain could indicate the intrusion of minor amounts of seawater into the CFA. However, the low EC measurements, ranging from 0.67 mS/cm to 0.78 mS/cm, for samples 67, 68 and 69, that occur along the coast of Mitchells Plain suggest otherwise (Figure 4.3).

The extremely high EC measurements recorded in Pinelands (samples 97, 227, 228, 229 and 231) may be the result of the underlying unconsolidated sand containing high amounts of salts. This cannot be due to seawater ingress because a) the EC measurements are up to 58.70 mS/cm which is higher than the expected EC for seawater and b) the Pinelands' groundwater samples have an identical isotopic composition to the springs on the lower slopes of Table

Mountain (Harris et al., 1999). Harris (2017) has therefore attributed the high EC in Pinelands groundwater to the composition of the aquifer (the aquifer contains salt within the sand) rather than to seawater infiltration into the aquifer. Therefore, the similarity of the stable isotope values of the water samples collected in this study with 'normal' groundwater (groundwater with EC values <1) indicates that the increase in EC measurements towards the north and northeast of the study area may be the result of the lithology i.e., it is a natural phenomenon. The decrease in the water quality in terms of EC appears to coincide with the change in the underlying lithology. In the Southern Suburbs, Camps Bay and Bakoven, the TMG, Cape Granite Suite and the Quaternary sediments are the bedrock, whereas, in the north and northeast of the study area in the suburbs of Greenpoint, the City Bowl, Salt River and Observatory, the Malmesbury Group predominantly occurs (figure 2.3). Shales generally weather more easily and contain minerals that are more soluble than granites and quartz-rich sandstones (USGS, n.d.). Therefore, water in fractures of the Malmesbury Group may have a relatively high salinity due to the dissolution of feldspar and other minerals within the Malmesbury Group that contain elements such as Na. The underlying lithology may also be an alternative explanation for the relatively moderate EC measurements of the Philippi and Mitchell's Plain samples collected from the southeast of the study area (Figure 4.3). Towards the northwest of Philippi, the Springfontyn Formation dominates, whereas towards the coast, the Witzands Formation dominates, and minor outcrops of the Langebaan Formation occur (figure 2.3; CoCT, 2019). It is possible that the Springfontyn Formation contains more dissolvable particles such as marine calcite or aragonite than the Witzands and Langebaan Formations. The presence of sediments such as beach sand could also increase the EC of groundwater. The pore water salinity of beach sand in intertidal zones has been found to have a higher EC than seawater due to evaporation removing water and increasing the concentration of salts and other dissolved particles (Geng et al., 2016). This phenomenon can be used to explain the EC readings that were measured across the Cape Flats. Towards the northwest of Philippi, paleo-lagoons may be present. These ancient surface water bodies would have experienced extensive evaporation which would have led to enhanced pore water salinities. Therefore, the influence of the substrate lithology or sediment desposits, and the build-up of dissolved chemicals inland at low elevations seems like the more plausible explanation(s) than the intrusion of seawater into the CFA.

The elevated EC at the SPCA located in Grassy Park (sample 53) seems to be a localized phenomenon (Figure 4.3). The SPCA is an animal shelter therefore the relatively high EC measurement of 5.53 mS/cm may be due to the contamination of the groundwater by excrement

or chemicals. Sample 239, collected from Three Anchor Bay, in the north of the study area, also appears to have an elevated EC measurement of 6.60 mS/cm. It is unclear what the source of the high EC is. Samples 112, 180, 186 and 187 were collected from Rustenberg High School in Rondebosch, Camps Bay High School, Jan Van Riebeeck Primary School in Gardens, and Jan Van Riebeeck Sportveld in Tamboerskloof, respectively. Their low to moderate EC measurements, ranging from 1.04 mS/cm to 2.17 mS/cm, may possibly be caused by the accumulation of dissolved chemicals from fertilizers used on the sports fields (Figure 4.3). Similarly, sample 126, collected from the Villagers Football Club in Claremont, may also be affected by the accumulation of chemicals from fertilizers. It has an EC of 1.39 mS/cm. Alternatively, irrigation or a local source point of pollution could be increasing the EC of these samples. The Red Cross Children's Hospital (sample 147) and the Groote Schuur Hospital (sample 135) samples, which are located at a relatively high altitudes in Rondebosch and Mowbray, have low to moderate ECs of 1.16 mS/cm and 1.53 mS/cm, respectively, which could possibly indicate the leakage of the hospitals' wastewater that could contain chemicals from pharmaceuticals, disinfectants and other solutions used for medical purposes (Emmanuel et al., 2009; Figure 4.3). This requires further investigation. Otherwise, the low to moderate EC reading of the Groote Schuur Hospital (sample 135) may primarily be a function of the underlying lithology. Sample 135 was collected from a depth of 200 m (Figure 4.14). Therefore, it appears that the borehole sample occurs in the Malmesbury Group. It is unclear why some of the other samples, which were collected at relatively high altitudes have moderate EC measurements such as samples 36, 162, 173, 174 and 176. Samples 36, 174 and 176 have EC measurements that range from 1.00 mS/cm to 1.57 mS/cm. They were collected from residential homes. Samples 162 and 173 have EC measurements of 1.11 mS/cm and 1.62 mS/cm, respectively. They were collected from office blocks. These samples may have been stored in open tanks above the ground. Therefore, they may have experienced extensive evaporation resulting in the increased concentration of dissolvable particles such as salts. The relatively high δ^{18}O value for sample 36 is consistent with this explanation (Figure 4.8). However, samples 162, 173, 174 and 176 have relatively low δ^{18}O values (Figure 4.8). Rather, they may be affected by a local source of contamination. The low to moderate EC of 1.41 mS/cm of sample 38, which is situated along the coast of Muizenberg, could be the result of salt spray from the ocean (Figure 4.3). Marine aerosols could either directly be washed out of the atmosphere by rainfall and recharge the groundwater or salt that accumulates at the surface could be dissolved by rainfall, which would then percolate into the groundwater system (Weaver et al., 1999). The coastal samples in Mitchells Plain (samples 67, 68 and 69) are

located somewhat more inland than sample 38 and may not be as affected by the salt spray from the ocean (Figure 4.3). They have lower EC measurements of 0.67 mS/cm, 0.78 mS/cm and 0.71 mS/cm, respectively.

Based on the research conducted by Harris (2017) on the Constantia groundwater samples, the EC would be expected to increase with increasing distance from the Table Mountain and Malmesbury Group unconformity because further away from the mountain, pool salts, chemicals from fertilizers, and other sources of dissolvable particles build up gradually as the water flows downslope in the aquifer (Harris, 2017). The EC of groundwater is generally lower in salinity and higher in quality closer to the TMG because the host rock is predominantly quartzite, which results in it being relatively unreactive (Wu, 2008). In addition, the Peninsula Formation is highly resistant and forms topographic highs where large amounts of rainfall dilute and flush out dissolvable particles such as salts (Wu, 2008). The EC of groundwater in the TMG Aquifer in pristine catchment areas is typically lower than 0.1 mS/cm (Rosewarne, 2002). The EC of the water samples collected in this study generally increases slightly as the distance from the TMG and Malmesbury Group unconformity increases (Figure 4.5). This relationship is statistically significant for a sample size of 249 and a correlation coefficient of 0.33 with a confidence interval of >99.99% (Figure 4.5). The groundwater samples collected from Pinelands (samples 97, 227, 228 and 229) are clear outliers, which indicates that they must have an additional source of dissolvable particles such as salt (Figure 4.5). This is consistent with Harris' (2017) findings, as discussed above.

Aquifers that have a marked increase in EC at a certain depth indicates that there is a significant source of dissolvable particles such as salt. This is often associated with seawater infiltration in coastal areas. The samples collected in this study were not collected at depths at regular intervals in the borehole i.e., packers were not used. Therefore, it would be useful to use packers in future studies to determine if there is a fresh-salt water interface. There are, however, extremely high EC measurements for the groundwater samples collected in Pinelands. Samples 226, 227 and 228, collected from Pinelands High School at variable depths of 4 m, 20 m, and 35 m, show an increase in EC with increasing depth from 2.96 mS/cm to 58.70 mS/cm. This may suggest that the source of the salt is located at a depth of 35 m or greater. Alternatively, the progressive increase in EC with increasing depth may just be a function of the influence of freshwater from rain or irrigation at Earth's surface i.e., the samples collected from shallower depths are diluted with freshwater more than the samples collected

from deeper depths. The δD and $\delta^{18}O$ values of the water samples were plotted against EC but there is no obvious relationship (Figure 4.6).

5.3 Stable isotope composition of the surface water samples

The positive δD and $\delta^{18}O$ values of the stagnant surface water samples (samples 39, 40 and 41) are primarily due to evapoconcentration. Samples 39, 40 and 41 plot along the trendline of the LEL (Figure 4.8). In contrast, almost all the spring samples (samples 113, 215, 240, 242 and 248) and river samples (samples 130, 219 and 247) plot between the LMWL and the GMWL, except for sample 101 which has been shifted slightly to the right of the LMWL and the GMWL. Sample 101 was collected from Elsieskraalrivier in Pinelands. Elsieskraalrivier is channelised, whereas the other rivers (Black River, Silvermynrivier and a stream in Glencairn Heights) that were sampled in this study are not. Therefore, this river may have an evaporative isotopic signature because it contains a smaller component of groundwater seepage than other rivers. The positive d-excess values of the spring and river samples, ranging from +4.94‰ (sample 101) to +14.40‰ (sample 242), suggests that their stable isotope compositions are closely related to the recent local precipitation and that the samples have experienced negligible evapoconcentration, besides sample 101 which appears to have experienced some isotopic enrichment due to evaporation. Therefore, it is assumed that most of the spring and river samples have not had enough time at the surface to experience significant evaporation.

5.4 Stable isotope composition of the groundwater samples

Groundwater is trapped below the surface of the Earth therefore it should not be directly affected by atmospheric conditions. However, several groundwater samples in the dataset, unexpectantly, have isotope compositions consistent with evaporation. For example, groundwater sample 152, collected from a home in Athlone, and groundwater sample 226 collected from a shallow wellpoint with a depth of 4 m in Pinelands, have very high δD and $\delta^{18}O$ values of +4.19‰ and -0.45‰, and +1.54‰ and +0.24‰, respectively. Sample 226 plots relatively close to the isotopic value of seawater (Figure 4.8). It is shifted significantly to the right of the GMWL and the LMWL (Figure 4.8). However, it is unlikely that it is related to seawater based on its EC measurement of 2.93 mS/cm and its pH reading of 6.86. In addition, the isotope ratios of the groundwater samples across the study area do not appear to indicate seawater ingress into the aquifers, as discussed below. The way it is stored could result in it

having experienced relatively extensive evaporation e.g., an open tank above ground. Sample 152 is shifted slightly to the right of the LMWL and the GMWL. Its storage conditions are unknown. Samples 137, 172 and 238 are similarly thought to be isotopically enriched due to their storage conditions. Alternatively, these samples could have a surface water component such as surface irrigation water, tap water or swimming pool water.

5.4.1 The source of recharge of the groundwater

As previously mentioned, the equations of the lines of best fit for the groundwater have a greater similarity to the 2009 – 2020 UCT LMWLs than the 1996 – 2008 UCT LMWLs. Kasolo (2020) suggests that the UCT LMWLs calculated for the two time periods of 1996 – 2008 and 2009 – 2020 differ due to an increased rate of evaporation of raindrops as they fall to the ground, particularly during early summer months, in the latter time period. The groundwater samples also plot closer to the weighted mean annual rainfall for 2009 – 2020 than 1996 – 2008. This indicates that the main source of recharge is local, present-day precipitation (Figure 4.11).

The isotopic composition of the Main and Albion spring water has slightly higher δD values for given $\delta^{18}O$ values in comparison to the 2021 groundwater (Figure 4.12). This could be due to several reasons. For example, the groundwater could be experiencing greater amounts of evaporation than the Main and Albion spring water, resulting in their isotope values shifting slightly to the right of the LMWL and GMWL. However, this seems unlikely because groundwater is trapped below the surface of the Earth and should not be susceptible to evaporation. However, many of the samples were collected from water tanks, which may have been open to the atmosphere, and therefore resulted in the groundwater samples experiencing more evaporation than the Main and Albion spring water samples. This does not, however, explain the samples that were collected directly from the borehole or wellpoint. These samples could have a surface water component such as irrigation water or pool water, as discussed previously. Alternatively, the difference in the isotopic values could be due to a difference in the time between recharge and outflow for the Main and Albion springs vs. groundwater i.e., the groundwater may contain water that is a different age to the spring water. The Main and Albion springs at the foot of Table Mountain could also be in a different recharge zone than the groundwater. For example, the springs could be recharged by orographic rain as well as

frontal rain whereas the groundwater samples, which predominantly occur at lower altitudes, could be recharged mainly by frontal rainfall.

5.4.2 Altitude of recharge of the aquifer(s)

The relationship of the groundwater samples from higher altitudes having more negative isotopic values than the samples from lower altitudes could be the result of the aquifers being dominantly unconfined and experiencing direct recharge by rainfall which vertically infiltrates into the underlying aquifer (Figure 4.7; Figure 4.9; DWAF, 2008). Previous studies have revealed that the isotopic composition of Cape Town's precipitation is influenced by an altitude effect (Dansgaard, 1964; Diamond and Harris, 2019).

An altitude effect seems like a suitable explanation for the broader range in the $\delta^{18}O$ values for the groundwater samples collected from the northern extent of the Southern Suburbs and City Bowl in this study in comparison to the $\delta^{18}O$ values of the spring water samples collected from the City Bowl by Diamond and Harris (2019) (Figure 4.8; figure 5.1). The samples collected in this study were obtained from an area with a wider range in altitudes than the spring water samples collected in the study performed by Diamond and Harris (2019) which were collected from a relatively steep and narrow altitude range (Figure 4.7; figure 5.1). Therefore, this appears to confirm that the groundwater and spring water inherit an altitude effect from the rainfall. Alternatively, the differences in the $\delta^{18}O$ values between this study vs. Diamond and Harris (2019) may be due to the time difference in the collection of the water samples i.e., rainfall experienced in 2010 – 2012 may have had slightly different $\delta^{18}O$ values than the rainfall experienced in 2017 – 2021.

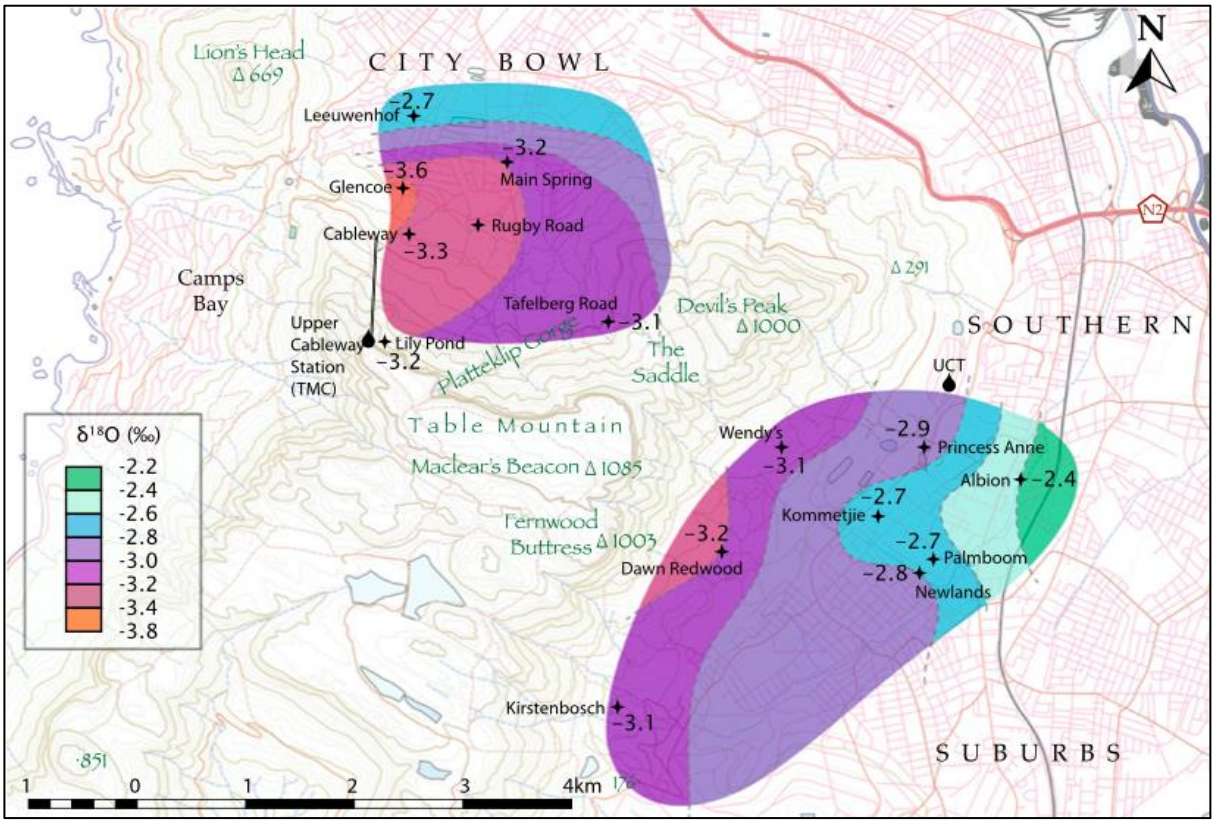

Figure 5.1: Contour map of the $\delta^{18}O$ composition of the Table Mountain springs produced by Diamond and Harris (2019) based on data collected from 2017 – 2021.

The groundwater samples could also be influenced by an amount effect. In summer, the south-easterly winds blow moist air from the southern Atlantic Ocean to the eastern slopes of Table Mountain (Cowling et al., 1995). The air rises, cools, and condenses to produce orographic rainfall, which accounts for up to 25% of Cape Town's annual precipitation (Cowling et al., 1995). In winter, the northwesterly winds are able to blow clouds over Table Mountain because it is not high enough to prevent it from doing so. This results in an uneven distribution of winter rainfall across Cape Town with more rain falling on the eastern slopes of the mountain, despite it being the leeward side (Figure 5.2; South African Weather Service [SAWS], 2021). Therefore, Newlands suburb which is located on the eastern slopes of Table Mountain, is one of the wettest suburbs in Cape Town.

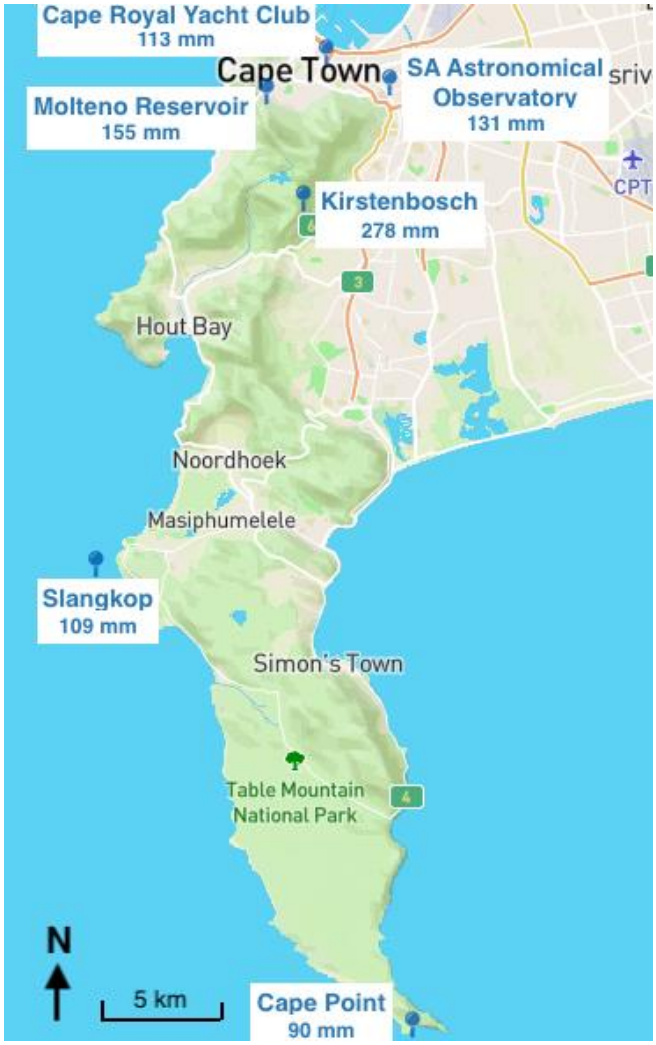

Figure 5.2: Preliminary winter rainfall for the month of July received by the SAWS (2021) weather stations by the 28th of July (month ending on the 01/08/2021).

Alternatively, this pattern of the water samples from lower altitudes having higher δD and $\delta^{18}O$ values could primarily be a function of evapoconcentration. The return flow of the abstracted water for irrigation purposes would become isotopically enriched due to evaporation. Therefore, areas such as Philippi Farmlands, located at relatively low altitudes, should show relatively high δD and $\delta^{18}O$ values that are shifted to the right of the LMWL and the GMWL due to extensive watering of crops. This is relatively consistent with the data presented. Evaporative enrichment also explains the occurrence of the samples with relatively high isotope ratios at high altitudes (>30 m) such as samples 49 & 250, 156 and 206, which were collected from Wynberg Girl's school, Kenilworth Centre, and Steenberg Golf course, respectively (Figure 4.7; Figure 4.8).

5.4.3 Number of primary aquifer(s)

The overall variation of the oxygen and hydrogen isotope composition of the groundwater samples across the study area indicates that the groundwater samples are derived from either: 1) a single aquifer or 2) multiple aquifers that are well-connected or 3) multiple aquifers that are recharged by the same water (Figure 4.8). The differences in the water quality in terms of EC and pH, as discussed above, suggest that the groundwater is derived from multiple aquifers across the CoCT that are recharged by the same water. For example, the low-quality groundwater derived from Pinelands and the Cape Flats seems to be associated with a different aquifer to the relatively high-quality groundwater derived from the eastern slopes of Table Mountain.

5.4.4 *Rate of recharge*

The overlap of the groundwater samples collected in 2021 with the Constantia groundwater data collected by Harris (2017) and the CFA groundwater samples collected in 2020, confirms the groundwater across the study area is recharged by the same source of water (Figure 4.10). However, the Constantia groundwater field plots at more negative $\delta^{18}O$ values than the groundwater samples collected from the CFA in 2020. This can be reconciled by the fact that Constantia generally occurs at a higher altitude than the area from which the groundwater samples in 2020 were collected i.e., the Cape Flats and Southern Suburbs. In addition, Constantia is also located relatively close to Newlands suburb, along the eastern slopes of the Cape Peninsula mountain range, which experiences relatively wet conditions. Therefore, the more negative isotope values of the Constantia groundwater could be the consequence of altitude and amount effects.

Samples 42, 49 and 52 collected in 2020 were resampled in 2021 as samples 251, 250 and 252, respectively. They have δD and $\delta^{18}O$ values that are extremely similar to the δD and $\delta^{18}O$ values of the samples collected in 2020 (Table 4.1). This suggests that recharge rates are greater than a year because the stable isotope values of rainfall (which recharges the aquifer) varies from year to year (Table 7.2). The similarity of the isotopic composition of the scree Constantia aquifer with the CFA and the groundwater samples collected across Cape Town in 2021 suggests that they have similar recharge rates. Harris et al. (2017) found that the scree aquifer in Constantia was recharged dominantly by rainfall experienced in 2013, which was the wettest year (1996 mm rainfall was experienced) between 2007 - 2017. The recharge rate

of the groundwater collected in this study is therefore thought to be slower than the recharge rates of the springs (which are recharged by up to 50% within <3 years) on the lower slopes of Table Mountain.

Samples 59 and 66, collected from Mitchells Plain, are not compositionally consistent with present-day rainfall because they have much lower δD and $\delta^{18}O$ values of -13.1‰ and -3.19‰, and -13.2‰ and -3.21‰, respectively, in comparison with the rest of the 2020 CFA groundwater data which has average δD and $\delta^{18}O$ values of -9.0‰ and -2.41‰, respectively (Figure 4.7). Samples 67, 68 and 69 also have lower isotopic values than expected with δD and $\delta^{18}O$ values of -10.6‰, -12.1‰, -10.3‰ and -2.64, ‰ -2.84‰, -2.5‰, respectively. They may contain water that has been trapped below ferricrete or peat, clay or calcareous rich layers within the Sandveld Group. Alternatively, these samples could contain water that has been trapped by man-made impermeable substrates. The Philippi horticultural area remains undeveloped, while according to the CoCT (2019), the rest of the CFA is largely covered by tar, concrete, and other impermeable substrates. The basis for the estimation of impermeable surface coverage by the CoCT (2019) is not described. Further research is required to resolve this.

Samples 214, 225, 242, 246, 247, 248 and 255, collected from the eastern slopes of Swartkop also appear to be compositionally different the rest of the samples in terms of stable isotope values (Figure 4.7). These samples have even lower δD and $\delta^{18}O$ values than samples 59 and 66, collected from the CFA. This appears to primarily be a function of an altitude affect. The samples collected along the slopes of Swartkop occur within a recharge zone located at a higher average altitude in comparison to the samples collected across the study area. The isotopic values of these samples are fairly similar to the samples collected by Daws (2021).

5.5 Aquifer flow models

Diamond and Harris (2019) propose that the springs at the foot of Table Mountain are stratified scree slope aquifers that consist of shallower, faster flowing water that is recharged by recent precipitation and deeper (>5 m below the surface), slower flowing water that is recharged by heavy rainfall events or periods of high-volume rainfall. This layered groundwater model reconciles the isotopic evidence that suggests that the springs have rapid flow rates of less than a year and the evidence that indicates that the springs continue to flow

during periods of drought i.e., it accounts for the deeper, slower water having more negative δD and $\delta^{18}O$ values than the shallower, faster flowing water (Diamond and Harris, 2019). This is based on the selection effect, which is the process whereby deep-water is recharged predominantly during events of heavy rainfall (Gat and Tzur, 1967). This results in the deep groundwater having more negative δD and $\delta^{18}O$ values than the ambient precipitation due to the amount effect (Diamond and Harris, 2019).

In the CFA, the average δD and $\delta^{18}O$ values of the groundwater samples collected from boreholes and wellpoints drilled to depths of <20 m is lower than the average δD and $\delta^{18}O$ values of the groundwater samples collected from boreholes drilled to depths of 20 – 60 m (Table 4.3). This is consistent with a selection affect. However, it is unclear why the average δD and $\delta^{18}O$ values of the groundwater samples collected from boreholes drilled to depths of >60 m is lower than the average δD and $\delta^{18}O$ values of the groundwater samples collected from boreholes drilled to depths of 20 – 60 m (Table 4.3). This is possibly caused by the age of the water. Older water may have a different isotopic composition to more recent rainfall. This suggests that the groundwater from the CFA lacks vertical mixing. The three samples collected from Pinelands High School appear to show this same pattern in the variation of the δD and $\delta^{18}O$ values with depth. The δD and $\delta^{18}O$ values decreased from +1.54‰ and +0.2‰ for sample 226 (located at a depth of 4 m) to -13.62‰ and -2.8‰ for sample 227 (located at a depth of 20 m), which then increased slightly to -13.61‰ and -2.4‰ for sample 228 (located at a depth of 35 m), respectively. However, the increase in the δD and $\delta^{18}O$ values of the Pinelands High School samples collected from depths of 20 m and 35 m is probably not statistically significant if the errors of the δD and $\delta^{18}O$ values of the water samples is greater than the errors of the δD and $\delta^{18}O$ values of Evian water. Whether or not the Pinelands aquifer shows the same pattern in the variation in the δD and $\delta^{18}O$ values with depth as the CFA or not, it is thought to be a subdivision of the CFA because it is located close to the CFA and it is an intergranular aquifer i.e. it occurs in a sandy substrate.

Overall, the relatively large number of CFA groundwater samples that were collected from depths of ~10 m and ~45 m indicates that the CFA is multi-layered (Figure 4.14). These findings are consistent with the models of hydraulic flow proposed for the CFA by DWAF (2008). The first model they propose suggests that the CFA is dominantly unconfined, and it consists of two layers: 1) an upper layer with lower hydraulic conductivity and 2) a basal layer

with higher hydraulic conductivity, in which groundwater flow is concentrated (figure 5.3A; DWAF, 2008). This basal layer may be semi-confined (DWAF, 2008). The second model proposed suggests that the CFA consists of an unconfined upper aquifer and two underlying semi-confined aquifers (figure 5.3B; DWAF, 2008). The groundwater flow in this model is concentrated in the basal coarse gravels that occur within palaeochannels (DWAF, 2008). The high hydraulic-conductivity aquifer units are made up of the Springfontyn Formation and paleo-channels infilled with gravels, whereas the low-hydraulic-conductivity confining units are comprised of discrete clay and calcareous rich layers in the Sandveld Group and recent sediments, or ferricrete. The very low hydraulic-conductivity bedrock is Malmesbury Group.

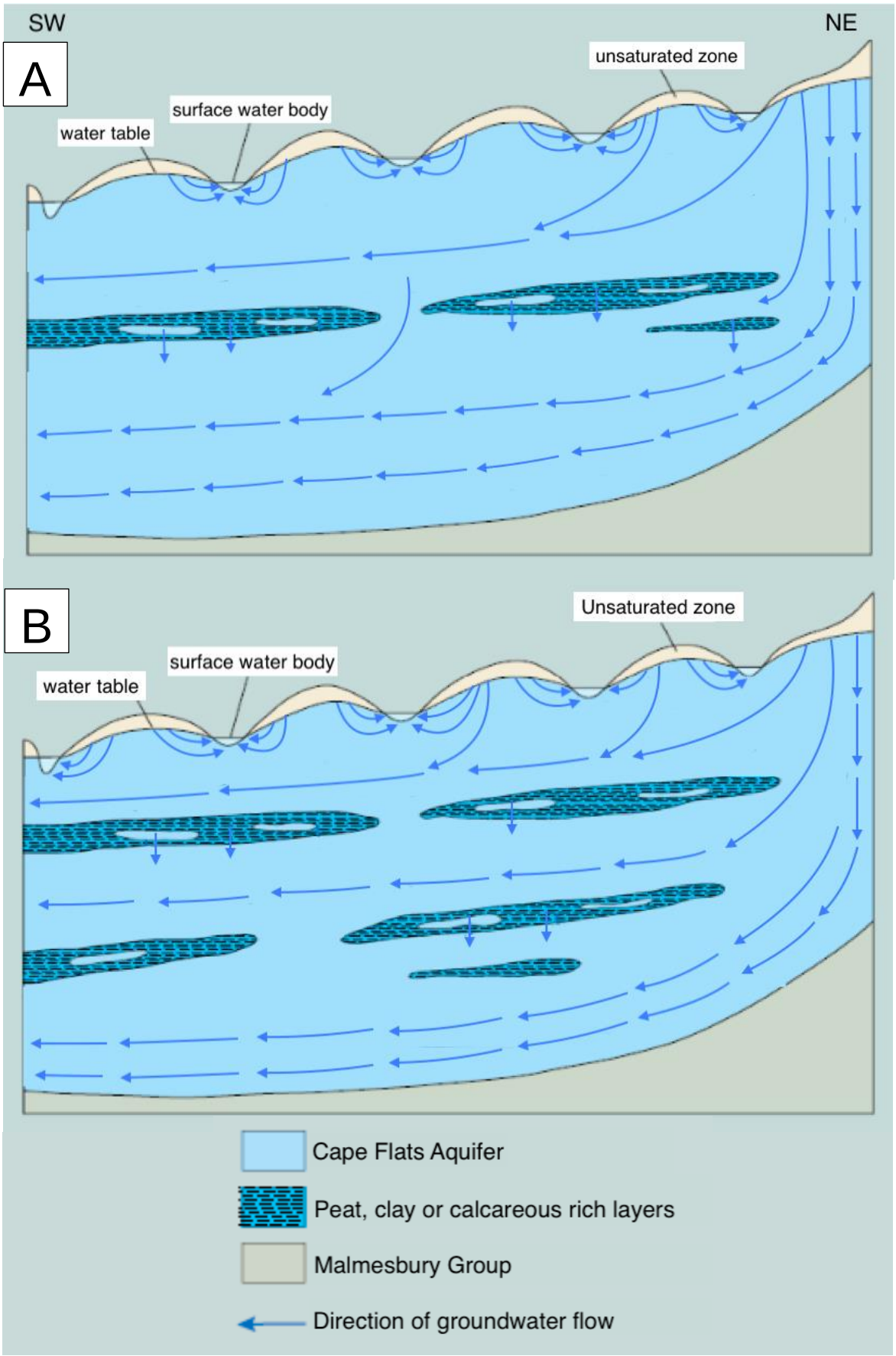

Figure 5.3: Proposed aquifer flow models for the CFA: A) 2-layered unconfined aquifer and B) unconfined upper aquifer and 2 underlying semi-confined aquifers (adapted from Sun, 1986). Diagram not to scale.

The majority of the 2021 water samples were collected from the eastern slopes of the Cape Peninsula mountain range. The overall decrease in the average δD and $\delta^{18}O$ values with increasing depth of the boreholes and wellpoints for the samples collected in 2021 (Table 4.3) is consistent with the layered model that Diamond and Harris (2019) have developed for the springs on the lower slopes of Table Mountain as shown below (figure 5.4) i.e. the shallower, faster flowing groundwater has more positive isotopic values than the deeper, slower flowing groundwater. The groundwater samples collected in this study therefore appear to have been collected from boreholes and wellpoints situated on the scree slopes of the mountain ranges (indicated in grey in their figure 5.4).

Stratification of groundwater has been found to be evident where freshwater lies above saline water due to difference in buoyancy (Simmons et al., 2002). However, the occurrence of saline water is not evident along the eastern slopes of the Cape Peninsula mountains in the study area. Zones of groundwater flow have also been found to occur in talus on the slopes of mountains such as the Canadian Rockies (Muir et al., 2011). However, these zones were horizontally segregated rather than vertically segregated and they have discrete discharge points (Muir et al., 2011). Both of these explanations for stratification therefore do not sufficiently explain the vertical layering of water with depth that is seen for the springs at the foot of Table Mountain and the groundwater samples collected in 2021. Furthermore, the thickness and hydraulic properties of the scree on the slopes of Table Mountain is poorly understood. It therefore remains unclear how the scree aquifers are stratified. Diamond and Harris (2019) propose that the lower section of the scree aquifer may be dominated by finer material that has settled out from above, or that more metasediments and weathered granite have been incorporated earlier in the formation of the scree slopes, resulting in the vertical variation in the flow dynamics with depth. Further research examining geophysical data (seismic refraction tomography, ground penetrating radar and electrical resistivity tomography), as outlined by Christensen et al. (2020) to investigate the groundwater flow paths within an alpine aquifer system in the Canadian Rockies, would be useful to gain an understanding of the scree slope deposits of the Cape Peninsula mountains.

The scree aquifer is thought to be complex because the unconsolidated sediment can create multiple groundwater flow paths, which may be disconnected from one another as demonstrated by McClymont et al. (2011). The springs at the foot of the slopes of Table Mountain have been found to be distinct from one another in terms of EC (Halenyane, 2017).

Halenyane (2017) states that this is associated with the substrate lithology. This suggests that the spring water, and in turn, the groundwater collected in this study, is derived from a number of different compartments within the scree zone which are split by topographic highs within the regional scree aquifer. Therefore, the local aquifers are thought to occur along existing streams within the valleys of Table Mountain.

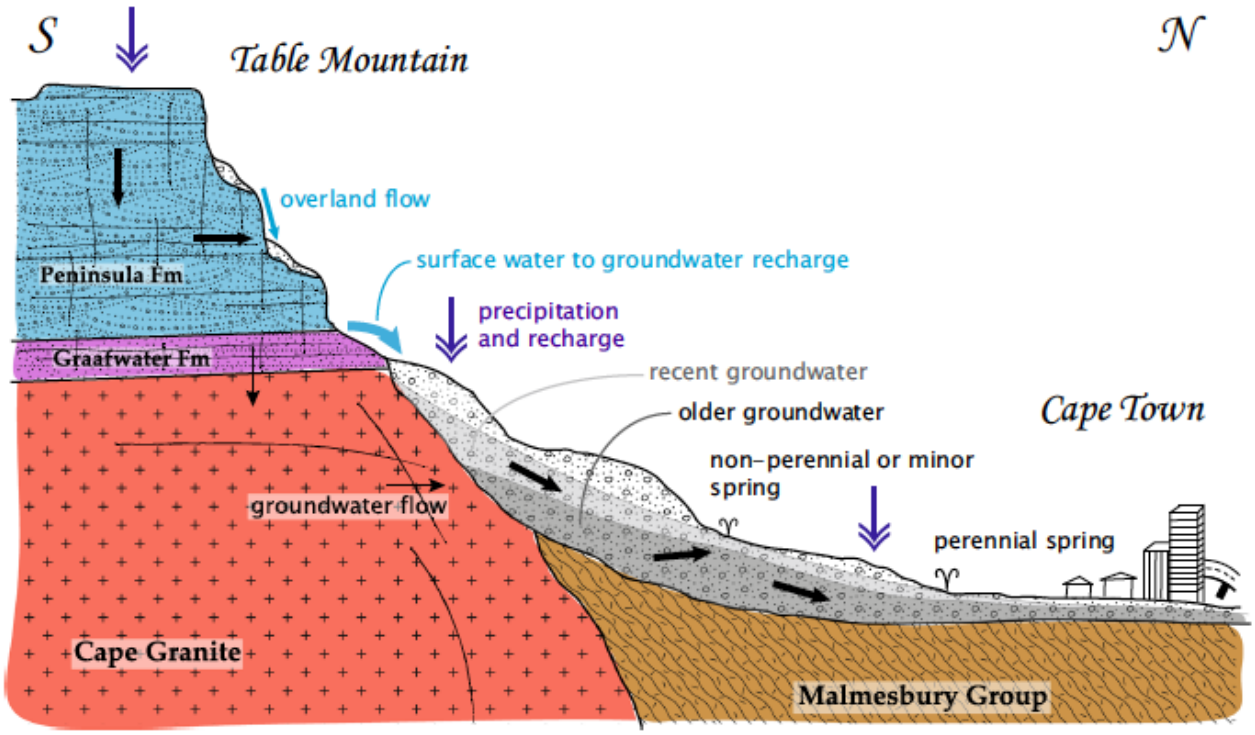

Figure 5.4: Scree aquifer flow model proposed by Diamond and Harris (2019) for the springs on the lower slopes of Table Mountain. Diagram not to scale.

Samples 135, 136, 167, 168, 169, 170, 171, 172, 173, 175, 176, 186, 187, 235, 238, 239 and 240 are located along the slopes of Table Mountain, towards the north and northeast of the study area, are thought to be collected from boreholes and wellpoints located in the Malmesbury Group and not the scree aquifers because the scree deposit is thin or absent in this area. The variation of the δD and $\delta^{18}O$ values with depth for groundwater residing in the Malmesbury Group could not be determined due to the lack of depth data. Previous research has revealed that the Malmesbury Group is generally impervious on a regional scale (DWAF, 2008). It has been found to have a low yield (0.2 – 2.0 L/s) of poor-quality water (Colvin and Saayman, 2017). However, the heterogenous nature of the highly folded strata of the Malmesbury Group has resulted in an uneven distribution of groundwater (Rozendaal et al., 1999). Conrad et al. (2019) have found that boreholes intersecting bedrock fractures of the Malmesbury Group in the Cape Flats can be high yielding of up to 9 L/s in the sandstone layers.

Conrad et al. (2019) proposes that these fractured aquifers of the Malmesbury Group are recharged by a variety of non-vertical sources such as recharge associated with the overlying quartzitic sandstones or Quaternary deposits. Alternatively, the fractured aquifers could simply be recharged by rainwater that is received in areas surrounding the faults (Conrad et al., 2019). The presence of relatively impermeable, thick weathered shale and clay layers above the fractured Malmesbury aquifer indicates that direct vertical infiltration of water is not a significant source of recharge to the Malmesbury aquifer in the Cape Flats region (Conrad et al., 2019).

5.6 The western slopes of the Table Mountain and Constantiaberg massifs

The greater number of samples collected over a broader area with a larger range in altitude and over a longer period of time may be contributors to the greater variability of the δD and $\delta^{18}O$ values of the groundwater samples collected in this study than the groundwater samples collected by Daws (2021) (Figure 4.13). The average altitude of the zone of recharge for the samples collected on the western slopes of the Table Mountain and Constantia massifs appears to be much higher and less variable than on the eastern side of the Cape Peninsula mountains. Therefore, the groundwater samples collected by Daws (2021) have a lower and narrower range in δD and $\delta^{18}O$ values than the eastern slopes because the groundwater samples were collected from closer proximities over higher and more limited altitudes i.e., the differences in the δD and $\delta^{18}O$ values of the two groundwater datasets can largely be attributed to an altitude effect. Alternatively, the more negative δD and $\delta^{18}O$ values of the groundwater samples collected by Daws (2021) could be a function of isotopic rainout. As a cloud producing rainfall is blown from the northwesterly direction (towards the southeast) it approaches the western slopes of the Table Mountain and Constantiaberg massifs. This results in the western slopes receiving rainfall with higher δD and $\delta^{18}O$ values than the eastern slopes of the Cape Peninsula mountain range because the vapour in the cloud becomes progressively depleted in heavier isotopes during the rainfall event. Furthermore, the data collected in this study was collected over 3 years whereas the data collected by Daws (2021) was collected within a year. Therefore, the differences in the gradients of slopes of the two datasets could be a function of the age of the recharge water i.e., the groundwater collected from 2017 – 2021 may contain 'older' water with δD and $\delta^{18}O$ values that differ to the δD and $\delta^{18}O$ values of more recent rainfall experienced in late 2020 and early 2021.

The similarity of the stable isotope values of the groundwater collected by Daws (2021) in spring 2020 and autumn 2021 indicates that there is no obvious seasonal variation in the stable isotope compositions of the groundwater samples on the western slopes of the Table Mountain and Constantiaberg massifs. This is suspected to also be the case for the eastern slopes of the Cape Peninsula mountain range because the temperature differences across Cape Town are not pronounced i.e., the conditions on either side of the mountains should be similar. Harris et al. (2010) found that there was a minor but discernible seasonal effect on the δD and $\delta^{18}O$ values of monthly rainfall collected at UCT between 1996 – 2008 due to the influence of amount and temperature effects. The δD and $\delta^{18}O$ values of the monthly precipitation were weakly correlated with the amount of rainfall and weakly anti-correlated with the temperature (Harris et al., 2010). Summer rainfall had higher δD and $\delta^{18}O$ values than the winter months. Over the long-term, seasonal variability becomes more apparent. The lack of a discernible seasonal effect on the groundwater samples collected by Daws (2021) from the western slopes of the Table Mountain and Constantiaberg massifs, could be the result of the groundwater being recharged predominantly by winter rainfall. If this is the case, it is unclear if the groundwater from the eastern slopes of the Cape Peninsula mountain range would lack a seasonal effect or not because it receives both winter rainfall and summer rainfall, whereas the western slopes mainly receive winter rainfall only. However, the volume of the stored groundwater is much greater than the volume of summer recharge therefore, it is assumed that the groundwater from the eastern slopes would also not show a season effect.

5.7 Strontium isotope composition of the water samples

Strontium differs from oxygen and hydrogen isotopes in that it is not affected by surficial processes such as evaporation. Therefore, $^{87}Sr/^{86}Sr$ is a good indicator of water-rock interaction and mixing, as previously discussed. Unfortunately, this study only analysed 10 samples because of cost.

Halenyane (2017) found that the springs at the base of Table Mountain had varying but relatively low concentrations of strontium of between 19 ppb measured at Main spring and 43 ppb at Albion spring. The concentration of strontium of the groundwater collected in this study was not measured due to expense. However, the concentration of strontium in the groundwater present in the study area is thought to be relatively low but higher than the spring water because the springs contain relatively good quality water with low EC readings. The groundwater with

higher EC measurements are therefore expected to have higher strontium isotope concentrations than the springs because they presumably contain waters with longer residence times during which the water can interact with the rocks through which it flows. The lack of correlation between $^{87}Sr/^{86}Sr$ and EC, indicated by the low correlation coefficient, reveals that the source of strontium is not the same as the source of the EC (Figure 4.18). Therefore, the sources of strontium and EC cannot both be primarily due to the substrate lithology, contamination, or rainfall. They must have different sources or a combination of sources.

Samples 152 and 213 have the lowest $^{87}Sr/^{86}Sr$ ratios with measurements of 0.70985 and 0.70935, respectively (Table 4.5). These values are very similar to the $^{87}Sr/^{86}Sr$ ratio of the modern ocean (0.7092). The analysis of stable isotopes of the groundwater samples has revealed that there is no seawater ingress into the groundwater system of Cape Town. Therefore, the most likely source for the strontium isotope measurements of the water samples chosen for analysis appears to be the interaction of the groundwater with the geology and sediment deposits. Sample 152 was collected from Athlone and sample 213 was collected from Fish Hoek (Figure 4.15; Figure 4.19). The calcareous and dolomite lenses in the Sandveld Group of the Cape Flats, and the shells and carbonate deposits along the coast of Fish Hoek could potentially be the cause of the low $^{87}Sr/^{86}Sr$ ratios of samples 152 and 213. Similarly, the relatively low $^{87}Sr/^{86}Sr$ ratios of samples 145, 195 and 227, collected from the suburbs of Athlone, Bergvliet and Pinelands which are located in (or close to) the Cape Flats could be a function of the consolidate or unconsolidated sediment deposits. Sample 183, collected from a borehole in Vredehoek, and sample 242, collected from a spring in Muizenberg, also have relatively low $^{87}Sr/^{86}Sr$ ratios of 0.71058 and 0.71036, respectively (Figure 4.15). These samples are collected in close proximity to the TMG. As previously discussed, it was found that the TMG contains a negligible concentration of strontium (Weaver et al., 1999). Therefore, the relatively low $^{87}Sr/^{86}Sr$ ratios of samples 183 and 242 could primarily reflect the strontium isotope ratio of the Sandveld Group which may be present in the area. The relatively low $^{87}Sr/^{86}Sr$ ratio of sample 167, collected from the V&A Waterfront, is low for Malmesbury Group but this area is actually reclaimed ground. Sample 181, has the highest $^{87}Sr/^{86}Sr$ ratio of 0.73023. It was collected from the suburb of Camps Bay which is underlain by Cape Granite which is likely the source of the high $^{87}Sr/^{86}Sr$ (Figure 4.15; Table 5.1). Sample 135 has the second highest $^{87}Sr/^{86}Sr$ ratio of 0.72054. It was collected from Groote Schuur Hospital from a depth of 200 m (Table 4.5). It is thought to have a relatively high $^{87}Sr/^{86}Sr$ ratio because it has interacted with the Malmesbury Group (Table 5.1). Therefore, the variation of the strontium

isotope ratios of the water samples collected from across Cape Town indicates the predominant source of strontium is interaction of groundwater with the geology and sediment deposits.

Strontium isotope analysis of Daws' dataset of groundwater samples from the western slopes of the Table Mountain and Constantiaberg massifs, reveals that they have a similar range in $^{87}Sr/^{86}Sr$ ratios to the samples analysed in this study (Figure 4.15). This suggests that the strontium in groundwater collected from the western slopes of the Table Mountain and Constantiaberg massifs is derived from different sources in similar proportions to the eastern slopes of the Cape Peninsula mountain range. Therefore, similarly to sample 181, the end-member from Daws' dataset with the highest $^{87}Sr/^{86}Sr$ ratio of 0.731182 (HB28) is thought to be derived from groundwater that has interacted with the Cape Granite Suite or the Malmesbury Group (present NW of Table Mountain, which both have high strontium isotope ratios), to the same extent as the water from the eastern slopes (Figure 4.15; Table 5.1).

The samples collected at altitudes of <20 mamsl ($\bar{x}$= 0.71148) have a lower average strontium isotope ratio than the samples collected at altitudes of >20 mamsl ($\bar{x}$= 0.72045) (Figure 4.16). This could reflect the influence of the geology and sediment deposits on the strontium isotope ratios of the groundwater. At lower altitudes calcareous and dolomite lenses in the Sandveld Group are present and at higher altitudes, the relatively resistant TMG and Cape Granite Suite occur. The decrease in the range of the $^{87}Sr/^{86}Sr$ ratios with increasing distance from the TMG and Malmesbury Group unconformity also suggests that the geology and sediment deposits could affect the strontium isotope ratios (Figure 4.17). Closer to the TMG and Cape Granite Suite, the average strontium isotope ratio of the tabular cluster of datapoints ($\bar{x}$= 0.71621) is slightly higher than the average strontium isotope ratio of the concave circular cluster of datapoints ($\bar{x}$= 0.71213) in areas located further away, such as the Cape Flats where the Sandveld Group contains calcareous and dolomite lenses with lower $^{87}Sr/^{86}Sr$ ratios (Figure 4.17).

Table 5.1: Comparison of the strontium isotope ratios of the major rock types of the southwestern Cape (Midgley et al. (2012).

Rock type	**$^{87}Sr/^{86}Sr$ ratio**
Late Precambrian carbonates	0.71025
Malmesbury Group	0.7208 - 0.7873
Cape Granite Suite	0.7701- 0.1.1600
TMG	Sr concentrations too low to detect

The low correlation coefficient (r= 0.30) between the $^{87}Sr/^{86}Sr$ and the $\delta^{18}O$ values indicates that the relationship is not significant for a sample size of 10 (Figure 4.19). The lack of correlation between these two variables could be a function of oxygen isotopes being constrained by different process to strontium isotopes e.g. oxygen isotopes are susceptible to the influence of surface processes such as evaporation, whereas strontium isotopes are not.

5.8 Limitations

There is an obvious spatial bias in this study. The majority of the boreholes and wellpoints sampled in this study are located on the predominantly the eastern slopes of the Cape Peninsula mountain range. In order to gain a more holistic view of the groundwater system, samples should be collected throughout the study area with a more even distribution. For example, more samples should be collected from areas such as Seapoint and the Cape Flats. It would also be useful to obtain proper depth data by using packers in deep boreholes in order to gain insights into the aquifer flow dynamics i.e. to determine if there is stratification or another mechanism of flow. In particular, it would have been interesting to investigate a model of the aquifer flow dynamics for the samples collected from boreholes and wellpoints occurring within the Malmesbury Group. It also would have been advantageous to have been more consistent with the temperature measurements - there are no temperature measurements for the Constantia water samples and for the samples collected via the crowd-sourcing method. The use of two different instruments to measure EC across the different rounds of data collection could also have affected the precision of the results. The WTW-conductivity multimeter is generally more sensitive to lower salinities than the Hannah instruments HI-199300 waterproof pH meter. The stable isotope analyses were also performed by different people across the different years, which could have introduced human error into the results. It would be useful to examine more

chemical data, which was limited in this study because it is expensive. For example, major cations and anions should be measured in future studies to assist in determining the source of the elements causing the EC and pH readings. In addition, hydrochemistry data could improve our understanding of the source of strontium in an aquifer. There is a tendency for near coast aquifer systems to have $^{87}Sr/^{86}Sr$ ratios that are similar to the $^{87}Sr/^{86}Sr$ ratios of the modern ocean due to the deposition of calcareous marine sediments with high proportions of shell material, and strontium supplied from fog events and sea spray (Scott et al., 2020). Therefore, hydrochemistry data could potentially assist with clarifying ambiguities associated with the source of strontium in groundwater in near coast regions. A study of tap water in conjunction to the groundwater may be helpful to determine if there are municipal water leaks in the study area. For example, sample 49 has an EC measurement that is very similar to tap water, therefore its reading could be affected by municipal water. A further investigation on the seasonal effects on groundwater from the eastern and western slopes of the Cape Peninsula mountain range may be useful in determining the ultimate sources of water to the aquifers. A greater temporal analysis of the groundwater is recommended in order to investigate the recharge rates and the response of the groundwater system to changing climatic conditions over time more thoroughly i.e. repeating the same exercise 3 years apart to see what change occurs.

Furthermore, it is unclear if the isoscapes represent the data appropriately (Figure 4.9). The aquifers are thought to be stratified. Therefore, it is not obvious if it is reasonable to compare water samples collected at different depths since it is thought that water at shallow depths is recharged by ambient rainfall and water at deep depths (>5 m) is recharged predominantly by heavy rainfall events (at least for the groundwater samples collected from the eastern slopes of the Cape Peninsula mountain range). In addition, the water samples are thought to be derived from two different aquifers. Many of the samples were also not collected directly from the borehole or wellpoint (e.g., they were collected from storage tanks etc.). Hence, constructing an isoscape may be misrepresentative.

Chapter 6: Conclusions

Approximately 48% of the groundwater samples have EC measurements that are within the potable range of <0.7 mS/cm and 93% are within the safety limit for human consumption. The δD and $\delta^{18}O$ values of the water samples (including stagnant surface, spring, river and groundwater) ranges from -19.9‰ to +13.7‰ and -4.37‰ to +2.35‰, respectively, whereas the groundwater samples range from -19.9‰ to +4.2‰ and -4.37‰ to +0.24‰ respectively. The relatively low EC, as well as the δD and $\delta^{18}O$ values of the groundwater samples being isotopically distinct from seawater indicates that there has been no seawater ingress into the parts of the groundwater system of Cape Town that were analysed (i.e. 256 samples were collected from an area of 330 km^2). Whereas a single aquifer can contain water with varying composition (e.g. the EC of Pinelands water) the data are consistent with either multiple localised aquifers or compartments within the regional CFA and scree aquifers**.** Pinelands is probably a subdivision of the CFA, in which the aquifer (unconsolidated sand) has a high concentration of salt.

The lines of best fit through the groundwater data (LSM: $\delta D = 5.20*\delta^{18}O + 3.17$; RMA method: $\delta D = 5.58*\delta^{18}O + 4.14$) are similar to one another but differ to the LMWL calculated at UCT for 1996 – 2008, in terms of the y-intercept values. They are more similar to the recent UCT LMWLs based on rainfall received from 2009 – 2020. This suggests a change in the δD and $\delta^{18}O$ values of the rainfall between the two time periods, which could be climate related. The correlation between the δD and $\delta^{18}O$ values of 0.94 is good, as is the case for meteoric water worldwide, but the overall variation of the oxygen and hydrogen isotope composition of the groundwater and its similarity with present-day rainfall indicates that the aquifers are recharged by local, present-day precipitation.

The majority of the groundwater samples that were collected at higher altitudes (>30 mamsl), on the eastern slopes of the Cape Peninsula mountains have EC measurements of <1 mS/cm. At lower altitudes (<30 mamsl) the EC measurements are generally higher. This pattern of increasing isotopic ratios of the groundwater at lower altitudes could be due to: 1) an inherited signature from the rainfall, which is affected by altitude and minor amount effects and/or 2) evaporative enrichment of the return flow of abstracted groundwater as a result of prolonged near surface residence, as a result of extensive irrigation in areas such as Philippi

Farmlands. The δD and $\delta^{18}O$ values of the groundwater samples, collected from the eastern slopes of the Cape Peninsula mountains, increase with depth. This indicates that the scree aquifer is stratified.

The $^{87}Sr/^{86}Sr$ ratios for the subset of the 10 samples range from 0.70935 to 0.73023 with an average of 0.71417. The $^{87}Sr/^{86}Sr$ ratios of the groundwater samples must be related to the interaction of the water with the local geology and sediment deposits. The $^{87}Sr/^{86}Sr$ ratios of the water samples collected by Daws (2021) from the western slopes of the Table Mountain and Constantiaberg massifs has similar $^{87}Sr/^{86}Sr$ ratios of 0.709507 to 0.731182 with an average of 0.71917. This reveals that they have strontium derived from different sources in similar proportions.

The stable isotope composition of the groundwater collected in this study is distinct from the data collected by Daws (2021) from the western slopes of the Table Mountain and Constantiaberg massifs. Daws' groundwater dataset likely differs due to the influence of an altitude effect and /or isotope rain-out in addition to the data being collected over different time periods. Furthermore, the groundwater from this study differs isotopically from water collected from the Main and Albion springs- these have lower δD values for given $\delta^{18}O$ values with an average d-excess value of +12.93‰ in comparison to the groundwater which has an average d-excess value of +10.44‰. The groundwater collected from the eastern slopes of the Cape Peninsula mountains have a similar stable isotope composition to the CFA and Constantia groundwater. Recharge of groundwater on the eastern slopes is therefore thought to be similar to the rates of recharge of the CFA and scree aquifer on the upper slopes of Constantia but slower than for the Table Mountain springs (which are recharged by approximately 50% within 3 years) because the recharge area and volume of water contained in the scree aprons from which the springs are derived is smaller than the groundwater. These findings are useful to assist with ensuring sustainable extraction of groundwater through the monitoring of abstraction vs. recharge rates.

References

Adamson, J. 2006. *ECN Technical Note 3*. Available: http://www.ecn.ac.uk/measurements/technical-notes/preparation-of-conductivity-and-ph-solutions/view [2021, August 11].

Adelana, S. and Xu, Y. 2006. Contamination and protection of the Cape Flats Aquifer, South Africa. In *Groundwater pollution in Africa*. Y. Xu and B. Usher, Eds. London: Chemical Rubber Company Press. 265-277. DOI: http://dx.doi.org/10.1201/9780203963548.ch23

Agyare-Dwomoh, Y. 2020. *The application of Radon-222 in constraining groundwater recharge in the City of Cape Town and its surrounds*. MSc Dissertation. Stellenbosch University. Available: https://scholar.sun.ac.za/handle/10019.1/108087 [2021, July 13].

Alfarrah, N. and Walraevens, K. 2018. Groundwater Overexploitation and seawater intrusion in coastal areas of arid and semi-arid regions. *Water*, 10(2): 143-166. DOI: https://doi.org/10.3390/w10020143

American Water Works Association. 2014. *Groundwater - Manual of Water Supply Practices, M21 (4th Edition)*. Denver, CO: American Water Works Association.

Anderson, H. and Cummings, D. 1999. *Measuring the salinity of water*. (Report no. LC0064). Victoria, Australia: Department of Sustainability and Environment.

Aza-Gnandji, C.D., Xu, Y., Raitt, L. and Levy, J. 2013. Salinity of irrigation water in the Philippi farming area of the Cape Flats, Cape Town, South Africa. *Water SA*, 39(2): 199-210. DOI: https://doi.org/10.4314/wsa.v39i2.3

Boelhouwers, J. 1993. A discussion regarding weathering in the Western Cape Mountains, South Africa: implications for Pleistocene cryoclastic debris production. *South African Geographical Journal*, 75(2): 46-52. DOI: https://doi.org/10.1080/03736245.1993.10586404

Botha, G.A. 2006. The coastal Cenozoic deposits. In *the geology of South Africa*. M.R., Johnson, C.R., Anhaeusser and R.J., Thomas, Eds. Pretoria, South Africa: Geological Society of South Africa and the Council for Geoscience: 605-628.

Bowen, G.J. 2010. Isoscapes: spatial pattern in isotopic biogeochemistry. *Annual Review of Earth and Planetary Sciences*, 38: 161-187. DOI: https://doi.org/10.1146/annurev-earth-040809-152429

Bowen, G.J., Putman, A., Brooks, J.R., Bowling, D.R., Oerter, E.J. and Good, S.P. 2018. Inferring the source of evaporated waters using stable H and O isotopes. *Oecologia*, 187: 1025-1039. DOI: https://doi.org/10.1007/s00442-018-4192-5

Brace W.F. 1984. Permeability of crystalline rocks: New in situ measurements. *Journal of Geophysical Research*, 89: 4327-4330. DOI: https://doi.org/10.1029/JB089iB06p04327

Brown, C., Colvin, C., Hartnady, C., Hay, R., Le Maitre, D. and Riemann, K. 2003. *Ecological and environmental impacts of large-scale groundwater development in the Table Mountain Group (TMG) Aquifer system. Discussion document for scoping phase. WRC project K5/1327.* (CSIR report no. ENV-S-C 2003-076). Stellenbosch, South Africa: CSIR Environmentek.

Browning, C. and Roberts, D.L. 2015. Lithostratigraphy of the Witzand Formation (Sandveld Group), South Africa. *South African Journal of Geology*, 118(3): 317-322. DOI: https://doi.org/10.2113/gssajg.118.3.317

"Cape Province". *Encyclopaedia Britannica online*. 2013. Encyclopaedia Britannica. Available: https://www.britannica.com/place/Cape-Province [2021, July 12].

City of Cape Town. 2018a. *How the City of Cape Town manages leaks and burst pipes guide and FAQs.* Cape Town, South Africa: City of Cape Town.

City of Cape Town. 2018b. *Water services and the Cape Town urban water cycle*. Cape Town, South Africa: City of Cape Town.

City of Cape Town. 2019. *Draft Cape Flats District baseline and analysis report 2019: state of the environment* (draft version 1.1). Cape Town, South Africa: City of Cape Town.

City of Cape Town Open Data Portal. 2015a. *Digital elevation model* [Shape file, September 15]. City of Cape Town Open Data Portal. Available: https://web1.capetown.gov.za/web1/opendataportal/DatasetSearchResult?&searchTerm=DEM [2021, September 07].

City of Cape Town Open Data Portal. 2015b. *Open watercourses* [Shape file, December 11]. City of Cape Town Open Data Portal. Available: https://web1.capetown.gov.za/web1/opendataportal/DatasetDetail?DatasetName=Open%20watercourses [2021, March 17].

City of Cape Town Open Data Portal. 2016. *Road centreline* [Shape file, January 13]. City of Cape Town Open Data Portal. Available: https://web1.capetown.gov.za/web1/opendataportal/DatasetDetail?DatasetName=Road%20centrelines [2021, March 17].

Christensen, C.W., Hayashi, M. and Bentley, L.R. 2020. Hydrogeological characterization of an alpine aquifer system in the Canadian Rocky Mountains. *Hydrogeology Journal*, 28: 1871-1890. DOI: https://doi.org/10.1007/s10040-020-02153-7

Cole, D.J. 2011. *Report on economically-viable mineral resources in the City of Cape Town's administrative area*. Cape Town, South Africa: Council for Geoscience.

Colvin, C. and Saayman, I. 2007. Challenges to groundwater governance: a case study of groundwater governance in Cape Town, South Africa. *Water Policy*, 9(2): 127-148. DOI: http://dx.doi.org/10.2166/wp.2007.129

Compton, J. 2004. *The rocks and mountains of Cape Town.* Cape Town, South Africa: Double Storey Books.

Conrad, J., Smit, L., Murray, K. and van Gend-Muller, J. 2019. The Malmesbury Group - an aquifer of surprising significance. *South African Journal of Geology*, 122(3): 331-342. DOI: https://doi.org/10.25131/sajg.122.0028

Copeland, S.R., Cawthra, H.C., Fisher, E.C., Lee-Thorp, J.A., Cowling, R.M., le Roux, P.J., Hodgkins, J. and Marean, C.W. 2016. Strontium isotope investigation of ungulate movement patterns on the Pleistocene Paleo-Agulhas Plain of the Greater Cape Floristic Region, South Africa. *Quaternary Science Reviews*, 141: 65-84. DOI: http://dx.doi.org/10.1016/j.quascirev.2016.04.002

Copernicus. 2021. *Digital elevation model*. [Shape file, 12 April]. Copernicus. Available: https://registry.opendata.aws/copernicus-dem [2021, November 30].

Council for Geoscience. 1990. *Cape Town 3318* [Map]. Scale 1:250 000. 1:250 000 Geological Series. Pretoria, South Africa: Council for Geoscience.

Cowling, R.M., MacDonald, I.A.W. and Simmons, M.T. 1995. The Cape Peninsula, South Africa: physiographical, biological and historical background to an extraordinary hot-spot of biodiversity. *Biodiversity & Conservation*, 5(5): 527-550. DOI: https://doi.org/10.1007/BF00137608

Craig, H. 1961. Isotopic variations in meteoric waters. *Science*, 133(3465): 1702-1703. DOI: https://doi.org/10.1126/science.133.3465.1702

Dansgaard, W. 1964. Stable isotopes in precipitation. *Tellus*, 16(4): 436-468. DOI: https://doi.org/10.1111/j.2153-3490.1964.tb00181.x

Day, L., Ollis, D., Ngobela, T. and Rivers-Moore, N. 2020. *Water quality of rivers and open waterbodies in the City of Cape Town: status and historical trends, with a focus on the period April 2015 to March 2020.* Cape Town, South Africa: City of Cape Town.

Deacon, H.J. and Deacon, J. 1999. *Human beginnings in South Africa: uncovering the secrets of the Stone Age*. Cape Town, South Africa: David Philip Publishers.

Department of Water Affairs. 2010. *Groundwater strategy 2010.* Pretoria, South Africa: Department of Water Affairs.

Department of Water Affairs and Forestry. 1996. *South African water quality guidelines*. 2nd ed. V.1. Domestic use. Pretoria, South Africa: Department of Water Affairs and Forestry.

Department of Water Affairs and Forestry. 2007. *The Assessment of Water Availability in the Berg Catchment (WMA 19) by Means of Water Resource Related Models: Groundwater Model Report Volume 4 – Regional Water Balance Model.* (Research report P WMA 19/000/00/0407). Pretoria, South Africa: Umvoto Africa (Pty) Ltd in association with Ninham Shand (Pty) Ltd on behalf of the Directorate : National Water Resource Planning.

Department of Water Affairs and Forestry. 2008. *The assessment of water availability in the Berg Catchment (WMA 19) by means of water resource related models: groundwater model report volume 5 – Cape Flats Aquifer model.* (Research report P MWA 19/000/00/0408). Pretoria, South Africa: Umvoto Africa.

de Beer, C.H. 2002. The stratigraphy, lithology and structure of the Table Mountain Group. In *A synthesis of the hydrogeology of the Table Mountain Group – formation of a research strategy*. (WRC report no. TT 158/01). K., Pietersen, and R., Parsons, Eds. Cape Town, South Africa: Water Research Commission: 9-18.

de Vries, J.J. and Simmers, I. 2002. Groundwater recharge: an overview of processes and challenges. *Hydrogeology Journal,* 10: 5–17. DOI: https://doi.org/10.1007/s10040-001-0171-7

de Wet, R.F., West, A.G. and Harris, C. 2020. Seasonal variation in tap water δ^2H and $\delta^{18}O$ isotopes reveals two tap water worlds. *Scientific Reports,* 10(2020). DOI: https://doi.org/10.1038/s41598-020-70317-2

Diamond, R.E. 2014. *Stable isotope hydrology of the Table Mountain Group*. Ph.D. Thesis. University of Cape Town. Available: https://open.uct.ac.za/handle/11427/21190 [2021, July 19].

Diamond, R.E. and Harris, C. 2000. Oxygen and hydrogen isotope geochemistry of thermal springs of the Western Cape, South Africa: recharge at high altitude? *Journal of African Earth Sciences,* 31(3/4): 467-481. DOI: https://doi.org/10.1016/S0899-5362(00)80002-0

Diamond, R.E. and Harris, C. 2019. Annual shifts in O-and H-isotope composition as measures of recharge: the case of the Table Mountain springs, Cape Town, South Africa. *Hydrogeology Journal*, *27*(8): 2993-3008. DOI: http://dx.doi.org/10.1007/s10040-019-02045-5

Dippenaar, M.A. 2016. *Hydrological heritage overview: Cape Town*. Pretoria, South Africa: The Water Research Commission.

Emmanuel, E., Pierre, M.G. and Perrodin, Y. 2009. Groundwater contamination by microbiological and chemical substances released from hospital wastewater: health risk assessment for drinking water consumers. *Environment international*, *35*(4): 718-726. DOI: https://doi.org/10.1016/j.envint.2009.01.011

February, E., Bond, W., Taylor, R. and Newton, R. 2004. Will water abstraction from the Table Mountain Aquifer threaten endemic species? A case study at Cape Point, Cape Town. *South African Journal of Science*, 100: 2-4. DOI: https://hdl.handle.net/10520/EJC96262

Fourie, F., Mbatha, K. and Verster, H. 2002. *The Effect of Vegetation (Prosopis spp.) on Groundwater levels in Rugseer River, Kenhardt, South Africa*. Pretoria, South Africa: Department of Water Affairs and Forestry. 1-8. (Unpublished).

Frimmel, H.E., Fölling, P.G. and Diamond, R. 2001. Metamorphism of the Permo-Triassic Cape Fold Belt and its basement, South Africa. *Minerology and Petrology*, 73(4): 325-346. DOI: http://dx.doi.org/10.1007/s007100170005

Gamal, H., Elkatatny, S., Basfar, S. and Al-Majed, A. 2019. Effect of pH on rheological and filtration properties of water-based drilling fluid based on bentonite. *Sustainability*, 11(23): 1-13. https://doi.org/10.3390/su11236714

Gat, J.R. 1996. Oxygen and hydrogen isotopes in the hydrologic cycle. *Annual Review of Earth and Planetary Sciences*, 24(1): 225-262. DOI: https://doi.org/10.1146/annurev.earth.24.1.225

Gat, J.R. and Carmi, I. 1970. Evolution of the isotopic composition of atmospheric waters in the Mediterranean Sea area. *Journal of Geophysical Research Atmospheres*, 75(15): 3039-3048. DOI: https://doi.org/10.1029/JC075i015p03039

Gat, J.R. and Tzur, Y. 1967. Modification of the isotopic composition of rainwater by processes which occur before groundwater recharge. *Conference: Symposium on Isotopes in Hydrology*. 14-18 November 1966. Vienna, Austria: International Atomic Energy Agency: 49–60.

Gee, G.W. and Hillel, D. 1998. Groundwater recharge in arid regions: review and critique of estimation methods. *Hydrological Processes*, 2: 255-266. DOI: https://doi.org/10.1002/hyp.3360020306

Geng, X., Boufadel, M.C. and Jackson, N.L. 2016. Evidence of salt accumulation in beach intertidal zone due to evaporation. *Scientific Reports*, 6(31486): 1-4. DOI: https://doi.org/10.1002/hyp.3360020306

Gerber, A. 1981. *A digital model of groundwater flow in the Cape Flats aquifer*. (Report C WAT 46). Pretoria, South Africa: National Institute for Water Research, Council for Scientific and Industrial Research.

Global Earth Observation System of Systems, South Africa. 2020. *Groundtruthing: establishing a citizen science groundwater monitoring network in Cape Town*. (Report no. 2019/11-02). Cape Town, South Africa: World Wide Fund for Nature.

Gomo, M. 2018. Conceptual hydrogeochemical characteristics of a calcite and dolomite acid mine drainage neutralised circumneutral groundwater system. *Water Science*, 32(2): 355-361. DOI: https://doi.org/10.1016/j.wsj.2018.05.004

Google Earth Pro 7.3.4.8248 (64-bit). 2019a. *Cape Town, ON South Africa* [Map, April 27]. 34° 04' 02.11"S, 18° 29' 03.24"E, Eye alt 49.57 km. NOAA, U.S. Navy, NGA, GEBCO 2021. Available: http://www.google.com/earth/index.html [2021, March 12].

Google Earth Pro 7.3.4.8248 (64-bit). 2019b. *Cape Town, ON South Africa* [Map, April 27]. 33° 57' 00.01"S, 18° 28' 00.62"E, Eye alt 9.09 km. NOAA, U.S. Navy, NGA, GEBCO 2021. Available: http://www.google.com/earth/index.html [2021, October 23].

Google Maps. 2021. *Cape Town, South Africa.* Available: https://www.google.com/maps/@-34.0575812,18.4052435,10.77z [2021, March 12].

Gresse, P.G., Von Veh, M.W. and Frimmel, H.E. 2006. Namibian (Neoproterozoic) to early Cambrian successions. In *the geology of South Africa*. M.R., Johnson, C.R., Anhaeusser and R.J., Thomas, Eds. Pretoria, South Africa: Geological Society of South Africa and the Council for Geoscience: 395-420.

Halenyane, K. 2017. *Investigating recharge rates in Table Mountain Springs using oxygen and hydrogen isotopes.* MSc Dissertation. University of Cape Town. Available: https://open.uct.ac.za/handle/11427/27834 [2020, November 27].

Hariall, Z. 2020. *Noble gas and radiocarbon constraints on the residence times of groundwater in and around the city of Cape Town*. MSc Dissertation. Stellenbosch University. Available: https://scholar.sun.ac.hemi/handle/10019.1/108020 [2021, June 03].

Harper, W.V. 2014. Reduced major axis regression: teaching alternatives to least squares. *9th International Conference on Teaching Statistics* . 13-18 July 2014. Flagstaff, AZ,: International Association for Statistical Education.

Harris, C. 2017. Report on the stable isotope composition of groundwater in the Constantia area. (Unpublished).

Harris, C., Burgers, C., Miller, J. and Rawoot, F. 2010. O-and H-isotope record of Cape Town rainfall from 1996 to 2008, and its application to recharge studies of Table Mountain groundwater, South Africa. *South African Journal of Geology, 113*(1): 33-56. DOI: http://dx.doi.org/10.2113/gssajg.113.1.33

Harris, C., Oom, B.M. and Diamond, R.E. 1999. A preliminary investigation of the oxygen and hydrogen isotope hydrology of the greater Cape Town area and an assessment of the potential for using stable isotopes at tracers. *Water SA,* 25(1): 15-24.

Harris, C. and Vogeli, J. 2010. Oxygen isotope composition of garnet in the Peninsula Granite, Cape Granite Suite, South Africa: Constraints on melting and emplacement mechanisms. *South African Journal of Geology,* 113(4): 385-396. DOI: https://doi.org/10.2113/gssajg.113.4.401

Hartnady, C. J. and Hay, R. 2000. *Reconnaissance investigation into the development and utilisation of Table Mountain Group artesian groundwater, using the E10 catchment as a pilot study area.* (Steffen, Robertson and Kirsten (SRK) and Umvoto Africa report no. 2.2(510)). Pretoria, South Africa: Department of Water Affairs and Forestry.

Hartnady, C. and Jones, M. 2007. *Geothermal studies of the Table Mountain Group Aquifer Systems*. (WRC Report No 1403/1/07). Cape Town, South Africa: Water Research Commission.

Harvey, F.E. and Silbray, S.S. 2001. Delineating ground water recharge from leaking irrigation canals using water chemistry and isotopes. *Ground Water*, 39(3): 408-421. DOI: https://doi.org/10.1111/j.1745-6584.2001.tb02325.x

Hay, R., McGibbon, D., Botha, F. and Riemann, K. 2015. Cape Flats Aquifer and False Bay–opportunities to change. *79th IMESA Conference 2015, Annual conference and exhibition of the Institute of Municipal Engineering of Southern Africa on changing the face of the municipal engineer*. 27-30 October 2015. Cape Town, South Africa: Institute of Municipal Engineering of Southern Africa.

HKS LAWGIBB. 1995. *Introductory study - environmental contamination and geotechnical conditions.* Culemborg - Black River, Cape Town. (Unpublished).

Hoefs, J. 2009. *Stable isotope geochemistry*. Heidelberg, Germany: Springer-Verlag Berlin. DOI: https://doi.org/10.1007/978-3-540-70708-0

International Atomic Energy Agency. 1992. *Statistical treatment of data on environmental isotopes in precipitation*. (Technical Report Series no. 331). Vienna, Austria: International Atomic Energy Agency.

International Atomic Energy Agency and World Meteorological Organization. 2006. *Station 6881600 'Malan' (Cape Town) South Africa. Global Network of Isotopes in Precipitation.* The GNIP database. Available: http://isohis.iaea.org [2021, August 14].

Intergovernmental Panel on Climate Change. 2021. Summary for policy makers. In *Climate change 2021: The physical science basis*. (Research report IPCC AR6 WG1). V., Masson-Delmotte, P., Zhai, A., Pirani, S. L., Connors, C., Péan, S., Berger, N., Caud, Y., Chen, L., Goldfarb, M. I., Gomis, M., Huang, K., Leitzell, E., Lonnoy, J.B.R., Matthews, T. K., Maycock, T., Waterfield, O., Yelekçi, R., Yu and B., Zhou, Eds. Cambridge, England: Cambridge University Press: 1-41.

Jolly, J.L. and Kotze, J.C. 2002. The Klein Karoo rural water supply scheme. In *A synthesis of the hydrogeology of the Table Mountain Group – formation of a research strategy*. (WRC report no. TT 158/01). K., Pietersen, and R., Parsons, Eds. Cape Town, South Africa: Water Research Commission: 198-201.

Jørgensen, N.O., Andersen, M.S. and Engesgaard, P. 2008. Investigation of a dynamic seawater intrusion event using strontium isotopes ($^{87}Sr/^{86}Sr$). *Journal of Hydrology*, 348: 257-269. DOI: https://doi.org/10.1016/j.jhydrol.2007.10.001

Kasolo, N. 2020. H and O isotope composition of Cape Town rainfall between 2009-2019: An isotopic perspective of the 2015-2017 'great drought'. BSc Hons thesis. University of Cape Town. (Unpublished).

Kharaka, Y.K. and Hanor, J.S. 2014. Deep fluids in sedimentary basins. *In Treatise on geochemistry.* 2nd ed. H.D. Holland and K.K. Turekian, Eds. California, CA: Elsevier Science.

Kotze, J.C., Verhagen, B.T. and Butler, M.J. 2000. An aquifer model based on chemistry, isotopes and lineament mapping: Little Karoo, South Africa. In *Groundwater: past*

achievements and future challenges. O., Sililo, Ed. Rotterdam, Netherlands: Balkema: 539-544.

Kotze, J. C. 2002. *Towards a management tool for groundwater exploitation in the Table Mountain sandstone fractured aquifer*. (WRC Report No. 729/1/02). Cape Town, South Africa: Water Research Commission.

Lin, L., Jia, H. and Xu, Y. 2007. Fracture network characteristics of a deep borehole in the Table Mountain Group (TMG), South Africa. *Hydrogeology Journal*, 15:1419-1432. DOI: http://dx.doi.org/10.1007/s10040-007-0184-y

Mary River Catchment Coordinating Committee. 2013. *Water quality salinity standards*. Available: https://mrccc.org.au/fact-sheets/ [2021, April 2013].

McClymont, A.F., Roy, J.W., Hayashi, M., Bentley, L.R., Maurer, H. and Langston, G. 2011. Investigating groundwater flow paths within proglacial moraine using multiple geophysical methods. *Journal of Hydrology*, 399(1-2): 57-66. DOI: https://doi.org/10.1016/j.jhydrol.2010.12.036

McMullen, C.C., Fritze, K. and Tomilson, R.H. 1966. The half-life of Rubidium- 87. *Canadian Journal of Physics*, 44(12): 3033-3038. https://doi.org/10.1139/p66-248

McNutt, R.H. 2000. Strontium isotopes. In *Environmental tracers in subsurface hydrology.* P.G. Cook, and A.L. Herczeg, Eds. Glen Osmond, Australia: Springer. DOI: https://doi.org/10.1007/978-1-4615-4557-6

Merriam-Webster. n.d. *Vlei.* Available: https://www.merriam-webster.com/dictionary/vlei [2021, September 02].

Meyer, P.S. 2001. *An explanation of the 1:500 000 hydrogeological map of Cape Town 3317*. Pretoria; South Africa: Directorate Geohydrology, Department of Water Affairs and Forestry.

Midgley, G.F., Chapman, R.A., Hewitson, B., Johnston, P., De Wit, M., Ziervogel, G., Mukheibir, P., Van Niekerk, L., Tadross, M., Van Wilgen, B.W. and Kgope, B. 2005. *A status quo, vulnerability and adaptation assessment of the physical and socio-economic effects of climate change in the Western Cape.* (Research report ENV-S-C 2005-073). Cape Town, South Africa: Department of Environmental Affairs and Development Planning, Provincial Government of the Western Cape. DOI: http://hdl.handle.net/11427/17144

Midgley, J.J., Harris, C., Harington, A. and Potts, A.J. 2012. Geochemical perspective on origins and consequences of heuweltjie formation in the southwestern Cape, South Africa. *South African journal of geology*, 115(4): 577-588. DOI: https://doi.org/10.2113/gssajg.115.4.577

Miller, J.A., Dunford, A.J., Swana, K.A., Palcsu, L., Butler, M. and Clarke, C.E. 2017. Stable isotope and noble gas constraints on the source and residence times of spring water from the Table Mountain Group Aquifer, Paarl, South Africa and implications for

large scale abstraction. *Journal of Hydrology*, 551: 100-115. DOI: http://dx.doi.org/10.1016/j.jhydrol.2017.05.036

Moorcroft, L.B. 2019. *Trace metal contamination of soil and groundwater in the Rietvlei Catchment, Cape Town.* MSc dissertation. North-West University. Available: https://repository.nwu.ac.za/handle/10394/34129?show=full [2021, June 04].

Mugabe, J.C. 2013. *Environmental report for Capricorn Business Park May/June 2013.* Muizenberg, South Africa: Cape Town Environmental Education Trust.

Muir, D.L., Hayashi, M. and McClymont, A.F. 2011. Hydrological storage and transmission characteristics of an alpine talus. *Hydrological Processes*, 25(19): 2954–2966. DOI: https://doi.org/10.1002/hyp.8060

Netili, K.F. 2007. *A preliminary understanding of deep groundwater flow in the Table Mountain group (TMG) aquifer system.* Ph.D. Dissertation. University of the Western Cape. Available: http://etd.uwc.ac.za/xmlui/handle/11394/2314 [2021, June 03].

Newlands Brewery. n.d. *Spring time in Newlands, since 1820*. Available: https://newlandsbrewery.co.za/newlands-spring/ [2021, July 13].

Otto, F.E., Wolski, P., Lehner, F., Tebaldi, C., Van Oldenborgh, G.J., Hogesteeger, S., Singh, R., Holden, P., Fučkar, N.S., Odoulami, R.C. and New, M. 2018. Anthropogenic influence on the drivers of the Western Cape drought 2015–2017. *Environmental Research Letters*, 13(12):1-9. DOI: http://dx.doi.org/10.1088/1748-9326/aae9f9

Oxford University Press. 2021. *Semi-confined aquifer*. Available: https://www.oxfordreference.com/view/10.1093/oi/authority.20110803100453961 [2021, June 03].

Ramjukadh1, C., Silberbauer, M. and Taljaard, S. 2018. An anomaly in pH data in South Africa's national water quality monitoring database – implications for future water use. *Water SA*, 44(4): 760 – 763. DOI: http://dx.doi.org/10.4314/wsa.v44i4.23

Rebelo, A.G., Holmes, P.M., Dorse, C. and Wood, J. 2011. Impacts of urbanization in a biodiversity hotspot: Conservation challenges in Metropolitan Cape Town. *South Africa Journal of Botany*, 77(1): 20-35. DOI: https://doi.org/10.1016/j.sajb.2010.04.006

Reid, D.L., Erlank, A.J. and Rex, D.C. 1991. Age and correlation of the False Bay dolerite dyke swarm, south-western Cape, Cape province. *South African Journal of Geology*, 94(2/3): 155-158.

Roberts, D.L., Bateman, M.D., Murray-Wallace, C.V., Carr, A.S. and Holmes, P.J. 2008. West coast dune plumes: climate driven contrasts in dunefield morphogenesis along the western and southern South African coasts. *Palaeogeography, Palaeoclimatology, Palaeoecology*, 271(1-2): 24-38. DOI: https://doi.org/10.1016/j.palaeo.2008.09.009

Rosewarne, P. 2002. Hydrogeological characteristics of the Table Mountain Group Aquifers. In *A synthesis of the hydrogeology of the Table Mountain Group – formation of a*

research strategy. (WRC report no. TT 158/01). K., Pietersen, and R., Parsons, Eds. Cape Town, South Africa: Water Research Commission: 33-43.

Rozendaal, R., Gresse, P.G. and Le Roux, J.P. 1999. Neoproterozoic to Early Cambrian crustal evolution of the Pan-African Saldania Belt, South Africa. *Precambrian Research*, 97(3-4): 303-323. DOI: https://doi.org/10.1016/S0301-9268(99)00036-4

Scheepers, R. 1995. Geology, geochemistry and petrogenesis of Late Precambrian S-, I-and A-type granitoids in the Saldania belt, Western Cape Province, South Africa. *Journal of African Earth Sciences*, 21(1): 35-58.

Scheepers, R. and Schoch, A.E. 2006. The Cape Granite Suite. In *the geology of South Africa*. M.R., Johnson, C.R., Anhaeusser and R.J., Thomas, Eds. Pretoria, South Africa: Geological Society of South Africa and the Council for Geoscience: 421-432.

Scott, M., le Roux, P., Sealy, J. and Pickering, R. 2020. Lead and strontium isotopes as palaeodietary indicators in the Western Cape of South Africa. *South African Journal of Science*, 116(5/6): 1-8. DOI: https://doi.org/10.17159/sajs.2020/6700

Sharp, Z. 2017. *Principles of stable isotope geochemistry*. 2nd ed. DOI: https://doi.org/10.25844/h9q1-0p82

Simmons, C.T., Pierini, M.L. and Hutson, J.L. 2002. Laboratory Investigation of Variable-Density Flow and Solute Transport in Unsaturated–Saturated Porous Media. *Transport in Porous Media*, 47: 215-244. DOI: https://doi.org/10.1023/A:1015568724369

Sophocleous, M. and Buchanan, R.C. 2003. *Ground-water recharge in Kansas.* Available: http://www.kgs.ku.edu/Publications/pic22/pic22_1.html [2021, July 13].

South African National Parks. 2021. *Table Mountain National Park.* Available: https://www.sanparks.org [2021, June 9].

South African National Standards. 2015. *Drinking water.* (SANS 241:2015). Pretoria, South Africa: South African National Standards.

South African Weather Service. 2021. *Monthly rainfall: preliminary monthly rainfall data ! Month ending at 08:00 on 2021-08-01* [Data file]. Available: https://www.weathersa.co.za/images/data/climate/nr_month_rai.pdf [2021, July 28].

Spangenberg, J.E. and Vennemann, T.W. 2008. The stable hydrogen and oxygen isotope variation of water stored in polyethylene terephthalate (PET) bottles. *Rapid Communications in Mass Spectrometry*, 22: 672– 676. DOI: https://doi.org/10.1002/rcm.3415

Stowe, C.W. 1995. Characteristics of jointing in the Malmesbury Group, harbour area, Cape Town. *South African Journal of Geology*, 98(2): 224 – 231. DOI: https://hdl.handle.net/10520/EJC-92a0f2b1f

Sun, R.J. 1986. *Regional aquifer-system analysis program of the U.S. Geological Survey summary of projects, 1978-84. U.S. Geological Survey Circular 1002*. Washington, DC: United States Department of the Interior, United States Geological Survey. DOI: https://doi.org/10.3133/cir1002

Tankard, A.J. and Rogers, J. 1978. Late Cenozoic palaeoenvironments on the west coast of southern Africa. *Journal of Biogeography*, 319-337. DOI: https://doi.org/10.2307/3038026

Theron, J.N. 1984. *The geology of Cape Town and environs. Explanation of sheets 3318CD, DC, 3418AB, AD and BA.* Pretoria, South Africa: Department of Mineral and Energy Affairs.

Tshehla, C. and Wright, C.Y. 2019. 15 years after the National Environmental Management Air Quality Act: Is legislation failing to reduce air pollution in South Africa? *South African Journal of Science:* 115, 9/10: 1 - 4. DOI: https://doi.org/10.17159/sajs.2019/6100

United States Geological Survey. 1997. *What is acid rain?* Available: https://pubs.usgs.gov/gip/acidrain/2.html [2021, June 12].

United States Geological Survey. 2021. *Measurement of pH: U.S. Geological Survey techniques and methods, book 9, chap. A6.4, 21 p.* DOI: https://doi.org/10.3133/tm9A6.4 [Supersedes USGS Techniques of Water-Resources Investigations, book 9, chap. A6.4, version 2.0.]

United States Geological Survey. n.d. *Chloride, salinity and dissolved solids.* Available: https://www.usgs.gov/mission-areas/water-resources/science/chloride-salinity-and-dissolved-solids?qt-science_center_objects=0#qt-science_center_objects [2021, June 12].

University of Cape Town. Department of Geological Sciences. 2021. *Cape Town geology.* Available: http://www.geology.uct.ac.za/cape/town/geology [2021, June 10].

van Gend, J., Francis, M.L., Watson, M.P., Palcsu, L., Horváth, A., Macey, P.H., le Roux, P.J., Clarke, C.E. and Miller, J.A. 2020. Saline groundwater in the Buffels River catchment, Namaqualand, South Africa: a new look at an old problem. *Science of the Total Environment*, 762: 1-15. DOI: https://doi.org/10.1016/j.scitotenv.2020.143140

van Schalkwyk, L. and Dyson, L.L. 2013. Climatological Characteristics of Fog at Cape Town International Airport. *Weather and Forecasting*, 28(3): 631-646. DOI: https://doi.org/10.1175/WAF-D-12-00028.1

van Wyk, Y. and Witthueser, K. 2011. A forced-gradient tracer test on the Hansrivier Dyke: Beaufort West, South Africa. *Water SA*, 37(4): 437-443. DOI: https://hdl.handle.net/10520/EJC116816

Von Veh, M.W. 1982. *Aspects of the structure, tectonic evolution and sedimentation of the Tygerberg terrane, Southwestern Cape province*. Msc Dissertation. University of Cape Town. http://hdl.handle.net/11427/16842 [2021, October 12].

Weaver, J.M.C., Talma, A.S. and Cavé, L.C. 1999. *Geochemistry and isotopes for resource evaluation in the fractured rock aquifers of the Table Mountain Group*. (WRC report no. 481/1/99). Pretoria, South Africa: Water Research Commission.

West, A.G., February, E.C. and Bowen, G.J., 2014. Spatial analysis of hydrogen and oxygen stable isotopes ("isoscapes") in ground water and tap water across South Africa. *Journal of Geochemical Exploration*, 145: 213-222. DOI: https://doi.org/10.1016/j.gexplo.2014.06.009

West, A.G, Goldsmith, G.R., Brooks, P.D. and Dawson, T.E. 2010. Discrepancies between isotope ratio infrared spectroscopy and isotope ratio mass spectrometry for the stable isotope analysis of plant and soil waters. *Rapid Communications in Mass Spectrometry*, 24(14): 1948-1954. DOI: https://doi.org/10.1002/rcm.4597

West, J.B., Sobek, A. and Ehleringer, J.R. 2008. A simplified GIS approach to modelling global leaf water isoscapes. *PLoS ONE*, 3(6). DOI: https://doi.org/10.1371/journal.pone.0002447

Western Cape Government. 2011a. *2010 Fifa World Cup, host city Cape Town, green goal legacy report.* Cape Town, South Africa: Western Cape Government.

Western Cape Government. 2011b. *Western Cape integrated water resources management action plan.* Cape Town, South Africa: Department of Water Affairs.

Western Cape Government. 2018. *State of environment outlook report for the Western Cape province: climate change*. (507350). Cape Town, South Africa: Department of Environmental Affairs and Development Planning.

Wigley, R.A. 2004. *Sedimentary facies from the Head of the Cape Canyon: Insights into the Cenozoic evolution of the western margin of South Africa*. Doctoral dissertation. University of Cape Town. Available: https://open.uct.ac.za/handle/11427/423 [2020, May 4].

Wolfgang, D. 2003. Dissolution: carbonate rocks. In *Encyclopedia of caves and karst science*. J. Gunn, Ed. New York, NY: Routledge. DOI: https://doi.org/10.4324/9780203483855

World Health Organization. 2007. *pH in drinking water, revised background document for development of WHO guidelines for drinking water quality*. (Report no. WHO/SDE/WSH/07.01/1). Available: https://www.who.int/water_sanitation_health/dwq/chemicals/ph_revised_2007_clean_version.pdf [2021, September 08].

Wu, C. 2008. *Groundwater occurrence of Table Mountain area in Cape Town, South Africa*. MPhil Dissertation. University of the Western Cape. Available: http://etd.uwc.ac.za/xmlui/handle/11394/2686 [2021, June 28].

Wu, Y. 2005. *Groundwater recharge estimation in Table Mountain Group aquifer systems with a case study of Kammanassie area.* Ph.D. Dissertation. Thesis. University of the Western Cape. Available: http://hdl.handle.net/11394/1319 [2021, July 13].

Xu, Y., Lin, L. and Jia, H. 2009. *Groundwater flow conceptualisation and storage determination of the Table Mountain Group (TMG) Aquifers*. (WRC report no. 1419/1/09). Pretoria, South Africa: Water Research Commission.

Youssef, A.M., Zabramwia, Y.A., Gutiérrezc, F., Bahamila, A.M., Otaibid, Z.A. and Zahrani, A.J. 2020. Sinkholes induced by uncontrolled groundwater withdrawal for agriculture in arid Saudi Arabia. Integration of remote-sensing and geophysical (ERT) techniques. *Journal of Arid Environments*, 177. DOI: https://doi.org/10.1016/j.jaridenv.2020.104132

Appendix

Monthly rainfall data, including the amount and stable isotope values, received by the roof top of the Geological building at UCT, are included below. The δD and $\delta^{18}O$ values range from -57.0‰ to +21.0‰ and from -8.10‰ to +3.47‰ with averages of -7.3‰ and -2.40‰, respectively. On average, 110 mm of rainfall is received monthly. The minimum amount of rainfall received in a month is 0 mm and the maximum amount of rainfall received in a month is 422 mm (August 2013).

Table 7.1: Monthly rainfall data collected from the rooftop of the Geological building at UCT from 1995 – 2021.

Year	Month	Amount (mm)	δD (‰)	$\delta^{18}O$ (‰)	d-excess (‰)
1995	June	120	-6.1	-3.81	24.39
	July	297	-5.0	-2.92	18.36
	August	138	-15.9	-4.92	23.45
	September	67	-2.1	-2.35	16.70
	October	160	-5.8	-3.12	19.16
	November	18	-25.0	-4.60	11.80
	December	15	-57.0	-8.10	7.80
1996	January	4	7.0	1.20	-2.60
	February	50	-31.2	-4.90	8.00
	March	56	-21.0	-5.40	22.22
	April	85	0.5	-2.10	17.30
	May	81	-14.8	-5.00	25.20
	June	248	-7.1	-3.50	20.93
	July	211	-19.0	-5.90	28.21
	August	159	-21.9	-4.97	17.86
	September	237	-10.8	-2.98	13.04
	October	126	-2.1	-1.87	12.86
	November	79	-15.9	-3.35	10.89
	December	96	-14.6	-2.57	5.96
1997	January	17	-11.2	-1.39	-0.06
	February	4	-0.9	-0.43	2.58
	March	13	4.0	-1.37	14.91
	April	94	-11.0	-3.41	16.29
	May	146	-23.8	-5.00	16.24
	June	158	-18.6	-4.72	19.21
	July	37	-2.4	-2.13	14.69

	August	306	-5.9	-2.24	12.03
	September	30	-5.4	-1.83	9.24
	October	41	-5.2	-2.15	12.04
	November	126	-15.4	-3.25	10.63
	December	19	3.8	-0.61	8.72
1998	January	23	-1.8	-1.57	10.76
	February	5	4.0	-0.91	11.23
	March	58	-5.3	-1.69	8.24
	April	114	-5.1	-1.55	7.26
	May	326	-24.0	-4.15	9.20
	June	191	-4.8	-2.11	12.08
	July	172	-8.8	-2.58	11.80
	August	67	-14.9	-3.27	11.31
	September	87	-3.7	-0.95	3.87
	October	80	-8.2	-2.26	9.84
	November	82	-4.5	-2.38	14.51
	December	52	-16.0	-2.59	4.69
1999	January	15	5.2	0.14	4.09
	February	13	6.8	-0.47	10.54
	March	5	2.7	-1.14	11.86
	April	79	-24.5	-5.44	19.04
	May	125	-6.7	-2.80	15.70
	June	169	-15.2	-3.69	14.28
	July	159	-10.5	-3.06	13.97
	August	253	-18.4	-4.66	18.92
	September	246	-17.3	-4.70	20.30
	October	5	6.6	-0.65	11.84
	November	58	2.1	-1.60	14.92
	December	4	-1.9	-1.30	8.53
2000	January	39	-5.2	-2.39	13.94
	February	0			
	March	8	-31.6	-5.59	13.09
	April	29	3.1	-1.23	12.98
	May	226	-4.1	-4.24	29.83
	June	162	-15.3	-3.13	9.72
	July	154	-14.5	-4.71	23.21
	August	163	-8.3	-2.65	12.94
	September	214	-2.9	-1.98	12.98
	October	24	-0.6	-1.16	8.67

	November	29	-11.1	-2.54	9.18
	December	37	-2.1	-1.64	11.06
2001	January	20	-12.8	-3.45	14.84
	February	38	-1.6	-1.20	8.05
	March	0			
	April	77	-20.8	-4.73	17.04
	May	277	-6.1	-3.24	19.81
	June	127	-5.4	-3.06	19.11
	July	442	-19.0	-4.77	19.13
	August	413	-18.0	-4.48	17.84
	September	152	-4.0	-2.66	17.28
	October	119	3.0	-1.50	15.00
	November	26	-18.0	-2.68	3.44
	December	6	7.0	-0.28	9.24
2002	January	138	-17.0	-5.50	27.00
	February	36	0.0	-2.40	19.20
	March	46	2.0	-2.06	18.48
	April	78	0.0	-4.14	33.12
	May	147	0.0	-2.65	21.20
	June	256	-3.0	-2.26	15.08
	July	259	0.0	-3.39	27.12
	August	95	-36.0	-6.43	15.44
	September	40	-14.0	-2.99	9.92
	October	105	-15.0	-3.85	15.80
	November	66	-9.0	-3.31	17.48
	December	8	18.0	3.47	-9.76
2003	January	25	18.0	3.30	-8.40
	February	25	11.0	0.28	8.76
	March	96	-22.0	-5.60	22.80
	April	33	-3.0	-2.30	15.40
	May	95	-7.0	-2.70	14.60
	June	93	-5.0	-2.90	18.20
	July	165	-16.0	-2.71	5.68
	August	296	-23.0	-5.04	17.32
	September	165	-12.0	-2.76	10.08
	October	88	-4.0	-2.18	13.44
	November	10	9.0	-0.66	14.28
	December	75	-1.0	-1.45	10.60
	January	13	-18.0	-3.55	10.40

2004	February	27	-10.0	-2.87	12.96
	March	30	-8.0	-2.75	14.00
	April	197	-15.1	-3.54	13.22
	May	64	-6.0	-2.79	16.32
	June	228	-21.0	-4.65	16.20
	July	263	-14.0	-3.47	13.76
	August	342	-10.0	-2.67	11.36
	September	98	-10.0	-2.38	9.04
	October	188	-31.0	-5.67	14.36
	November	18	-4.0	-1.51	8.08
	December	39	5.0	-0.50	9.00
2005	January	63	-6.6	-1.94	8.92
	February	5	-4.0	-1.40	7.20
	March	15	0.0	-1.16	9.28
	April	134	-37.0	-5.37	5.96
	May	309	-26.0	-3.22	-0.24
	June	321	-14.0	-3.15	11.20
	July	187	-14.0	-1.67	-0.64
	August	287	-15.0	-3.13	10.04
	September	98	-6.0	-2.40	13.20
	October	55	1.0	0.00	1.00
	November	23	4.0	0.97	-3.76
	December	0			
2006	January	0			
	February	60	-3.0	-1.71	10.68
	March	17	-4.0	-1.50	8.00
	April	85	-18.0	-3.83	12.64
	May	289	-18.0	-3.40	9.20
	June	117	-13.0	-3.02	11.16
	July	251	-11.0	-2.74	10.92
	August	213	-14.0	-2.91	9.28
	September	76	-15.0	-2.60	5.80
	October	86	-7.0	-2.18	10.44
	November	112	-24.0	-4.38	11.04
	December	30	-9.0	-2.42	10.36
2007	January	27	11.0	1.27	0.84
	February	46	0.0	-3.03	24.24
	March	49	-3.0	-2.82	19.56
	April	156	-2.0	-2.72	19.76

	May	162	-14.0	-3.36	12.88
	June	353	-22.0	-4.62	14.96
	July	334	-15.0	-3.66	14.28
	August	229	-21.0	-4.06	11.48
	September	115	-2.0	-1.84	12.72
	October	46	0.0	-3.58	28.64
	November	177	-4.0	-1.66	9.28
	December	40	11.3	1.52	-0.85
2008	January	30	-1.4	-2.40	17.83
	February	43	13.9	-1.22	23.61
	March	10	-6.6	-2.23	11.26
	April	20	-7.3	-2.66	13.97
	May	224	0.5	-1.78	14.72
	June	262	-13.3	-3.27	12.79
	July	358	-14.8	-4.66	22.47
	August	262	-24.8	-4.03	7.43
	September	337	-16.3	-3.07	8.26
	October	47	-1.1	-1.87	13.87
	November	52	-16.0	-3.61	12.80
	December	38	-2.0	-0.90	5.20
2009	January	3	-2.9	-0.30	-0.52
	February	14	-3.7	-0.28	-1.51
	March	5	7.2	2.03	-9.13
	April	72	-4.8	-1.88	10.26
	May	220	-10.1	-3.25	15.87
	June	393	-13.2	-2.71	8.48
	July	220	-22.6	-4.53	13.66
	August	393	-23.2	-4.50	12.80
	September	169	-8.1	-2.21	9.61
	October	76	-16.7	-3.16	8.52
	November	185	-32.0	-5.09	8.72
	December	16	-0.7	-0.56	3.75
2010	January	9	9.7	0.75	3.63
	February	12	-5.8	-0.54	-1.50
	March	7	0.4	-0.83	7.06
	April	44	-12.1	-2.25	5.93
	May	277	-8.4	-2.78	13.88
	June	222	-17.0	-3.31	9.45
	July	166	-15.0	-3.69	14.45

	August	121	-4.9	-1.74	8.99
	September	100	-3.3	-2.24	14.59
	October	102	-3.3	-2.15	13.91
	November	73	-6.2	-2.39	12.95
	December	17	-39.9	-5.06	0.52
2011	January	16	-5.2	-0.15	-4.04
	February	3	13.9	3.19	-11.56
	March	16	-23.6	-4.12	9.34
	April	111	-5.8	-2.73	16.11
	May	145	-12.3	-3.69	17.16
	June	191	-18.3	-4.82	20.20
	July	49	-14.6	-4.68	22.85
	August	209	-3.8	-2.63	17.18
	September	141	-0.1	-1.51	11.97
	October	41	-17.0	-3.48	10.80
	November	72	-12.0	-3.21	13.67
	December	62	-1.6	-2.05	14.78
2012	January	46	5.4	0.78	-0.84
	February	21	-2.5	-0.68	2.95
	March	69	-11.9	-3.07	12.64
	April	133	-9.8	-3.12	15.13
	May	143	-10.4	-3.08	14.24
	June	226	-6.4	-4.15	26.80
	July	293	-8.8	-2.67	12.56
	August	214	-13.5	-3.25	12.48
	September	172	-10.8	-2.36	8.15
	October	44	-7.1	-3.16	18.20
	November	60	0.9	-1.13	9.95
	December	9	7.2	-0.21	8.87
2013	January	26	0.4	-2.04	16.69
	February	55	3.0	-1.12	11.96
	March	76	-8.6	-1.13	0.43
	April	186	-17.4	-2.81	5.12
	May	231	-4.6	-2.07	11.95
	June	347	-18.3	-4.09	14.36
	July	185	-4.6	-1.43	6.87
	August	422	-23.3	-5.16	18.01
	September	238	-8.2	-2.68	13.28
	October	90	-10.3	-2.85	12.49

	November	129	-26.1	-3.87	4.85
	December	13	12.7	1.56	0.25
2014	January	49	-4.0	-2.36	14.87
	February	16	12.7	2.32	-5.90
	March	158	-8.0	-2.84	14.74
	April	54	-13.5	-4.46	22.20
	May	93	-2.5	-2.27	15.64
	June	274	-9.5	-3.53	18.75
	July	243	-12.6	-4.05	19.81
	August	212	-13.0	-3.54	15.33
	September	43	-10.8	-3.31	15.75
	October	7	-3.8	-3.04	20.52
	November	59	-1.7	-3.11	23.21
	December	33	6.1	-0.25	8.08
2015	January	67	0.6	-1.58	13.22
	February	23	12.7	0.32	10.06
	March	6	11.6	0.27	9.41
	April	18	-5.2	-2.97	18.50
	May	85	-5.5	-1.75	8.53
	June	293	-5.3	-3.76	24.74
	July	187	-15.5	-3.85	15.28
	August	94	0.4	-1.42	11.79
	September	101	-1.8	-1.69	11.70
	October	91	-6.2	-3.10	18.57
	November	24	-0.1	-1.70	13.50
	December	17	13.8	1.70	0.20
2016	January	61	-1.2	-2.25	16.80
	February	3	-13.1	-1.52	-0.94
	March	72	-6.0	-2.93	17.44
	April	152	-3.8	-2.03	12.44
	May	44	-4.3	-3.02	19.86
	June	255	-4.8	-2.83	17.84
	July	234	-28.9	-5.24	12.99
	August	121	-17.8	-3.19	7.76
	September	90	-6.7	-2.90	16.50
	October	34	-2.6	-0.80	3.76
	November	12	5.7	0.94	-1.80
	December	111	8.1	-0.10	8.94
	January	40	-1.8	-2.44	17.70

2017	February	0			
	March	45	-9.0	-2.32	9.61
	April	68	-4.5	-1.86	10.41
	May	15	0.8	-1.29	11.12
	June	311	-5.4	-2.45	14.19
	July	108	-6.4	-2.93	17.07
	August	203	-4.0	-2.22	13.75
	September	58	4.0	-0.31	6.42
	October	87	-3.3	-1.84	11.43
	November	58	-8.1	-2.87	14.86
	December	46	0.5	-1.26	10.56
2018	January	30	-4.1	-1.20	5.50
	February	10	5.7	0.80	-0.71
	March	47	-11.3	-2.38	7.68
	April	68	-9.2	-2.88	13.80
	May	176	-5.8	-2.21	11.84
	June	303	-8.1	-2.59	12.63
	July	95	-17.0	-3.97	14.78
	August	204	-7.5	-2.76	14.54
	September	192	-5.1	-2.12	11.81
	October	12	-17.5	-3.63	11.57
	November	20	5.1	-0.97	12.89
	December	66	0.0	-1.27	10.18
2019	January	22	18.4	3.41	-8.86
	February	7	-2.2	-1.03	6.04
	March	58	-13.6	-3.17	11.73
	April	36	2.2	-1.68	15.67
	May	115	-9.7	-2.45	9.89
	June	236	-17.5	-3.77	12.70
	July	347	-5.6	-2.37	13.44
	August	155	1.1	-1.60	13.86
	September	56	-0.1	-1.12	8.88
	October	135	-13.3	-2.89	9.82
	November	7	0.8	-1.17	10.19
	December	26	21.0	2.58	0.36
2020	January	8	-12.2	-3.02	12.00
	February	22	2.5	-0.18	3.88
	March	86	1.4	-0.18	2.88
	April	4	-7.5	-1.57	5.10

	May	160	-3.6	-2.13	13.48
	June	185	-8.2	-3.21	17.50
	July	168	-6.4	-2.64	14.69
	August	261	-8.7	-3.34	18.00
	September	157	-3.4	-2.29	14.95
	October	32	-1.8	-2.35	17.01
	November	87	-8.6	-2.59	12.18
	December	13	1.5	-1.36	12.37
2021	January	22	8.4	0.28	6.19

The rainfall amount, the arithmetic mean (Ar. mean) and the weighted mean (Wt. mean) annual stable isotope values of the rainfall received on the roof of the Geology building at UCT are presented below (Table 7.2). The arithmetic mean annual δD and $\delta^{18}O$ values range from -12.6‰ to -0.1‰ and from -3.45‰ to -1.27‰ with averages of -8.4 and -2.62 in time period 1 (1996 – 2008) and -5.8‰ and -2.09‰ in time period 2 (2009 – 2020), respectively. The weighted mean annual δD and $\delta^{18}O$ values range from -17.2‰ to -4.3‰ and from -3.53‰ to -2.19‰ with averages of -8.2‰ and -2.64‰ in time period 1 (1996 – 2008) and -8.8‰ and -2.11‰ in time period 2 (2009 – 2020), respectively.

Table 7.2: The arithmetic mean (Ar. mean) and the weighted mean (Wt. mean) annual δD and $\delta^{18}O$ values of UCT rainfall from 1995 – 2020.

Time period	Year	Amount (mm)	Ar. mean δD (‰)	Ar. mean $\delta^{18}O$ (‰)	Wt. mean δD (‰)	Wt. mean $\delta^{18}O$ (‰)	Ar. mean δD (‰)	Ar. mean $\delta^{18}O$ (‰)	Wt. mean δD (‰)	Wt. mean $\delta^{18}O$ (‰)
1	1996	1432	-12.6	-3.45	-12.6	-3.83	-8.4	-2.62	-8.2	-2.64
	1997	992	-7.6	-2.38	-7.6	-3.20				
	1998	1256	-7.8	-2.17	-7.8	-2.65				
	1999	1131	-5.9	-2.45	-5.9	-3.83				
	2000	1085	-8.4	-2.84	-8.4	-3.12				
	2001	1697	-8.7	-2.91	-8.7	-3.76				
	2002	1274	-6.2	-2.96	-6.7	-3.48				
	2003	1166	-4.6	-2.06	-4.6	-3.22				
	2004	1506	-11.8	-3.03	-11.8	-3.53				
	2005	1495	-10.7	-2.04	-10.7	-2.87				
	2006	1334	-12.4	-2.79	-12.4	-2.57				
	2007	1733	-5.1	-2.38	-6.5	-3.34				
	2008	1683	-7.4	-2.64	-7.5	-3.25				
2	2009	1766	-10.9	-2.20	-17.2	-3.53	-5.8	-2.09	-8.8	-2.11
	2010	1150	-8.8	-2.18	-10.0	-2.73				
	2011	1056	-8.4	-2.49	-9.0	-3.13				
	2012	1430	-5.6	-2.17	-8.7	-2.85				
	2013	1996	-8.8	-2.31	-14.0	-3.17				
	2014	1241	-5.1	-2.54	-8.9	-3.26				
	2015	1006	-0.1	-1.63	-5.1	-2.70				
	2016	1188	-6.3	-2.16	-9.4	-2.87				
	2017	1038	-3.4	-1.98	-4.3	-2.19				
	2018	1221	-6.2	-2.10	-7.3	-2.45				
	2019	1200	-1.5	-1.27	-7.2	-2.35				
	2020	1182	-4.6	-2.07	-5.7	-2.52				